Mathematical Modelling and Design Software for Pulse Tube Cryocoolers

Dissertation submitted in partial fulfilment
of the requirements of the degree of

Master of Technology (Research)

in

Mechanical Engineering

by

Debashis Panda

(Roll Number: 614ME1003)

based on research carried out

under the supervision of

Prof. Sunil Kumar Sarangi

January, 2017

Department of Mechanical Engineering
National Institute of Technology Rourkela

Mechanical Engineering
National Institute of Technology Rourkela

January 11, 2017

Certificate of Examination

Roll Number: *614ME1003*
Name: *Debashis Panda*

Title of Dissertation: *Mathematical modelling and Design software for Pulse Tube Cryocoolers*

We the below signed, after checking the dissertation mentioned above and the official record book (s) of the student, hereby state our approval of the dissertation submitted in partial fulfilment of the requirements of the degree of *Master of Technology (Research)* in *Mechanical Engineering* at *National Institute of Technology Rourkela*. We are satisfied with the volume, quality, correctness, and originality of the work.

Prof. Sunil K. Sarangi
(Principal Supervisor)

Dr. Suman Ghosh (ME)
Member, MSC

Prof A.K. Panda (EE)
Member, MSC

Prof. P.Viswakarma (PH)
Member, MSC

Prof. K.P. Maity
Chairperson, MSC

Prof. T.K. Nandi (IIT Kharagpur)
External Examiner

Mechanical Engineering
National Institute of Technology Rourkela

Sunil Kumar Sarangi
Professor

January 11, 2017

Supervisor's Certificate

This is to certify that the work presented in this dissertation entitled "*Mathematical modelling and Design software for Pulse Tube Cryocoolers"* by *Debashis Panda*, Roll Number 614ME1003, is a record of original research carried out by him under my supervision and guidance in partial fulfilment of the requirements of the degree of *Master of Technology (Research)* in *Mechanical Engineering*. Neither this dissertation nor any part of it has been submitted for any degree or diploma to any institute or university in India or abroad.

_____
Sunil Kumar Sarangi
Professor

Declaration of Originality

I, *Debashis Panda*, Roll Number *614ME1003* hereby declare that this dissertation entitled *Mathematical modelling and Design software for Pulse Tube Cryocoolers* presents my original work carried out as a postgraduate student of NIT Rourkela and, to the best of my knowledge, contains no material previously published or written by another person, nor any material presented by me for the award of any other degree or diploma of NIT Rourkela or any other institution. Any contribution made to this research by others, with whom I have worked at NIT Rourkela or elsewhere, is explicitly acknowledged in the dissertation. Works of other authors cited in this dissertation have been duly acknowledged under the section "References". I have also submitted my original research records to the scrutiny committee for evaluation of my dissertation.

I am fully aware that in case of any non-compliance detected in future, the Senate of NIT Rourkela may withdraw the degree awarded to me on the basis of the present dissertation.

January 11, 2017

NIT Rourkela ***Debashis Panda***

Dedicated

To my Parents

Acknowledgement

The research through my M.TECH (Research) study would not have been complete without the help and support of many individuals who deserve my appreciation and special thanks.

At First, I would like to express my deep sense of gratitude and respect to my supervisor **Prof. S. K. Sarangi** for his excellent guidance, suggestions, and constructive criticism. I feel proud that I am one of his research student. I will always remember his helping hands and moral support in my good and evil day during this period. I would like to express my deep sense of gratitude and respect to **Prof A. K. Satapathy** for some helpful suggestions, and constructive criticism during my research period. I would also like to express my sincere gratitude to the Head of the Department of Mechanical Engineering **Prof. S. S. Mahapatra** for his timely help during the entire course of my research work.

Very special thanks to my family members for their consistent support and faith shown upon me. Their love and patience made this work possible, and their encouragement immensely helped me in my work for this thesis. I am also thankful to all those who have directly or indirectly helped during my research period.

I am incredibly thankful to my research colleagues **Dr. Sachindra Rout**, **Rudra Narayan Kandi, Sai Manoj** and **Somen Biswal** for their friendship during my stay at NIT Rourkela and for making the past few years more delightful.

Finally, but most importantly, I am thankful to **Almighty**, my Lord for giving me the will power and strength to make it this far.

(January 11, 2017)

Debashis Panda

Abstract

Pulse tube refrigerators are increasingly become popular because of its higher reliability, absence of any moving parts at its cold end, easy design and fabrication technique, less maintenance, less wear and tear etc. However its design is quite complicated because of the complex heat and mass transfer process occurring inside it, so it is a challenging problem to the scientists and engineers pursuing this field to design pulse tube cryocoolers in order to achieve the desired performance.

The work presented in this thesis is directed towards the detailed mathematical analysis of regenerator, a critical component of not only pulse tube cryocoolers but also all other types of regenerative cryocoolers. Based on the mathematical analysis, a software package has been developed for simulation of regenerator and validated with the experimental results available in the literature. Also, a parametric study has been performed to identify the effect of essential parameters that affect the cooling performance of the regenerator for cryogenic based applications.

Detailed mathematical analysis of pulse tube refrigerator has been carried out for both Stirling and Gifford Mc-Mohan type pulse tube refrigerators of various geometrical configurations including different losses in various components that affect its performance. Based on the mathematical analysis, a general purpose simulation software package has been developed to design pulse tube refrigerators and validated with the numerical results available in previous results.

Also, CFD analysis of inertance type pulse tube refrigerator has been carried out not only to visualise the inside fluid flow and heat transfer processes, but also to identify the essential changes that happen due to increase in operating frequency. The effect of various losses, those explained theoretically by various scientists, has been illustrated graphically in the present work.

Keywords: Pulse tube cryocoolers, Software, CFD, Regenerator

Table of Contents

List of Figures

List of Tables

Nomenclature

A_{di}	Opening area of double inlet valve [m^2]
A_l	Interfacial heat transfer area [m^2]
A_m	Area of matrix [m^2]
A_o	Opening area of orifice valve [m^2]
A_r	Regenerator heat transfer area [m^2]
A_s	Heat transfer area [m^2]
A_{wl}	Area of wall [m^2]
C_{di}	Coefficient of discharge for double inlet valve
C_{do}	Coefficient of discharge for orifice valve
C_f	Forchheimer inertial coefficient
C_r	Capacity of matrix [J/kg-K]
F	Shape factor
G	Flow rate [kg/m^2 sec]
I, II, III	Sections shown in pulse tube
Ie	Inefficiency
L	Length [m]
M	Mass of regenerator [kg]
N_I	Number of insulation layer
N_s	Number of screens
N_t	Number of time steps
N_z	Number of spatial nodes

$NSTEP$	Number of time step
P	Pressure [Pa]
P_H	High pressure in system [Pa]
P_L	Low pressure in system [Pa]
Q_c	Cooling capacity [W]
Q_{ideal}	Ideal refrigeration power [W]
Q_{IL}	Ineffectiveness loss [W]
QC_m	Conduction loss in regenerator matrix [W]
Q_{pd}	Pressure drop Loss [W]
QC_{pt}	Conduction loss in pulse tube [W]
QC_{rg}	Conduction loss in regenerator [W]
QC_{total}	Total conduction Loss [W]
Q_{ts}	Temperature swing loss [W]
R	Gas constant [J/mol-K]
T_c	Cold end temperature [K]
T_h	Hot end temperature [K]
T_{mrg}	Logarithm mean temperature difference in regenerator [K]
T_{rgo}	Temperature at the outlet of regenerator [K]
T_{wl}	Temperature of wall [K]
$\bar{T}_{c-out}$	Average temperature at outlet [K]
V	Volume [m^3]
V_{chx}	Volume of cold heat exchanger [m^3]

V_d	Dead volume at cold end [m^3]
V_{drg}	Dead volume of regenerator [m^3]
V_{hhx}	Volume of hot heat exchanger [m^3]
V_o	Dead volume of compressor [m^3]
V_{res}	Volume of reservoir [m^3]
V_s	Swept volume of compressor [m^3]
W	Work supplied by compressor [W]
c_p	Specific heat capacity at constant pressure [J/kg-K]
c_v	Specific heat of gas at constant volume [J/kg-K]
d_h	Hydraulic Diameter [m]
d_o	Outer diameter of regenerator [m]
d_w	Wire diameter [m]
dq	Heat transfer [W]
du	Change in internal energy
dw	Work done [W]
e_c	Emissivity of cold surface
e_s	Emissivity of surface
f	Frequency [Hz]
fr	Friction factor
h	Heat transfer coefficient [W/m^2 - K]
k_f	Thermal conductivity of fluid [W/m-K]
m_I	Mass of section I of pulse tube [kg]
$\dot{m}$	Mass flow rate [kg/sec]

n	Number of mesh opening
r_h	Hydraulic radius [m]
s	Space between meshes
t_s	Thickness of screens [m]
u	Velocity [m/s]
wl	Wall

Greek symbols

α	Porosity of regenerator
β	Area density
γ	Ratio of specific heats
Δp	Pressure drop
Δt	Small change in time
Δz	Small change in space
$\Delta\xi$	Control volume length
$\Delta\eta$	Time step
δA_s	Small change in surface area
δV	Small change in volume
ε	Effectiveness of regenerator
ζ	Matrix conductivity factor
θ	Angle in rotary valve, System angle with respect to gravity
μ	Viscosity [Pa-s]
σ	Stefan Boltzmann's constant [W/m^2K^4]
τ	Period
φ	Permeability [m^2]
ψ	Angle in pulse tube, Geometrical parameters
ω	Angular frequency [rad/sec]

Dimensionless numbers

Re	Reynolds number
Pr	Prandtl number
NTU	Number of transfer units
Nu	Nusselt number
St	Stanton Number

Subscripts

ac	Aftercooler
c	Cold end
cp	Compressor
di	Double inlet
f	Fluid
h	Hot end
i	Inlet
m	Matrix
o	Orifice
o	Outlet
res	Reservoir
r	Rotary valve
s	Solid
w	Wall

Superscripts

cp	Compressor
chx	Cold heat exchanger

hhx	Hot heat exchanger
pt	Pulse tube
rg	Regenerator
l	Current time step
′	Heating period
′′	Cooling period

Constants

C_{IIO}, m_{IO}	Constants
K_{mo}, K_{wl}	Constants
$K_1, ...K_6$	Constants

Abbreviations

AFTC	After cooler
BPTR	Basic pulse tube refrigerator
CHX	Cold end heat exchanger
COMP	Compressor
COP	Coefficient of performance
CRESP-PTR	Cryo Engineering Simulation Programme-Pulse Tube Refrigerator
CRESP-REGEN	Cryo Engineering Simulation Programme-Regenerator
CRESP-SPTR	Cryo Engineering Simulation Programme-Stirling Pulse Tube Refrigerator
DIPTR	Double inlet pulse tube refrigerator
GM	Gifford Mc-Mahon
HHX	Hot end heat exchanger
HP	High pressure

IPTR	Inertance tube pulse tube refrigerator
LP	Low pressure
OPTR	Orifice pulse tube refrigerator
PT	Pulse tube
PTR	Pulse tube refrigerator
REG	Regenerator

Chapter 1

Introduction

1.1 General

Pulse tube cryocoolers are considered to be efficient and reliable cryocoolers to achieve a cryogenic temperature within a single stage or multi-stage operation using helium as working fluid. The concept of pulse tube refrigerator was first given by Gifford and Longsworth [1] in 1963. They wanted to improve the performance of GM-cryocooler and observed that the cold end of the tube becomes cold, thus, by further improvement invented the first pulse tube refrigerator. Pulse tube refrigerator is named so due to the production of pulsatile pressure wave inside a hollow stainless steel tube known as pulse tube. This configuration is known as basic pulse tube refrigerator. The working mechanism of basic pulse tube refrigerator has been explained elaborately with the aid of surface heat pumping mechanism in literature [2]. Pulse tube refrigerator is one kind of regenerative cryocooler that provides a wide variety of technical merits such as absence of any moving parts at its cold end besides smooth operation, better reliability and less vibration as well.

One significant technical modification in the geometry to improve the performance of basic pulse tube refrigerator was given by Mikulin *et al.* [3]. They proposed that the performance of basic pulse tube refrigerator could be further improved by changing the phase angle between pressure wave and volumetric flow rate at the cold end of pulse tube. They achieved it by placing an orifice valve and a reservoir and, they were able to achieve 105 K temperature using air as working fluid. This is considered to be the second generation of pulse tube refrigerator, known as orifice pulse tube refrigerator. Later, Radebaugh *et al.* [4] were able to achieve 60 K by changing the position of orifice valve and using helium as working fluid.

The third generation pulse tube refrigerator is termed as double inlet pulse tube refrigerator developed by Zhu *et al.* [5]. This technical configuration is quite similar to that of orifice type pulse tube refrigerator except that another orifice valve is present between the hot end of regenerator and hot end of pulse tube. As a result, the phase angle (between mass flow rate and pressure wave) changes and lower temperature could be achieved as compared to orifice pulse tube refrigerator. However, this configuration leads to one significant loss known as DC Loss that reduces the cooling capacity [6]. The most successful generation of pulse tube refrigerator is known as inertance pulse tube refrigerator. Here a long neck and small diameter tube, known as inertance tube, is present in place of an orifice in an orifice pulse tube refrigerator [7]. This tube is named as inertance tube due to the production of inertance effect inside it. However, multivalve pulse tube refrigerators have been developed to improve the performance that will be explained in subsequent chapters. Double inlet pulse tube refrigerator provides a trade-off between refrigerating capacity and technical configuration, as in the case of GM-type pulse tube refrigerator. Nevertheless, inertance tube configuration is mostly suited for Stirling type pulse tube refrigertaor.

Pulse tube is closed at the top end where a substantial heat transfer area exists between the working gas and the surrounding to dissipate heat. The bottom end is connected to the pressure wave generator via regenerator. The working principle of a basic pulse tube refrigerator will be explained in following pages. The gas parcels inside the pulse tube refrigerator will undergo pressurization and depressurization processes alternatively to produce a cooling effect. The working cycle is close to Stirling cycle [8] and GM cycle [9]. During compression part of the cycle, each element of gas in pulse tube refrigerator moves towards the closed end and at the same time experience a temperature rise due to adiabatic compression. At this stage, the pressure is at its peak value. During platue in pressure wave, the gas is cooled somewhat by transfer of heat to the tube wall. During expansion part of the cycle, the same element of gas moves towards the open end of pulse tube and experience a cooling effect due to adiabatic expansion. During expansion stage pressure is at its lowest value. During platue, the gas is warmed through heat transfer from the tube wall. Due to the imperfect thermal contact between the gas element and tube wall, compression and expansion process are between isothermal and adiabatic. The overall effect of these entire mechanism is to generate

refrigeration effect, and this mechanism is termed as the shuttle heat transfer mechanism (or, surface heat pumping mechanism) [8]. This will be explained in detailed in subsequent pages.

1.2 Motivation

Pulse tube cryocoolerss are used in a wide variety of applications, e.g. cooling of space satellites, cooling of military vehicles, cooling of IR sensors, storage of biological cells, MRI scanners, etc. For better working of space satellites, MRI etc. proper design of pulse tube cryocoolers is very much essential. So it is necessary to understand the cooling mechanism of pulse tube cryocoolers to improve its performance further. Detailed understanding of physical phenomena and mathematical principles is very much essential for the design of pulse tube refrigerator to achieve necessary refrigeration temperature with desired refrigerating capacity. The commercial software packages (e.g. SAGE, FZKPTR) developed by various organisations are not in an open form besides it is hard to modify it according to one's needs. Therefore, NIT Rourkela has initiated an R&D programme to develop an indigenous software package to cater the contemporary needs in research and development. Over 40 years of research and development (in cryocooler technology division), it was noticed that regenerator is the heart of not only pulse tube cryocooler but also of all other types of regenerative cryocoolers. Therefore, particular attention has been concentrated on the detailed mathematical study of the regenerator (a perticular chapter is dedicated towards regenerator mathematical analysis) and a software named as CRESP-REGEN has been developed in this work. Another package CRESP-PTR is also developed for simulation of pulse tube refrigerator.

1.3 Organization of the Thesis

Regenerator is a crucial component in many regenerative types of machines. The existing REGEN series software is used for simulation of regenerator. It is a widely used popular software and it is based on the assumption of sinusoidal variation of mass flow rate and pressure. However, in GM-type cryocoolers and GM-type pulse tube cryocoolers, the variation is not usually sinusoidal due to the presence of rotary valve. Also, it is only applicable for cryogenic temperature range application. In the present work, a software is developed by using numerical method presented by Ackerman *et al.* [10] and has been validated with the published experimental results.

Detailed mathematical modelling of pulse tube refrigerator such as isothermal model, adiabatic model and numerical model are presented in the thesis including the effect of various losses encountered in different components. CFD analysis of inertance type pulse tube refrigerator is also performed by using the commercial software package FLUENT to visualise the heat transfer and fluid flow phenomena and various losses.

The present dissertation has been organized into six chapters.

- The current chapter (first chapter) describes introduction on pulse tube cryocoolers, motivation for the current work and organisation of the thesis.

- The second chapter provides a detailed understanding of basic concepts of the regenerator and pulse tube refrigerator. Different types of pulse tube refrigerators and their mechanism of the cold production are also well explained. The ideal refrigeration capacity produced is different from actual refrigeration capacity due to various losses encountered in the regenerator, heat exchangers, pulse tube and all other components. The detailed analysis of different losses are presented in a summarised manner. A comprehensive review of mathematical models of regenerator and pulse tube cryocoolers of various configurations are also included. A detailed examination of analytical models, numerical models and CFD models related to pulse tube refrigerator technology is discussed. In addition, a list of commercially available software packages for simulation of pulse tube refrigerator is also presented in tabular form.

- The third chapter explains the mathematical model of regenerator and description of CRESP-REGEN software.Validation of CRESP-REGEN software with previously published results are also presented. A parametric study is performed by using REGEN 3.3, and the effect of the various operating and geometrical parameters on cooling power and coefficient of performance is explained with interactive charts.

- The fourth chapter describes the isothermal model, adiabatic model and numerical model of a pulse tube refrigerator including various losses. In this chapter, the end-user procedure to deal the CRESP-PTR software package has been elaborated and its validation with published resulte are also explained.

- Fifth chapter presents CFD Simulation of IPTR using commercial software package FLUENT. Various governing equations, modelling procedure from geometry creation up to results has been explained in detail.
- Sixth chapter includes an end note remark and valuable suggestions have been highlighted for future extension of the present work.

Chapter 2

Review of Literature

2.1 Basic Concepts of regenerator

Regenerator is of two types such as static regenerator and dynamic regenerator. In the case of a static regenerator, matrix of the regenerator is stationary whereas in dynamic regenerator matrix of regenerator is rotating. Rotary regenerators are further classified into two different categories such as axial flow rotary regenerator and radial flow rotary regenerator, depending upon the direction of flow. Regenerator is a critical component in all regenerative type of machines including Stirling cryocoolers, GM-cryocoolers, pulse tube cryocoolers, VM-cryocoolers and Stirling engines, etc. The performance of these regenerative machines is strongly dependent upon the performance of the regenerator. Thus, it is essential to study the physics involve in the working of the regenerator. Regenerator is a hollow tube filled with meshes or lead balls and these meshes are known as matrix.

A typical woven mesh is shown in Fig. 2.1. When hot fluid passes through the matrix, heat will be transferred into the matrix and the fluid gets cooled. This period is known as a heating period. After the heating period, flow reversal takes place where the cold fluid passes through it. The fluid absorbs heat from the matrix and gets heated, this period is known as cooling period. The flow inside the regenerator is periodic (or, oscillating, alternating), hence the design of a regenerator is a critical issue to the scientists and engineers pursuing in this field.

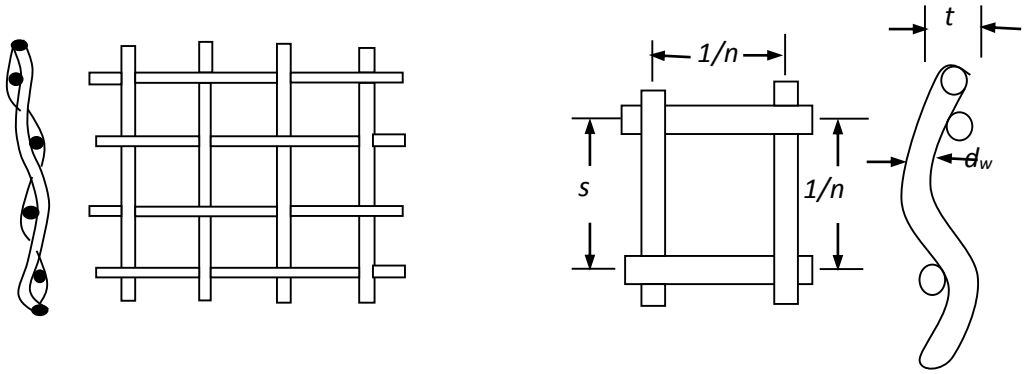

Figure 2.1: Regenerator meshes.

The complete heat transfer and fluid flow phenomena inside the regenerators are governed by a set of complex nonlinear, coupled and non-homogeneous differential equations. The complete analytical solution of this may be impossible. These sets of equations, however, can be solved using finite difference, finite volume or finite element methods by using high-speed computers [10].

2.1.1 Important terminologies

2.1.1.1 Porosity

$$\text{Porosity } (\alpha) = \frac{\text{total volume of void space}}{\text{total volume of the matrix}} \tag{2.1}$$

2.1.1.2 Area Density

$$\text{Area density } (\beta) = \frac{\text{total surface area of connected voids}}{\text{total volume of the matrix}} \tag{2.2}$$

2.1.1.3 Hydraulic Radius

$$r_h = \frac{\alpha}{\beta} = \frac{\text{Fluid volume}}{\text{Heat transfer area}} = \frac{\text{Area}}{\text{Wetted perimeter}} \tag{2.3}$$

2.1.1.4 Capacity Ratio

It is defined as the ratio between the thermal capacities of the matrix to the thermal capacity of fluid.

$$\frac{C_r}{C_{\min}} = \frac{(Mc_p)_m}{(\dot{m}c_p)_f \tau_h} \tag{2.4}$$

If capacity ratio is large then temperature swing loss of regenerator matrix is smaller. Hence to avoid temperature swing loss, capacity ratio must be large.

2.1.1.5 NTU (Number of Transfer Units)

It is a non-dimensional parameter related to the size of regenerator (heat exchangers). A lower value of NTU signifies that the effectiveness is small.

$$NTU = \frac{hA_S}{2\dot{m}c_p} \tag{2.5}$$

2.1.1.6 Stanton Number

$$St = \frac{h}{Gc_p} \tag{2.6}$$

2.1.1.7 Nusselt Number

It is defined as the ratio between convective heat transfers to conduction heat transfer.

$$Nu = \frac{hd_h}{k_f} \tag{2.7}$$

If it is large, then convention heat transfer dominates over conduction heat transfer and vice-versa.

2.1.1.8 Period

$$\tau = \frac{1}{2 \times f} \tag{2.8}$$

2.1.1.9 Reynolds Number

It is defined as the ratio between inertia force to viscous force. It is used to identify that whether the flow is laminar or turbulent.

$$Re = \frac{Gd_h}{\mu} \tag{2.9}$$

2.1.1.10 Prandtl Number

It is defined as the ratio between thermal boundary layer to momentum boundary layer.

$$Pr = \frac{\mu \times c_p}{k_f} \tag{2.10}$$

2.1.2 Desirable characteristics of an efficient regenerator

- Heat transfer area should be maximum.
- Pressure drop should be minimum.
- Finer mesh size.
- Heat capacity should be maximum.
- Small dead volume.
- Conduction loss should be minimum.
- Large capacity ratio (Minimum temperature swing loss).

2.2 Basic concepts of pulse tube refrigerator

2.2.1 Classification of pulse tube refrigerator

2.2.1.1 Based upon type of compression mechanism

Stirling-type pulse tube refrigerator

The operating principle of Stirling-type pulse tube refrigerator is mainly based on Stirling cycle. It is also known as valve less pulse tube refrigerator (Fig. 2.2). The operating frequency of Stirling pulse tube refrigerator is higher than GM-type pulse tube refrigerator, so miniaturisation can be achieved. Due to miniaturisation and more sophisticated operation over Stirling cryocoolers, it is suitable for space and defence applications. Its refrigeration capacity is greater than GM-type pulse tube refrigerator. Special compressor known as pressure wave generator is used in Stirling pulse tube refrigerator to generate the pressure wave.

GM-Type pulse tube refrigerator

GM-type pulse tube refrigerators are also referred as valved pulse tube refrigerator due to the presence of a rotary valve in between compressor and regenerator. The working mechanism is

based upon GM-cycle. Its operating frequency is low (1 Hz to 3 Hz) and refrigeration capacity is less than Stirling-type pulse tube refrigerator. It is possible to achieve a temperature of less than 4 K using 2-stage GM-pulse tube refrigerator. It is bulky and heavier over Stirling type machines. It mostly uses normal compressor suitable for cooling of MRI and laboratory purpose applications.

VM-Type pulse tube refrigerator

VM- type pulse tube refrigerator developed by Matsubara *et al.* [11] is different than another type of pulse tube refrigerators (e.g. Stirling type and GM-type) in the sense that thermal compressor is used in place of a mechanical compressor. Due to the temperature difference, pressure wave will be generated in the thermal compressor. It consists of displacer, expander, work transfer tube, regenerator, pulse tube and heat exchanger immersed in liquid nitrogen as shown in Fig. 2.3. The primary phase shifter is expander placed at the hot end of pulse tube. Three regenerators are present inside the VM-type pulse tube refrigerator. Displacer, work transfer tube, and first regenerator work as a thermal compressor.

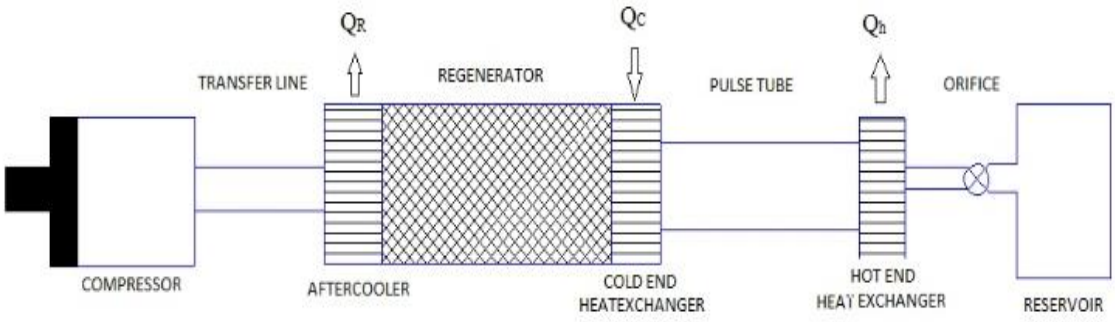

Figure 2.2: Stirling pulse tube refrigerator.

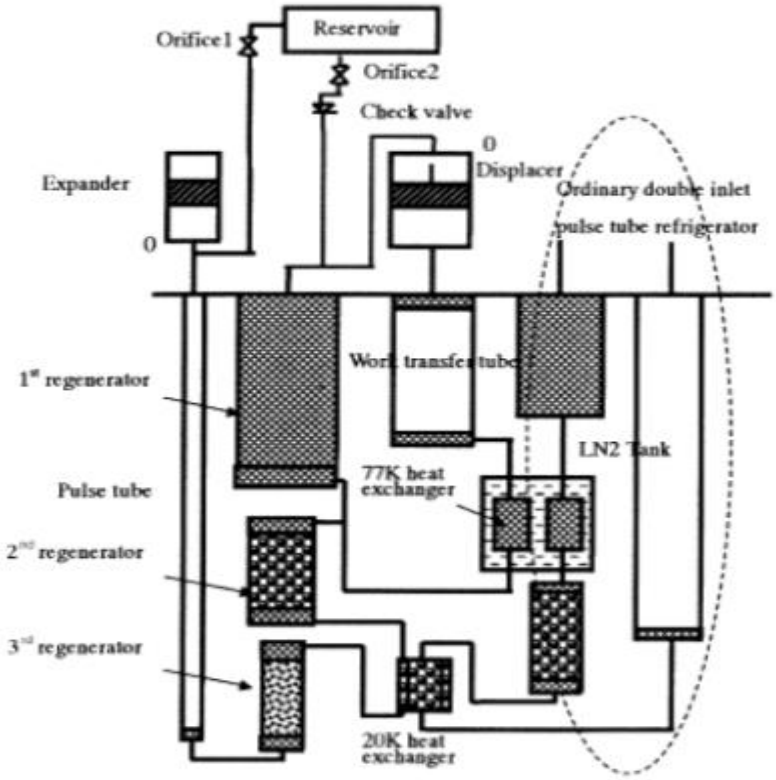

Figure 2.3: Schematic of VM Type pulse tube refrigerator [4].

2.2.1.2 Based upon configuration

Basic pulse tube refrigerator

The early generation of pulse tube refrigerator developed by Gifford and Longworth [1] in 1963 is termed as basic pulse tube refrigerator. It consists of a compressor, transfer line, aftercooler, regenerator, cold heat exchanger, pulse tube and hot heat exchanger (Fig. 2.4). In GM type pulse tube refrigerator, a rotary valve is present in between compressor and regenerator [12].

Orifice pulse tube refrigerator

Mikulin *et al.* [3] observed that performance of a basic pulse tube refrigerator could be further improved by changing the phase angle between volume flow rate and pressure at the cold end of the pulse tube refrigerator. He proved that by placing an orifice and reservoir before hot end heat exchanger and allowing some gases pass through it. By doing so, the orifice acted as

resisting device and observed a temperature of 105 K using air as working fluid (Fig. 2.5). This second generation of pulse tube refrigerator is termed as orifice pulse tube refrigerator. After one year Radebaugh *et al.* [4] placed the orifice after the hot heat exchanger and got a temperature of 60 K using helium as working fluid.

Double inlet pulse tube refrigerator

Zhu *et al.* [5] placed another orifice valve between the hot end of the regenerator and hot end of the hot heat exchanger; this valve is termed as a bypass valve (Fig. 2.6). Through bypass valve, some fluid passes through it and further decreases the phase angle between pressure and mass flow rate, so its performance is better than an orifice type pulse tube refrigerator. This configuration is known as bypass pulse tube refrigerator, or double inlet pulse tube refrigerator because of the presence of bypass valve.

Inertance pulse tube refrigerator

A most successful version of pulse tube refrigerator is inertance type pulse tube refrigerator [7], in this type of pulse tube refrigerator, an inertance tube is present in place of the orifice valve as in orifice pulse tube refrigerator (Fig 2.7). At high-frequency, inertance effect is generated inside the inertance tube which is long and narrow hollow tube. Inertance effect that is produced is equivalent to the inductance effect that is generated in the electric circuit. This inertance effect is capable of producing a negative phase shift between pressure and mass flow rate, so its performance is better than the earlier version of pulse tube refrigerator. High-frequency miniature inertance pulse tube refrigerators are capable of producing higher refrigeration power hence mostly used in space applications.

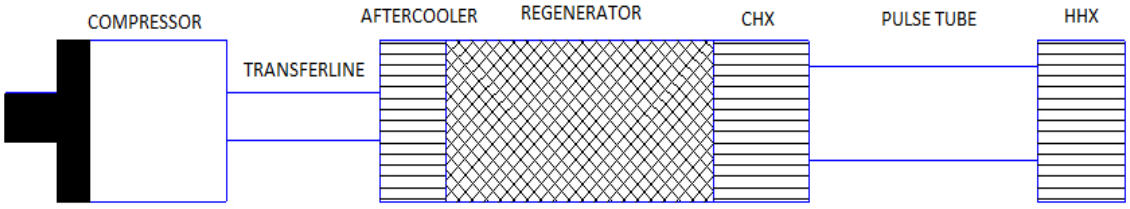

Figure 2.4: Basic pulse tube refrigerator.

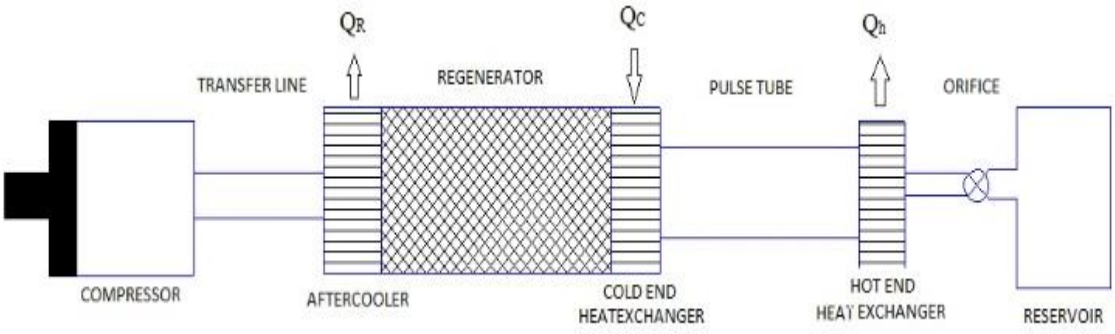

Figure 2.5: Orifice pulse tube refrigerator.

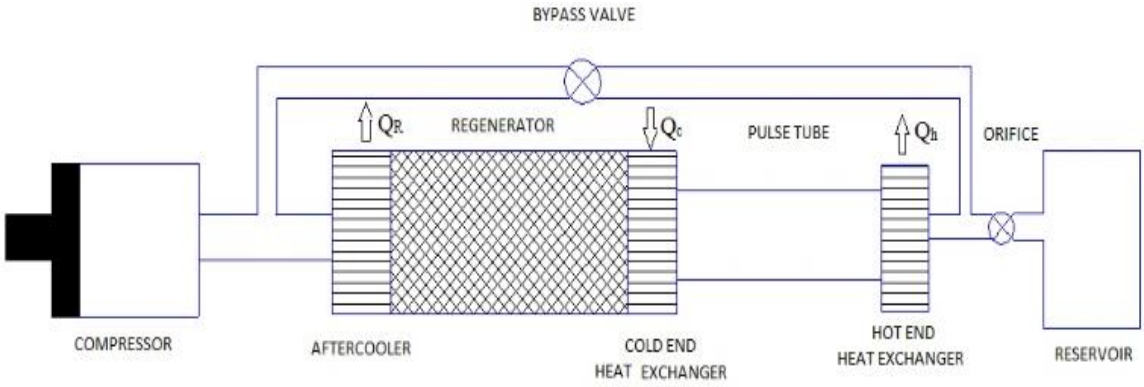

Figure 2.6: Double inlet pulse tube refrigerator.

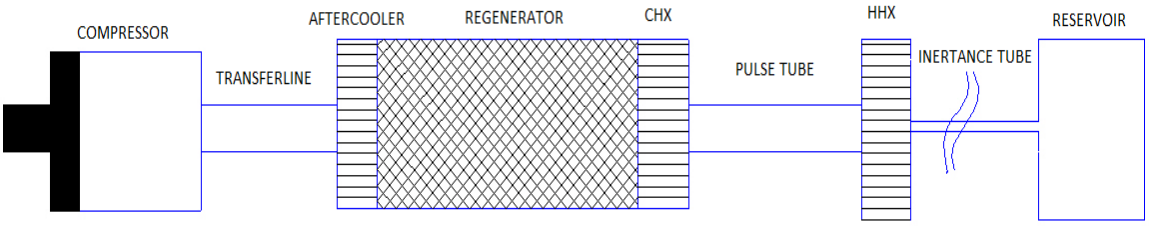

Figure 2.7: Inertance type pulse tube refrigerator.

Four valve pulse tube refrigerator

This is a particular type of pulse tube refrigerator in which reservoir is absent; the outlet from the hot end of pulse tube refrigerator is directly connected to the high-pressure and low-pressure ports of the compressor as shown in Fig. 2.8. Suitable valve timing mechanism has been provided to open and close the valves to improve its performance. DC flow loss is a major problem in this type of pulse tube refrigerator.

Five valve pulse tube refrigerator

Five valve pulse tube refrigerator is an improvement in four valve pulse tube refrigerator but a reservoir is placed at the hot end of pulse tube, and it is connected to the compressor by an orifice valve as shown in the Fig. 2.9. This additional mechanical arrangement not only reduces the DC flow loss but also improve the refrigerating capacity with the same size of a four valve pulse tube refrigerator [13].

Active buffer pulse tube refrigerator

Active buffer pulse tube refrigerator contains more than one reservoir or buffer in hot side pulse tube as shown in the Fig. 2.10. Due to this arrangement, its pressure inside the pulse tube is nearly equal to high pressure before the high-pressure valve is opened. After high-pressure valve closes gas in the pulse tube expands adiabatically near to low pressure, then the low-pressure valve will open as a result of which irreversibility losses inside the pulse tube will decrease and its performance improves. The principal components of a typical active buffer pulse tube refrigerator are compressor, regenerator, high-pressure valve, low-pressure valve, on-off valve and buffers [14].

Multiple inlet pulse tube refrigerator

Multiple inlet pulse tube refrigerator is a promising refrigerator in which a connecting tube and orifice valve is present between the middle of regenerator and intermediate of pulse tube as in Fig. 2.11. The orifice controls mass flow from or to the pulse tube by matching the resistance of the device, resulting in pressure drop in the regenerator. Due to similar temperature and pressure variation in the regenerator and pulse tube, its performance is slightly increased.

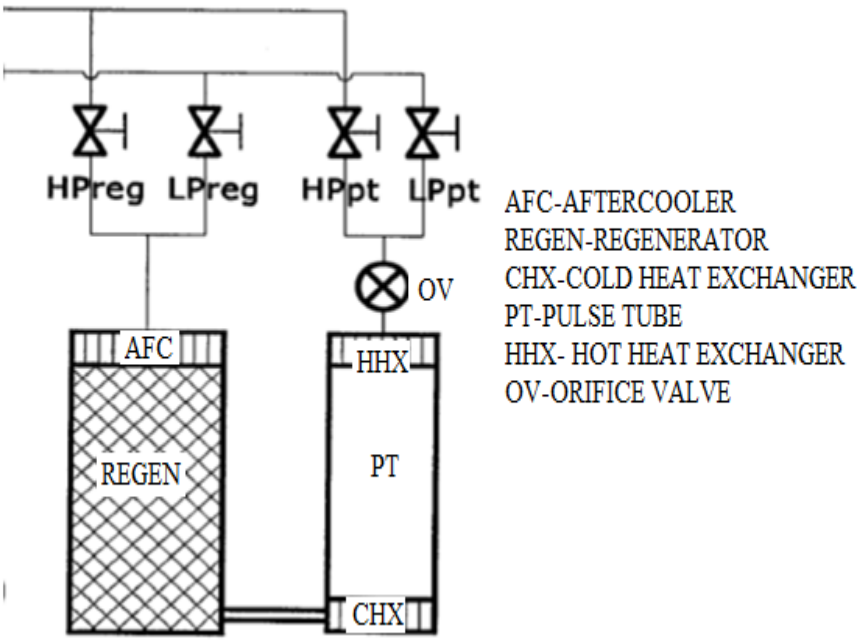

Figure 2.8: Four valve pulse tube refrigerator.

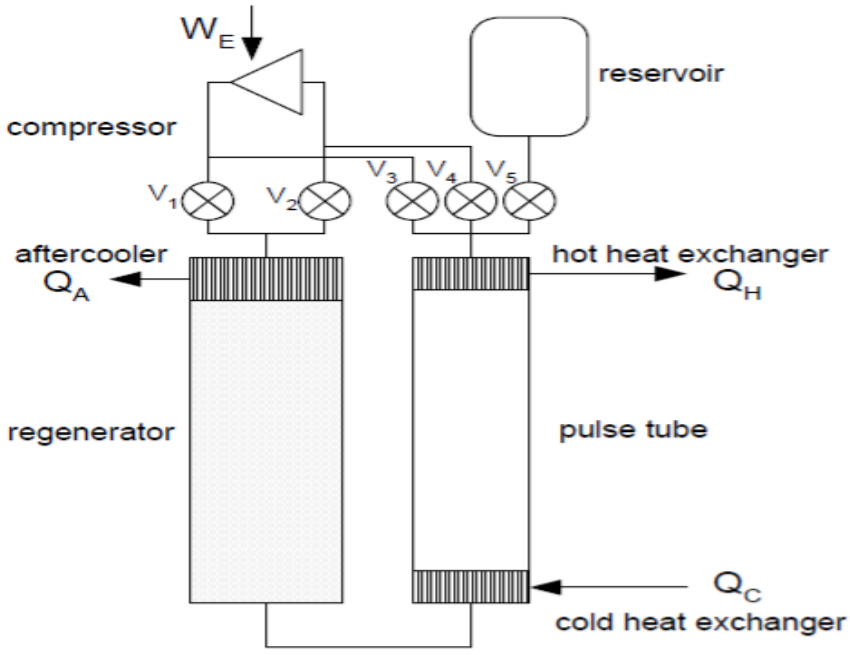

Figure 2.9: Five valve pulse tube refrigerator [13].

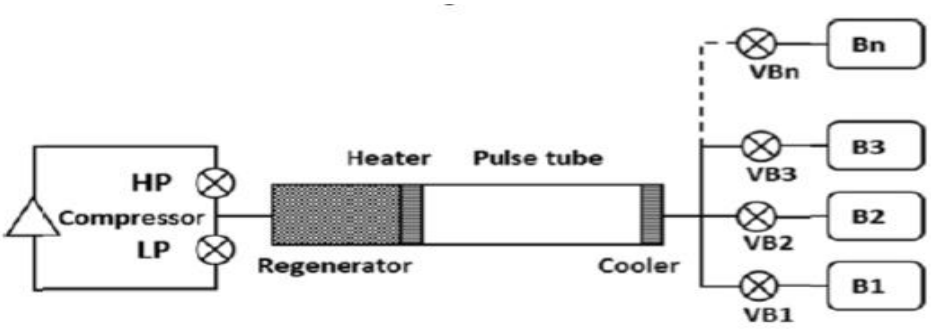

Figure 2.10: Active buffer pulse tube refrigerator [14].

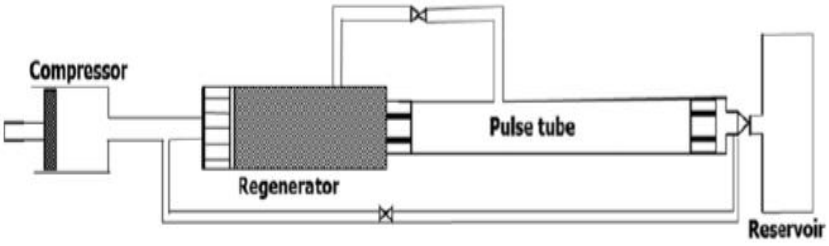

Figure 2.11: Multiple inlet pulse tube refrigerator.

DIPTR with Diaphragm configuration

DC flow loss is a significant loss in the double inlet pulse tube refrigerator that decreases its performance, to avoid this loss a diaphragm shape composed of two flanges with cone shaped hollow and circular tube made up of polyethene film is used (Fig. 2.12). The overall size of the diaphragm controls the gas flow that suppresses the DC flow loss and able to improve its cooling performance [15].

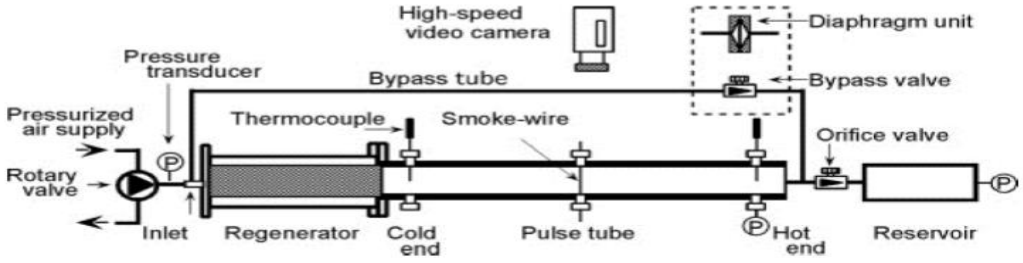

Figure 2.12: Double inlet pulse tube refrigerator with diaphragm configuration [15].

2.2.1.3 Based upon Geometry

Inline pulse tube refrigerator

In inline type pulse tube refrigerator, all components of pulse tube refrigerator starting from the compressor to the reservoir are placed in one straight line, so no loss due to U-bend (Figs 2.4-2.7). However, due to this configuration, the cold end heat exchanger is positioned in the middle becomes difficult and the best way is to put the hot heat exchanger outside the vacuum chamber [16].

U-bend pulse tube refrigerator

In U-bend pulse tube refrigerator, a U-shaped connecting tube is placed between the cold end of the regenerator and cold end of pulse tube, so it is easy to put it inside a vacuum chamber (Fig. 2.13). However, due to U-bending, its performance is lower than that of inline pulse tube refrigerator [16].

Coaxial pulse tube refrigerator

Coaxial pulse tube refrigerators are compact sized pulse tube refrigerators in which regenerator are ring-shaped surrounding the pulse tube (Fig. 2.14). As the pulse tube is placed inside the regenerator, its performance is deteriorated due to heat transfer between the regenerator and pulse tube wall. To overcome this difficulty a thin layer of insulation has been given between the regenerator and pulse tube wall [16].

Annular pulse tube refrigerator

Its technical constructions are nearly similar to that of coaxial pulse tube refrigerator except that, here regenerator is placed inside the pulse tube, rather pulse tube inside regenerator unlike a coaxial configuration. A thin layer of insulation is provided in the walls of pulse tube to improve its performance [16].

L-Shape pulse tube refrigerator

In L-shaped pulse tube refrigerator, pulse tube is English alphabet L-shape (Fig. 2.15) so that it can simplify the structure of pulse tube at cold end structure. However due to the large thickness of pulse tube at the cold end, it decreases the performance of the system.

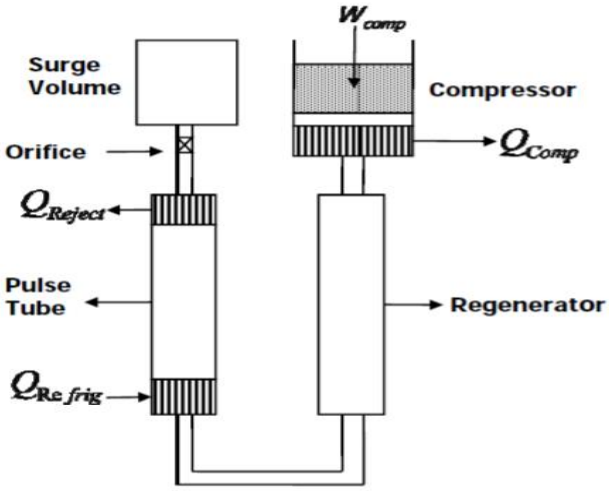

Figure 2.13: U-tube double inlet pulse tube refrigerator.

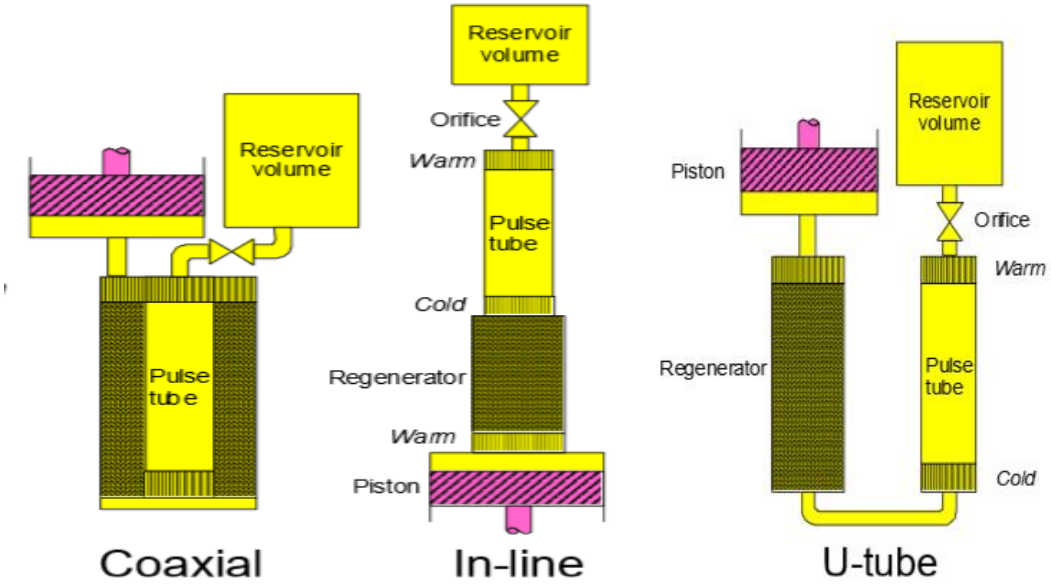

Figure 2.14: Coaxial, inline-tube pulse tube refrigerator [16].

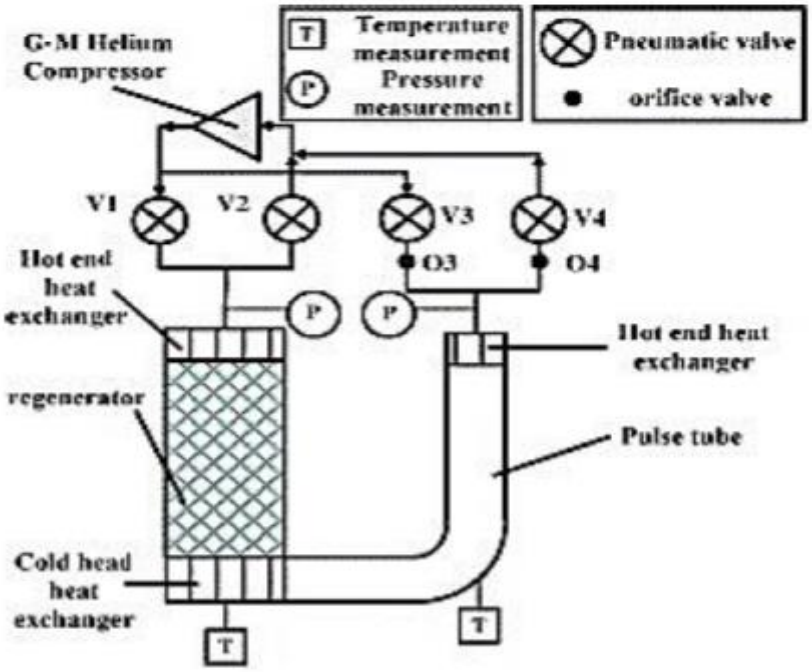

Figure 2.15: Pulse tube refrigerator with L-shaped pulse tube [10].

2.2.1.4 Based upon staging

It is impossible to achieve liquid helium temperature by using a single-stage pulse tube refrigerator. So it is necessary to improve the number of stages of pulse tube refrigerator. The advantage of this is, the gas in the second stage will be precooled by the first stage of pulse tube refrigerator. The cold end heat exchanger of fist stage is connected to cold end of first stage pulse tube and the hot end of second stage regenerator as shown in Fig. 2.16. As a result of this cooling temperature decreases and refrigeration capacity improves [17-19].

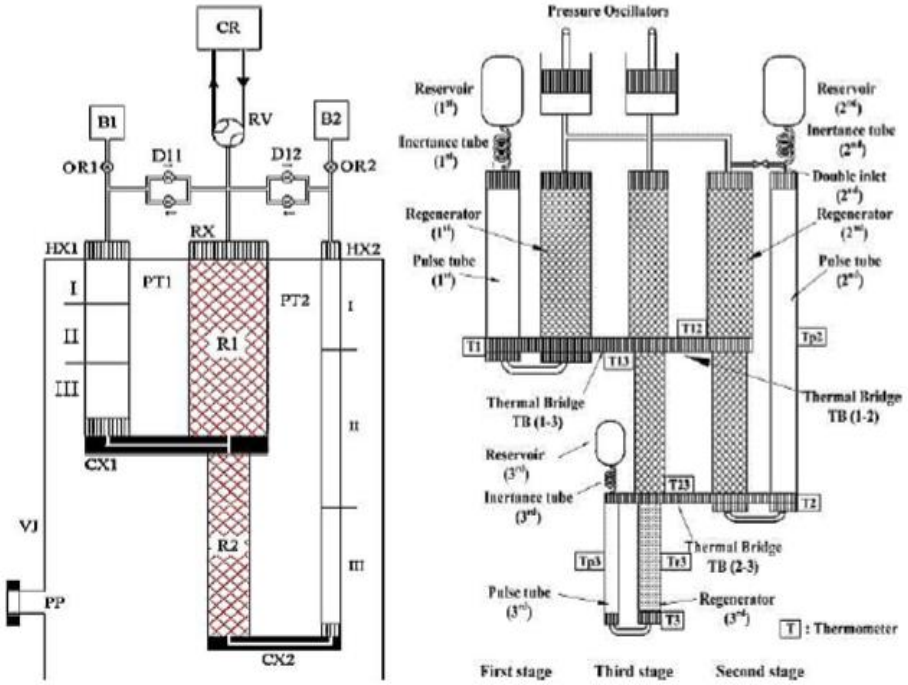

Figure 2.16: 2-Stage, 3-Stage pulse tube refrigerator [17-19].

The connection between one stage to another is carried out by thermal coupling and fluid coupling. In thermal coupling, the two stages concurrently exist, and a unique thermal bus connection is made between the cold heat exchanger of the first stage and the aftercooler of the second stage. The second stage has a pre-cooling regenerator between the compressor end and the aftercooler of the second stage. This regenerator produces heat that must be absorbed by the first stage. Hence, the first stage has a heat capacity larger than that the amount that must be absorbed from the precooling regenerator. This coupling scheme allows for the second stage warm temperature to be that of the first stage cold temperature. In fluid coupling, the flow of working fluid splits, for example, flow between the cold heat exchanger and corresponding pulse tube gets broken where a portion of the mass flow travels to the pulse tube, and the remaining mass flow visits another regenerator, which is the entrance to the second stage [16].

2.2.2 Components of pulse tube refrigerator

2.2.2.1 Compressor

Compressor or pressure wave generator is used to generate the pulsating pressure waves. In Stirling-type pulse tube refrigerator, particular types of the compressor are used, whereas in GM-type pulse tube refrigerator reciprocating compressors are used. Many investigators used different type of compressors and modified it to helium compressor to increase its performance.

2.2.2.2 Transfer line

A transfer line is simply a connecting tube that connects compressor and aftercooler.

2.2.2.3 Regenerator

Regenerator is the critical component of regenerative type cryocoolers. It consists of a hollow tube filled with porous matrix, wrapped meshes, parallel plates, parallel tubes or lead balls. When hot gas passes through it, heat will be transfer into it, and fluid gets cooled. After that flow reversal takes place and cold gas passes through it, and it absorbs heat flow from the matrix becomes heated. Hence, the flow here is alternating.

2.2.2.4 Heat exchangers

Three heat exchangers are presents in a typical single-stage pulse tube refrigerator; aftercooler is present after compressor to remove the heat of compression, so the performance of regenerator will improve. The second heat exchanger is present at the cold end of the regenerator and cold end of pulse tube, known as a cold heat exchanger; here refrigeration load is applied. The third one is present at the hot end of pulse tube to remove the heat after expansion and referred as a hot heat exchanger.

2.2.2.5 Pulse tube

This is a hollow thin stainless steel tube inside which pulsatile pressure wave is generated. Due to the presence of pulse tube, it is named as pulse tube refrigerator. Inside the pulse tube, the gas undergoes compression and expansion process. Near about more than 80% of gas never leaves the pulse tube and acts as a gas displacer.

2.2.2.6 Orifice Valve, Double inlet valve

These are valves present in pulse tube refrigerator to adjust the phase difference between pressure wave and mass flow rate to improve the performance of system.

2.2.2.7 Inertance tube

It is a long neck small diameter hollow tube inside which inertance effect is generated due to the gas flow. Inertance effect produced is equivalent to the inductance in electric circuits.

2.2.2.8 Reservoir

Reservoir or buffer is simply a storage cylinder present right side of inertance tube or orifice. The pressure in the buffer is nearly equal to the atmospheric pressure.

2.2.2.9 Rotary Valve, Solenoid valve

Rotary valves or solenoid valves are integral parts of GM-type pulse tube refrigerators present between the compressor and hot end of the regenerator (Fig. 2.17). Its design and construction are typically complicated tasks for the designers. Rotary valve will work as a phase shifter present on the hot side of the regenerator. Isenthalpic compression and isenthalpic expansion process occur here.

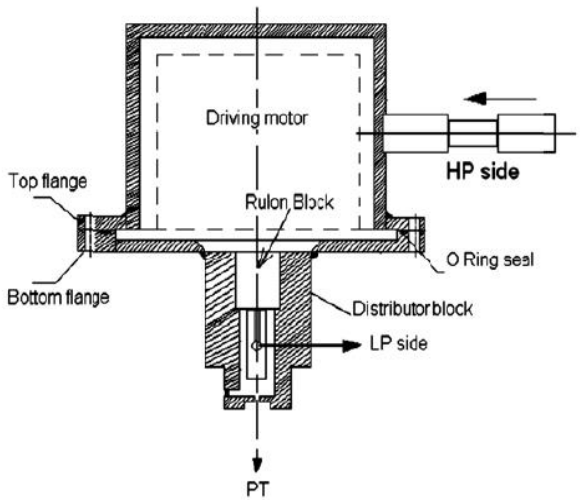

Figure 2.17: Rotary valve.

2.2.3 Basic theories of pulse tube refrigerator

After the development of basic pulse tube refrigerator several theories and mathematical models have been proposed by various scientists and researchers to explain its basic mechanism of cold production. Some of the relevant principles will be described in the following section.

2.2.3.1 Surface heat pumping theory

After the development of basic pulse tube refrigerator, Gifford and Longsworth [2] proposed surface heat pumping theory to explain its working principle. As mentioned above the working consists of four steps. Figure 2.18 shows the pulse tube connected to the compressor via regenerator in its cold end and attached to a hot heat exchanger in its hot end. In the first step, the gas parcel undergoes adiabatic compression (1-2 as shown in the Fig. 2.18), so its temperature is higher than wall temperature as a result of this heat transfer from gas parcel to the wall. In the next step after transfer of heat from gas parcel to wall, gas undergoes from step 2 to 3. Then gas parcels undergoes adiabatic expansion process (3-4 in the Fig 2.18), its temperature is lower than the temperature of the wall as a result of which heat transfer takes place from wall to gas parcels, and this process repeats.

2.2.3.2 Enthalpy flow theory

The cyclic average enthalpy flow in various components of pulse tube refrigerator is calculated by an integration of the governing equations. Time-averaged enthalpy flow in different components of pulse tube refrigerator are calculated. This helps to calculate losses in different components of pulse tube along with the net refrigeration power produced. By using enthalpy flow theory and phasor analysis Radebaugh *et al.* [4] compared the performance of various types of pulse tube refrigerator.

2.2.3.3 Thermoacoustic theory

Thermoacoustic devices are either of heat engines and prime mover type or refrigerator type. In prime movers heat flow is converted into workflow on the other hand in refrigerator type workflow is converted into heat flow. Thermoacoustic is a product of two words thermo means heat and acoustic means oscillating wave. All thermoacoustic devices consist of two media such as solid medium and fluid medium. Solid medium consists of walls of tubes, matrix or plates of regenerator whereas fluid medium are the working fluid which is oscillating in nature.

According to thermoacoustic theory when a large temperature gradient developed inside a tube which is closed at one end, the gas parcels starts oscillating. The reverse of this statement is also true that is a gas parcel starts oscillating inside a tube that is closed at one end, a temperature gradient develops at both ends. In pulse tube refrigerator, pressure wave generator is to generate the oscillating pressure wave when it passes through the pulse tube closed at one end there is a time average enthalpy flow across the tube and temperature gradient develops across both ends of pulse tube. The amount of work transferred from the pulse tube the same amount of heat transfer from cold end to hot end of the regenerator. This is the required thermoacoustic theory to explain cold production mechanism in pulse tube refrigerators and also in all thermoacoustic devices [20].

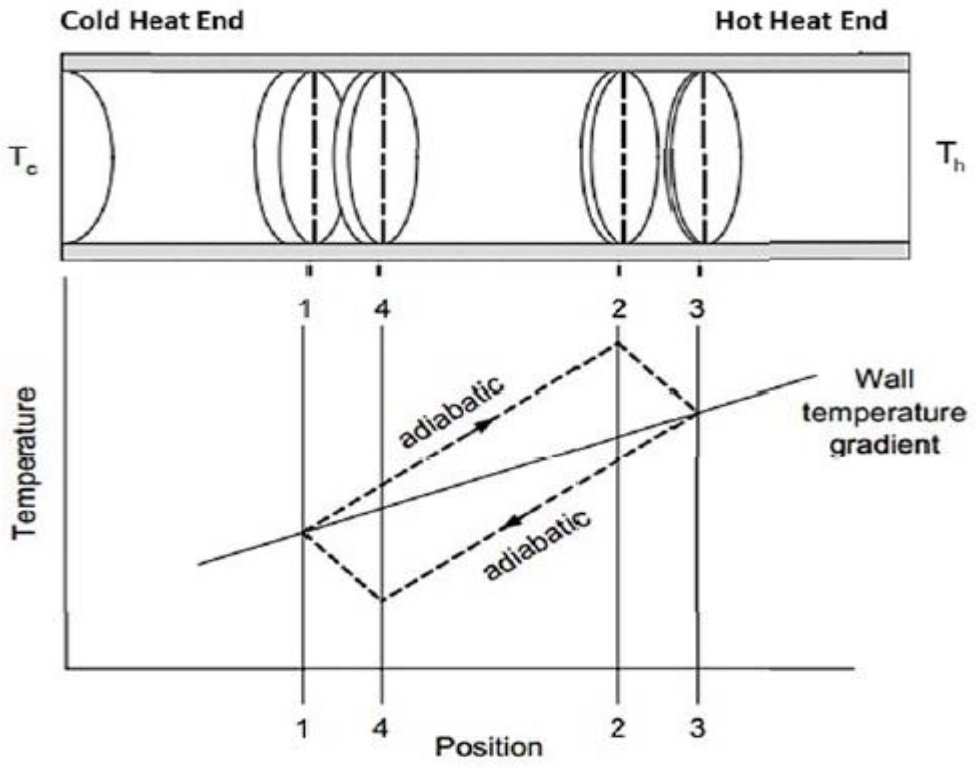

Figure 2.18: Surface heat pumping theory [2].

2.2.4 Pulse tube refrigerator loss mechanism

In pulse tube refrigerator acoustic power generated by the pressure wave generator is converted to the thermal energy which is responsible for the cooling effect. However, performances of real pulse tube machines are different from the ideal one due to the loss of exergy in each and every component due to the production of entropy. So to design a mathematical model to get reasonable accurate results, it is essential to account the effect of various loss mechanisms. The multiple losses occur in pulse tube refrigerator decreases the performance of pulse tube refrigerator, which include boundary phenomena, convection loss and boundary loss and turbulence loss [21].

2.2.4.1 Boundary loss

These losses occur within the boundary layer of the pulse tube and responsible for degradation of its performance. It includes

- Surface heat pumping or shuttle heat transfer
- Acoustic streaming (Rayleigh streaming)
- DC Streaming (Gedeon Streaming)

Surface heat pumping

Surface heat pumping phenomena as discussed above is responsible for the formation of refrigeration in basic pulse tube refrigerator. On the other hand, in other types of pulse tube refrigerator (e.g. OPTR, DIPTR, IPTR) surface heat pumping occurs in the reverse direction due to stepper temperature gradient. As a result of this, there is a net loss of acoustic power which degrades its performance (Fig. 2.19). This effect is termed as surface heat pumping loss.

Acoustic streaming

Rayleigh streaming or acoustic streaming is a loss mechanism that is responsible for degradation of refrigeration power of pulse tube refrigerator which occurs within the boundary layer of the pulse tube. Inside the boundary layer of the tube, due to viscosity effect, gas in the adjacent wall lags behind the velocity at the centre of the tube. The gas parcels inside the pulse tube undergo compression and expansion, so there is a change in temperature. As viscosity is a

function of temperature it induces a different level of shear stress within the tube that decreases its performance. This effect is termed as Rayleigh streaming (Fig. 2.20). This loss can be reduced by designing an appropriately tapered pulse tube as explained by Swift *et al.* [22].

DC streaming

DC streaming or Gedeon streaming is another loss phenomenon that occurs inside the pulse tube refrigerator for inviscid fluid. DC streaming is a function of phase difference between the acoustic velocity and pressure perturbation.

2.2.4.2 Convection Loss

The convection losses are classified as follows [21]:

- Jet driven streaming
- Turbulent mixing
- Free convection

Jet driven streaming

This loss occurs at the junction of two components due to sudden change in the area. When the fluid flows from the inertance tube to buffer, there is a sudden change in the area, also the high-velocity fluid is not diffused properly in pulse tube. As a result of this the acoustic power is not converted into thermal energy correctly and decreases performance. This loss can be reduced to some extent by using flow straightener.

Turbulent Mixing

The flow inside the compliance tube is laminar in nature, however if the design of pulse tube is wrong, so turbulence will be induced inside the pulse tube. This will cause parasitic energy transport and the concept of gas piston no longer holds good.

Free convection

This loss takes place due to the orientation of buffer tube, if the gravity vector is not aligned correctly with pulse tube axis (Fig 2.21). The analytical modeling of this has been considered by Swift *et al.* [23] by comparing this loss analogous to an inverted pendulum.

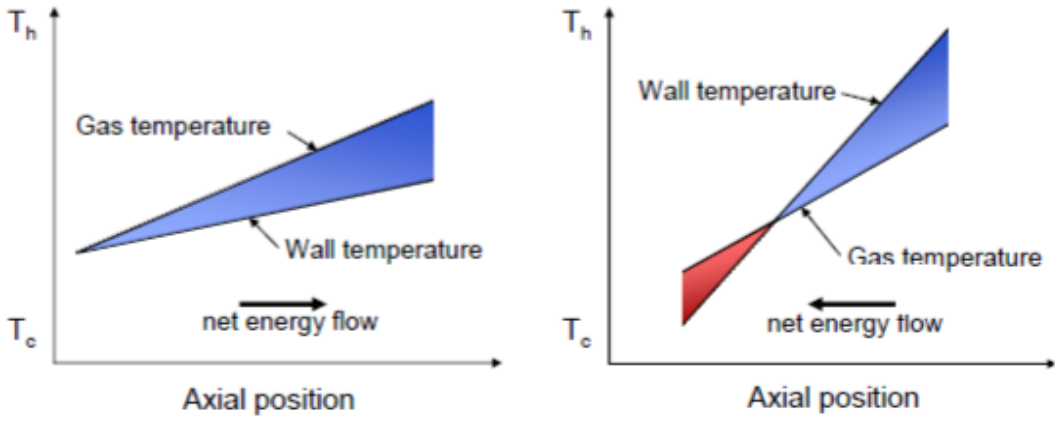

Figure 2.19: Surface heat pumping loss mechanism [21].

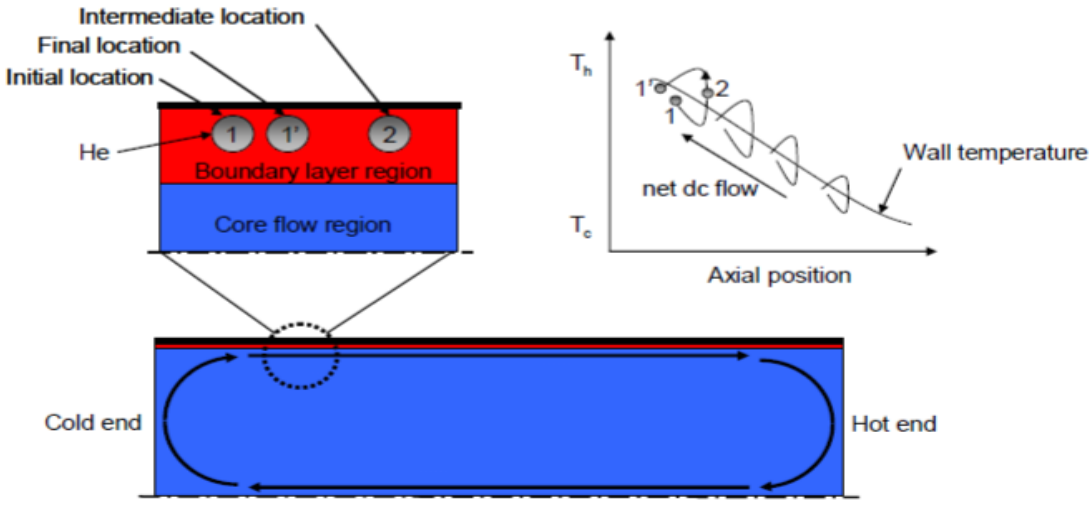

Figure 2.20: Rayleigh convection loss [21].

2.2.4.3 DC flow loss

The performance of an orifice pulse tube refrigerator increases by connecting a double inlet valve between the hot end of pulse tube and hot end of the regenerator. As a result of this, phase difference between pressure wave and mass flow rate decreases further, thereby cooling capacity also increases. On the other hand, some gasses passing through the bypass valve enters into the pulse tube hot end and passes through the regenerator, which will create a circulating gas flow in a closed loop and decreases the performance of pulse tube refrigerator. The DC flow is negative if the gas flows from hot end of the regenerator to hot end of pulse tube through the double inlet valve and positive if gas flows from hot end of pulse tube to hot end of regenerator via the double inlet valve. This loss can be reduced by providing multi-bypass method [24].

2.2.4.4 Hot end Loss

This loss is due to the presence of hot end heat exchanger at the hot end of the pulse tube. As the gas flows alternatively (periodically) it again passes through the hot heat exchanger. As a result of this hot heat exchanger acts not only as a recuperative heat exchanger but also as a regenerative heat exchanger; this regenerative effect serves as the loss in pulse tube refrigerator and termed as hot end loss of pulse tube refrigerator. This has been described by enthalpy flow model. As there is no hot heat exchanger in four valve pulse tube refrigerator its performance is slightly better [25].

2.2.4.5 Double inlet work loss

This loss is also associated with the double inlet valve. The mass flow through the bypass valve have two components: first, in phase with pressure wave (called as standing wave) and other, is out of phase with the pressure wave (called as a progressive wave). The component of mass flow rate in phase with the pressure wave is responsible for work loss, on the other hand part of mass flow rate out of phase with pressure wave is capable of adjusting the phase angle to improve refrigeration power [26].

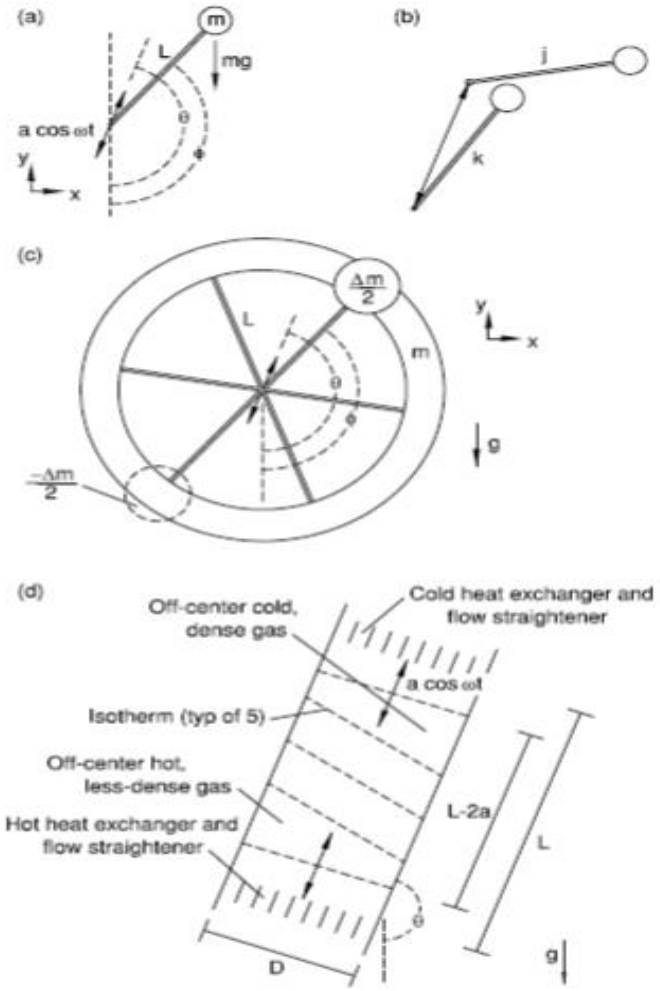

Figure 2.21: Free convection loss mechanism [23].

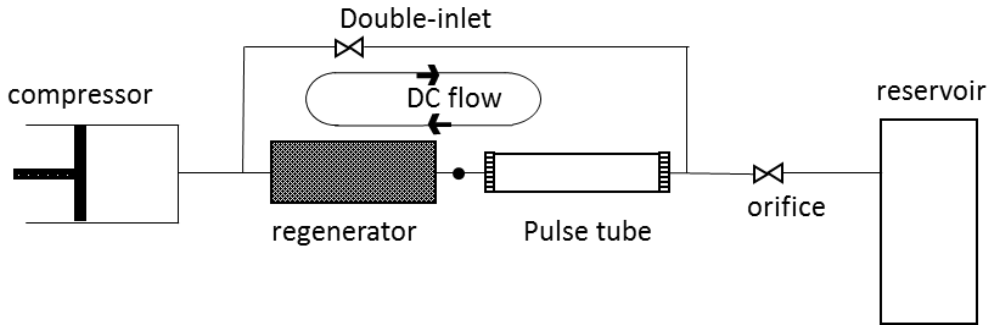

Figure 2.22: DC flow loss [24].

2.2.5 Modeling of pulse tube refrigerator

Mathematical modelling of a pulse tube refrigerator helps the users and designers to understand the physical processes occurring inside the pulse tube refrigerator. A properly tested mathematical model not only helps the designer to predict the performance of pulse tube refrigerator but also to design a pulse tube refrigerator. A mathematical model is a mathematical representation of the complex physical phenomena occurring inside the pulse tube refrigerator. A set of governing differential equations are used to represent the complete physical processes (heat transfer and fluid flow) that occur inside the pulse tube refrigerator. Since the entire physical processes inside the pulse tube refrigerators are complex due to oscillating nature of working gas, transient nature of flow in pulse tube, regenerator and valves, there are different types of mathematical models available for pulse tube refrigerator. These models are categorised into three main different types such as:

- First order model
- Seconder order model
- Third order model

2.2.5.1 First order models

First order analysis is the simplest mathematical model that does not consider the effect of any losses inside pulse tube refrigerator. Fist order model takes a very small computational time to predict the performance of pulse tube refrigerator, which is considered as the biggest advantage of this model over other models (second order models and third order models). However, the accuracy of first order model is far away from the experimental results. Assumptions taken for analysis in first order model are: ideal working gas, perfect regenerator and heat exchangers, no pressure drop in the regenerator, isothermal compression and expansion process etc. Enthalpy flow model is a first order model developed by Radebaugh *et al.* [4].

2.2.5.2 Second order models

Second order analysis considers the effect of losses in the regenerator, heat exchangers, pulse tube, etc. Complete sets of differential equations are used to represent the physical processes

inside the pulse tube refrigerator. Its complexity is more as compared to the first-order model whereas its accuracy is better than first order models. Various second order models are

- Isothermal model
- Adiabatic model
- Phasor analysis

2.2.5.3 Third order models

Third order model gives an accurate prediction of performance of pulse tube refrigerator, but it needs high-speed computers and long computational time. Third order models are:

- Numerical model
- CFD Model

2.3 Review of mathematical models of regenerator

Mathematical modelling of regenerator covers the detailed mathematical representation of physical phenomena of the regenerator considering variation of matrix and fluid temperature as a function of spatial and temporal coordinates. The complex heat transfer, fluid flow phenomena inside the regenerator is governed by a set of differential equations for which there are no closed form solutions. Many researchers performed the mathematical modelling by reducing the equations by making some assumptions. Nusselt [10] did the mathematical analysis of regenerator assuming infinite matrix heat capacity. Hausen[10] published an article making a fundamental comparison of heat transfer processes of regenerator with recuperator. Later several reports had been produced assuming the behaviours of regenerator is ideal. IIiffe [10] improved the Nusselt model by considering 1-D longitudinal heat flow, no thermal conduction and infinite azimuthal and radial thermal conductions in a matrix. By using above assumptions, he solved the equations by "reduced length reduced period" (RLRP) method [10]. Anzelius and Nusselt [10] developed the first closed form solution of governing equations of regenerator by using RLRP method as developed by Hausen. The effect of longitudinal heat conductions on the performance of regenerator has been studied by Bahnke and Howard [10] by using heat conduction equation of matrix. They have introduced a term known as

dimensionless heat conduction parameters that take the effect of conduction into accounts. Kays and London [27] did a number of experimental analysis to understand the effect of various parameters on regenerator performance. His study covers the effect of NTU, variable specific heat capacity of the matrix, longitudinal conduction on regenerator. Rios and Smith studied the effect of variable specific heat mathematically by using specific heats variation with temperature by using Debye equation. Wilmott *et al*. [28-38] performed the numerical analysis of regenerator to understand the effect of various parameters on performance of regenerator. Sarangi *et al.* [39-42] solved the mathematical model developed by Wilmott and studied the effect of variable specific heat, variable mass flow rate and longitudinal heat conduction numerically. Radebaugh *et al*. [43-46] developed a simplified mathematical model for the design of regenerator for cryogenics applications. Daney and Radebaugh [45] studied the effect of a mixture of fluid on the rate of cold production. Daney and Radebaugh examined the effect of void volume of regenerator. Gary *et al.* developed a software package for the design of regenerator REGEN. An improved version of REGEN developed by NIST group named as REGEN 3.2 and 3.3 for the design and simulation of the regenerator. Many researchers [19, 47-50] used REGEN to investigate the effect of various operating and geometrical parameters on regenerator performance.

2.4 Review of mathematical model of pulse tube refrigerator

2.4.1 Basic pulse tube refrigerator

The credit of development of pulse tube refrigerator technology goes to Gifford and Longsworth [1]. At Syracuse University, Gifford and Longsworth planned to improve the performance of GM-type cryocoolers. They reported that the cold end of the tube becomes cold which by further improvement they produced the first pulse tube refrigerator in 1963. This initial generation of pulse tube refrigerator is term as basic pulse tube refrigerator (BPTR). The cold production mechanism is based on surface heat pumping [2].

2.4.2 Orifice pulse tube refrigerator

Mikulin *et al.* [3] proposed that the performance of a pulse tube refrigerator can be improved by changing the phase angle between pressure and volume flow rate at the hot end of pulse tube

refrigerator. They have added an orifice valve and a reservoir after hot end heat exchanger and able to achieve 105 K by using air as working fluid. Radebaugh *et al.* [4] able to reach 60 K by changing the position of the orifice valve. This configuration is termed as orifice pulse tube refrigerator (OPTR). Radebaugh and Stroch [51] proposed phasor analysis to explain the working principle of OPTR. The phasor is a vectorial representation of pressure wave, mass flow rate and temperature. They observed that the refrigeration power is proportional to frequency, average pressure, square of the dynamic pressure ratio and mass flow rate.

The isothermal model proposed by Zhu *et al.* [52] is an improvement of phasor analysis to compute the performance of OPTR. In this model, the pulse tube is divided into three parts: left and right portions are isothermal whereas middle portion is adiabatic. The isothermal analysis is simpler, robust and consumes less computational time. Neglecting the effect of pressure drop in regenerator, Wu *et al.* [53] presented the numerical analysis of an orifice pulse tube refrigerator. Nodal analysis of regenerator and the effect of residual gas velocity on pulse tube refrigerator was considered by Lee *et al.* [54]. The importance of regenerator on the performance of pulse tube refrigerator has been reviewed by de Bore *et al.* [55]. He presented the effect of expansion ratio and compression ratio on refrigeration capacity and COP. Richardson *et al.* [56] proposed that transient behaviour of radial heat transfer is a significant effect on cold production. He observed that for a particular value of pulse rate the rate of cold production could be optimum. Regenerator and pulse tube are the two principal source of loss of refrigeration power due to entropy generation and irreversibility. Razani *et al.* [57] proposed a number of mathematical models based on exergy analysis to understand the effect of irreversibility and its impact on performance of pulse tube refrigerator.

Zhang *et al.* [58] reported that, if the ratio of reservoir volume to pulse tube volume is less than five, the entropy generation increases which reduce the cooling power of OPTR. The effect of time averaged entropy flow and hydrodynamic workflow upon the performance of OPTR have been investigated by Rawlins *et al.* [59] . The detailed mathematical modelling of OPTR is also found in some open literature [60-68]. CFD analysis on pulse tube refrigerators has been performed by using commercially available CFD packages to understood the fluid flow, heat transfer processes [69].

2.4.3 Double inlet pulse tube refrigerator

One significant improvement in the geometry of orifice pulse tube refrigerator achieved by addition of another orifice valve between hot end of the regenerator and hot end of pulse tube. By the addition of another orifice, the mass flow rate through the orifice or double inlet valve leads to pressure wave at the cold end of regenerator. This will create a negative phase shift between mass flow rate and pressure, thus cooling capacity increases and refrigeration temperature decreases [5]. The mass flow rate through the double inlet valve have two components: one is along the pressure wave and other leads pressure wave by 90 degrees. The sine component of mass flow rate is responsible for adjusting the phase shift to improve the cooling capacity and cosine component causes double inlet work loss. Another important loss in DIPTR is DC flow loss. In DIPTR, a certain quantity of mass flow occurs through the bypass valve, thus refrigeration power per unit mass flow rate decreases [70].

The performance of a double inlet pulse tube refrigerator can be further increased in putting a tapered regenerator as suggested by Ying-wen *et al.* [71]. They have used enthalpy flow model, and results have been validated by using experimental data. Convergent type regenerator geometry with a particular taper angle increases the performance but if the angle exceeds from optimum value, its performance however decreases. If a regenerator is either of convergent type or convergent-divergent type, its performance decreases. Ju *et al.* [70] studied the heat transfer and fluid mechanics process inside the pulse tube refrigerator by solving the complex sets of coupled nonlinear equations. Wang *et al.* [72] studied the effect of amplitude and phase of dependent quantities on the performance of pulse tube refrigerator. They suggested that the cooling power in a DIPTR will be more than that of conventional OPTR consuming less acoustic power. Mirels *et al.* [73] developed an analytical model to study the performance of a double inlet pulse tube refrigerator by using a stepped piston compressor.

Zhu *et al.* [26] presented an analytical expression to compute the double inlet work loss in a double inlet pulse tube refrigerator. They proposed that the double inlet work loss can be decreased by increasing void volume ratio of regenerator over buffer, increase in temperature ratio of ambient temperature over refrigeration temperature and increase in double inlet factor. Nika *et al.* [74, 75] suggested two methods to simulate a miniature DIPTR: first, the thermodynamic analysis and second, the electrical analogy method. In the thermodynamic

analysis, they have derived a complex set of governing equations by using fundamental principles of thermodynamics, fluid mechanics and heat transfer. Solutions of these equations have been carried out by using numerical methods to investigate the performance of DIPTR. They found that the performance of pulse tube refrigerator decreases due to axial conduction along the pulse tube wall. In their second part, they have studied the effect of pressure drop in the regenerator, temperature discontinuities due to internal flows. They have validated their both models by using experimental results.

Xiao *et al.* [76] studied the performance of double inlet pulse tube refrigerator by using thermoacoustic theory. By using the thermoacoustic theory, Hoffman [77] developed FZKPTR software package for design and simulation of pulse tube refrigerators to obtain desired refrigerating capacity based on given refrigeration temperature. Exergy method has been used by them to study the performance of pulse tube refrigerator. They found that most exergy loss occurs at the regenerator and orifice valve [78]. De Bore [79] developed a linearized 1-D model to study the performance of pulse tube refrigerator where the effect of void volume upon the performance was considered. The results show that, there is a substantial improvement in the performance of DIPTR as compared to OPTR. They derived the cooling power as a function of regenerator void volume and frequency. Chokhawala *et al.* [80] developed a phasor analysis to compare the performance of double inlet pulse tube refrigerator with orifice pulse tube refrigerator. The effect of geometrical parameters (e.g. length and diameter) and operating parameters (e.g. operating frequency, pressure difference between various components, coefficient of discharge of orifice valve and double inlet valve) of pulse tube refrigerator on cold production was considered.

Banjare *et al.* [81, 82] studied the performance of a DIPTR of GM-type geometry by using commercial software FLUENT. To explore the multi-dimensional effects, they performed CFD modelling of a 3D geometry. They reported that the performance of DIPTR is optimum when the double inlet valve is 30% opened and orifice valve is 60% opened [82]. Ju *et al.* [83] developed an excellent numerical model by using continuity equation, N.S. equation and energy equation. In this model, they have considered two energy equations for regenerator, one for fluid and the other for regenerator matrix. Also the effects of viscous loss, inertial loss and pressure loss was considered by them. Dash *et al.* [84] developed an improved numerical model

by combining phasor analysis with exergy analysis and reported that, below a particular frequency value the performance of a DIPTR decreases. When DIPTR operates below critical frequency, there is no cold production and its performance is a function of average system pressure only. Wang *et al.* [85] investigated the accuracy of local energy loss correlations in sudden expansion or contraction of joints under oscillating flow conditions of pulse tube cryocoolers using a 1-D model and also FLUENT software. The results were compared to 2-D model and reported that steady friction factors do not possess sufficiently accurate predictions of losses under oscillating flow conditions. In addition to the numerical analysis, much experimental analysis have been investigated by a number of researchers to understood the basic losses and its effects on cold production [86-91].

2.4.4 Inertance pulse tube refrigerator

The new generation of pulse tube cryocooler technology is an inertance type pulse tube refrigerator. The term inertance is equivalent to inductance in electrical circuits. Inertance effect is an acoustic effect generated in pulse tube refrigerator due to the inertia of moving gas. The inertance effect is more significant in higher operating frequency [7]. De Boer *et al.* [92] stated that the rate of refrigeration produced in inertance pulse tube depends on some particular relevant parameters. In the simplified case of an infinite volume of the reservoir and zero dead volume of the regenerator, these parameters are the dimensions of the inertance tube, the volume of the pulse tube, the conductance of the regenerator, charging pressure and operating frequency. A simple turbulent flow model was introduced to calculate the effective conductance of the inertance tube and reported that the performance of the ITPTR is higher to that of the OPTR over a limited range of frequencies. The improvement is explained regarding the pressure amplitude in the pulse tube, the flow rate between the regenerator and the pulse tube and the phase angle between these parameters. This analysis was extended to the case of finite reservoir and regenerator volumes [92].

To design inertance tube, various models have been proposed by various eminent persons. Radebaugh *et al.* [93] developed a transmission line model to design inertance tube. Roach *et al.* [94] developed lumped parameter model. Distributed component model proposed by Schunk *et al.* [95] predicts better performance as compared to above two models, since in this model, the inertance tube is divided into a number of divisions. In this model, the resistance,

capacitance and inductance has been determined in each division. INERTANCE software developed by Radebaugh *et al.* is based on transmission line model. This software along with ISOHX and REGEN is used by various research centres to design the miniature pulse tube cryocoolers for academic and industrial applications. Zhu *et al.* [96] developed a control volume method based on conservation of mass, momentum and energy to design and simulate inertance pulse tube refrigerator. In this model, an implicit method is used for time derivatives and first/second order upwind method is used for convection term to improve the speed of calculation. To improve the speed of calculation, they combined the continuity and the momentum equation to a single algebraic equation by using the ideal gas equation.

Cha *et al.* [97] used commercial CFD package FLUENT to study the multidimensional effects in pulse tube refrigerator. Luo *et al.* [98] considered the effect of turbulent flow and heat transfer inside the inertance tube. They have used acoustic turbulent flow model to solve the governing equations. Their numerical results gave very good agreement with experimental results. They also used CFD model and suggested that results of CFD model are more accurate than their model but computational time is more in CFD as it takes 2D effects. Dei *et al.* [99] proposed an inertance pulse tube refrigerator without reservoir which is driven by the thermoacoustic prime mover. After conducting an experimental investigation, they found that its performance is better than orifice pulse tube refrigerator with the reservoir. As the reservoir is absent is this type pulse tube refrigerator it is more reliable and compact as compared to conventional IPTR [99]. A lot of experimental studies have been performed on inertance pulse tube refrigerator [100-103]. Ashwin *et al.* [104] studied the performance of IPTR by using commercial code FLUENT by applying the thermal non-equilibrium model. In thermal non-equilibrium model FLUENT solves two energy equations, one for fluid and the other for matrix of porous media, yielding more accurate results. A parametric study of pulse tube refrigerators of various types of pulse tube refrigerators (e.g. IPTR, OPTR, DIPTR) was carried out by his team.

Pulse tube cryocoolers are of different kinds based on the formation of pressure waves. A detailed analysis of the design of a compressor/pressure wave generator is a challenging problem to the engineers and researchers in the field of cryogenics. The design and fabrication of pressure wave generators are available in open literature [105-108]. On the other hand, GM-

type pulse tube refrigerators use a GM- compressor. Its operating frequency is only few Hz (1-5 Hz). A rotary valve (sometimes solenoid valve) is present between compressor and PTR system. As its operating frequency is low, normal household compressor may be used for this purpose [109]. Some numerical and experimental analysis on the coaxial type pulse tube refrigerator is found in the open literature [103, 110-114].

2.4.5 Other multistage pulse tube refrigerator

Two, three and four stage pulse tube refrigerators are developed to achieve liquid helium temperature. This low refrigeration temperature is very much helpful for cooling of superconducting magnets. Tanka *et al.* [115] first developed a 2-stage pulse tube refrigerator and changed regenerator's dimensions to visualise the lowest refrigeration temperature. They found a no-load temperature of 20 K. Matsubara *et al.* [116, 117] developed a three stage GM-type pulse tube refrigerator operating at 2 Hz, 15 bar pressure and was able to achieve a refrigeration temperature of 3.6 K at 3rd stage cold end heat exchanger. Several experimental results published by them are available in the open literature. Different losses that affect the refrigeration power of a pulse tube refrigerator is explained by Gawali *et al.* [118]. Wang *et al.* [119] performed experimental studies on a two-stage pulse tube refrigerator. Wang *et al.* [120, 121] performed a numerical and experimental investigation and achieved a no-load temperature of the 2.23 K at the cold end. Wang *et al.* [122, 123] developed a numerical model taking the actual properties of gas, magnetic properties of material into account. Their results is very much close to the experimental value [122, 123] . The mathematical model presented by Ju *et al.* [124] uses mixed Eulerian-Langarian method.

Some existing software developed by various scientists and research institutes to design PTRS are presented in Table 2.1:

Table 2.1 : Commercially available software packages for simulation.

Year	Software Developed	Author	Institute/Organization	Reference
2014	StirlinGUIDE	Atrey *et al.*	IITBombay, INDIA	[125]
2013	Sharif PTR	Jahanbakhshi *et al.*	Sharif University of Technology, Iran	[126]
2010	SAGE	Gedeon D.	Gedeon Associates, Athens, OH, USA	[127]
2006	DELTAEC	Ward, Clark, Swift	Los Alamos National Lab, Los Alamos, USA	[128]
2005	FZKPTR	Hofmann	Forschungszentrum Karlsruhe, Institute fur Technische Physik, D-76021 Karlsruhe,	[77]
2002	MS∗2	Mitchell and Bauwens	Berkely, California, USA University of Calgary, Calgary, Alberta, Canada	[129]
1996	ARCOPTR	Roach and Kashani	NASA Ames Research Centre, Atlas Scientific, CI, USA	[65]
-	REGEN3.3,ISOHX,INERTANCE	Radebaugh *et al.*	NIST, Boulder, Colorodo, USA	-

2.5 Regenerative cryocooler research in India

In India mainly four centres are working for the development of regenerative cryocoolers. Apart from NIT Rourkela, namely IIT Bombay, IISc Bangalore, NIT Surat and recently NIT Calicut also started working in cryocoolers. Also ISRO is doing research on Stirling and pulse tube cryocoolers for space-based applications. The cyclic simulation of Stirling cryocooler has been performed by Atrey *et al.* [130]. A lot of experimental models and test prototypes of Stirling cryocoolers and pulse tube cryocoolers of Stirling type geometries are developed by their team. IIT Bombay is considered to be the pioneer of cryocoolers in India. Atrey *et al.* [131] developed a second order isothermal model for pulse tube refrigerator considering the effect of various losses encountered in the regenerator, pulse tube and heat exchangers. IIT Bombay and SVNIT

Surat are working collaboratively to develop mathematical modelling and prototype testing of GM type pulse tube refrigerators. StirlinGUIDE developed by Atrey *et al.* [125] is a simplified mathematical tool for the design and education of Stirling type machines (Stirling cryocoolers and Pulse Tube cryocoolers). In IIS Bangalore, Prof. Kasthurirengan *et al.* [17, 18] developed a two-stage GM cryocooler and achieved a cold end temperature of 2.5 K, which is the lowest temperature achieved by anyone in India. Indigenous pressure wave generators are also developed by Prof. Jacob *et al.* [132] for Stirling-type pulse tube cryocoolers and Stirling cryocoolers. Isothermal model of pulse tube refrigerator (proposed by Zhu *et al.* for the single-stage pulse tube refrigerator) has been developed for two stage pulse tube refrigerator by Kasthurirengan *et al.* [17]. Indigenous pressure wave generators are developed by Prof. Jacob *et al.* [132] at IISc Bangalore in collaboration with ISRO for space based application purposes. DRDO is also developing Stirling cryocoolers for cooling of IR Sensors. IUAC and BARC also evolve GM-cryocoolers for their indigenous applications.

Chapter 3

Mathematical Analysis and Design of Software for Regenerator

3.1 Mathematical modeling

In the present chapter, the detailed mathematical modelling of regenerator is presented. The mathematical model is classified under three sections. The first section describes an ideal regenerator, the second section considers regenerator including the effect of longitudinal conduction and the third describes the effect of both longitudinal as well as wall conduction [10]. In this chapter, a first order model is assumed, where the mass flow rate through the regenerator is constant during hot and cold periods and does not change with time. The fluid temperature during both heating and cooling period is constant and equal to T_h during the heating period, and equal to T_c during the cooling period. The void volume within the regenerator is assumed to be zero.

3.1.1 Ideal model

Energy equation for the matrix of regenerator is

$$(\rho c_p \delta V)_m \frac{\partial T_m}{\partial t} = h\delta A_s (T - T_m) \tag{3.1}$$

Energy equation for the fluid is

$$(\rho c_p \delta V)_f w_z \frac{\partial T}{\partial z} = h\delta A_s (T_m - T) \tag{3.2}$$

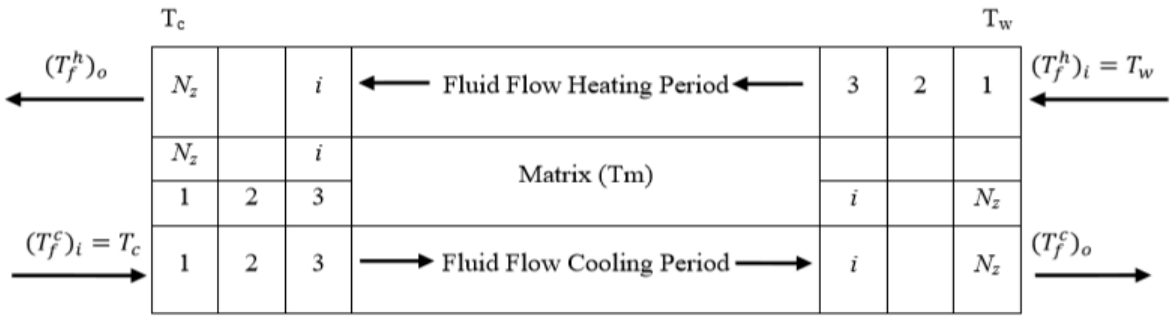

Figure 3.1: Temporal and spatial node distribution [10].

where, i is number of spatial nodes and j is number of time step (in Fig. 3.1) given as follows:

$$i = 1, 2, 3, \ldots\ldots\ldots\ldots N_z$$

$$j = 1, 2, 3, \ldots\ldots\ldots\ldots N_t$$

where, N_z is total number of spatial nodes and N_t is the total number of the time step. By using the procedure given in [10], the Eqs. (3.1) and (3.2) will be converted into following two algebraic equations:

Fluid temperature at outlet is

$$(T)_o = (T)_i - K_1\left[(T)_i - (T_m)_i\right] \tag{3.3}$$

Matrix temperature at outlet is

$$(T_m)_o = (T_m)_i + K_2\left[(T)_i - (T_m)_i\right] \tag{3.4}$$

In Eqs. (3.3) and (3.4), K_1 and K_2 are constants calculated as follows:

$$K_1 = \frac{1}{\left[1 + \dfrac{(\dot{m}c_p)_f \Delta t}{\left[(Mc_p)_m\right]_{\Delta z}}\right]} \left\{1 - \exp\left[-\frac{(hA_s)_{\Delta z}}{(\dot{m}c_p)_f}\right]\left[1 + \frac{(\dot{m}c_p)_f \Delta t}{\left[(Mc_p)_m\right]_{\Delta z}}\right]\right\} \tag{3.5}$$

$$K_2 = \frac{1}{\left\{1+\frac{\left[(Mc_p)_m\right]_{\Delta z}}{(\dot{m}c_p)_f \Delta t}\right\}}\left\{1-\exp\left[-\frac{(hA_s)_{\Delta z}}{(\dot{m}c_p)_f}\right]\left[1+\frac{(\dot{m}c_p)_f \Delta t}{\left[(Mc_p)_m\right]_{\Delta z}}\right]\right\} \tag{3.6}$$

Non-ideal effect of regenerator has been considered including the effect of longitudinal conduction.

3.1.2 Longitudinal conduction effect

By considering longitudinal effects, matrix thermal equation becomes

$$\frac{\partial}{\partial z}\left(k_m \frac{\partial T_m}{\partial z}\right)\delta V_m + h\delta A_s (T - T_m) = (\rho c_p \delta V)_m \frac{\partial T_m}{\partial t} \tag{3.7}$$

Fluid thermal equation becomes

$$(\rho c_p \delta V)_f w_z \frac{\partial T}{\partial z} = h\delta A_s (T_m - T) \tag{3.8}$$

For a finite regenerator element of width Δz, the matrix volume is equal to matrix area normal to flow and width. Hence,

$$\delta V_m = A_m \Delta z \tag{3.9}$$

Matrix conductivity k_m is defined by interfacial conductance between matrix elements which will be defined for a screen mesh as follows:

$$k_m = K_{mo}\left(\frac{T_m}{300}\right)^a \tag{3.10}$$

$$\frac{\partial k_m}{\partial T_m} = \frac{a k_m}{T_m} \tag{3.11}$$

Matrix thermal equation then becomes

$$\left[\frac{a k_m}{T_m}\left(\frac{\partial T_m}{\partial z}\right)^2 + k_m \frac{\partial^2 T_m}{\partial z^2}\right] A_m \Delta z + \left(hA_s\right)_{\Delta z}(T - T_m) = [(Mc_p)_m]_{\Delta z} \frac{\partial T_m}{\partial t} \tag{3.12}$$

Fluid thermal equation becomes

$$(\dot{m}c_p)_f \frac{\partial T}{\partial z} = -\left(hA_s\right)_{\Delta z}(T - T_m) \tag{3.13}$$

By using the procedure given in [10], Eqs. (3.12) and (3.13) results into the following algebraic equations:

Fluid temperature at outlet is given by

$$(T)_o = (T)_i - K_1\left[(T)_i - \left(T_m\right)_i\right] \tag{3.14}$$

Matrix temperature at outlet is calculated as

$$\left(T_m\right)_o = \left(T_m\right)_i + K_2\left[(T)_i - \left(T_m\right)_i\right] + K_3\left[\frac{a}{4\left(T_m\right)_i}(T_m')_i^{\,2} + (T_m'')_i\right] \tag{3.15}$$

where K_1 and K_2 are constants calculated from Eqs. (3.5) and (3.6). K_3 will be computed as

$$K_3 = \frac{k_m A_m \Delta t}{\left[\left(Mc_p\right)_m\right]_{\Delta z}\Delta z} \tag{3.16}$$

3.1.3 Longitudinal conduction and wall effect

Energy equation for regenerator matrix is

$$[(Mc_p)_m]_{\Delta z}\frac{\partial T_m}{\partial t} = \left[\frac{ak_m}{T_m}\left(\frac{\partial T_m}{\partial z}\right)^2 + k_m\frac{\partial^2 T_m}{\partial z^2}\right]A_m\Delta z + \left(hA_s\right)_{\Delta z}(T - T_m) \tag{3.17}$$

Energy equation for regenerator wall is

$$[(Mc_p)_{wl}]_{\Delta z}\frac{\partial T_{wl}}{\partial t} = \left[\frac{bk_{wl}}{T_{wl}}\left(\frac{\partial T_{wl}}{\partial z}\right)^2 + k_{wl}\frac{\partial^2 T_{wl}}{\partial z^2}\right]A_{wl}\Delta z + \left(hA_{wl}\right)_{\Delta z}(T - T_{wl}) \tag{3.18}$$

Energy equation of fluid is

$$(\dot{m}c_p)_f \frac{\partial T}{\partial z} + \left(hA_s\right)_{\Delta z}(T - T_m) + \left(hA_{wl}\right)_{\Delta z}(T - T_{wl}) = 0 \tag{3.19}$$

where, k_{wl} is a constant given as

$$k_{wl} = 14.80\left(\frac{T_{wl}}{300}\right)^{b} \tag{3.20}$$

Following the procedure [10], Eqs. (3.17), (3.18) and (3.19) results in following algebraic equations:

Fluid thermal equation becomes

$$(T)_o = (T)_i - K_1\left[(T)_i - (T_m)_i\right] - K_4\left[(T)_i - (T_{wl})_i\right] \tag{3.21}$$

Matrix thermal equation becomes

$$(T_m)_o = (T_m)_i + K_2\left[(T)_i - (T_m)_i\right] + K_3\left[\frac{a}{4(T_m)_i}(T_m')_i^{\,2} + (T_m'')_i\right] \tag{3.22}$$

Wall equation becomes

$$(T_{wl})_o = (T_{wl})_i + K_5\left[(T)_i - (T_{wl})_i\right] + K_6\left[\frac{a}{4(T_{wl})_i}(T_{wl}')_i^{\,2} + (T_{wl}'')_i\right] \tag{3.23}$$

where, constants K_1, K_2 and K_3 are given in Eqs. (3.5), (3.6) and (3.16) respectively.

$$K_4 = \frac{1}{\left\{1 + \dfrac{(\dot{m}c_p)_f\,\Delta t}{\left[(Mc_p)_{wl}\right]_{\Delta z}}\right\}}\left\{1 - \exp\left[-\frac{(hA_{wl})_{\Delta z}}{(\dot{m}c_p)_f}\right]\left[1 + \frac{(\dot{m}c_p)_f\,\Delta t}{\left[(Mc_p)_{wl}\right]_{\Delta z}}\right]\right\} \tag{3.24}$$

$$K_5 = \frac{1}{\left\{1 + \dfrac{\left[(Mc_p)_{wl}\right]_{\Delta z}}{(\dot{m}c_p)_f\,\Delta t}\right\}}\left\{1 - \exp\left[-\frac{(hA_{wl})_{\Delta z}}{(\dot{m}c_p)_f}\right]\left[1 + \frac{(\dot{m}c_p)_f\,\Delta t}{\left[(Mc_p)_{wl}\right]_{\Delta z}}\right]\right\} \tag{3.25}$$

$$K_6 = \frac{k_{wl} A_{wl} \Delta t}{\left[\left(Mc_p\right)_{wl}\right]_{\Delta z} \Delta z} \tag{3.26}$$

3.1.4 Boundary conditions and solution procedure

The above equations (Eqs (3.3-3.4), Eqs (3.14-3.15) and Eqs (3.21-23)) give outlet matrix temperature and fluid temperature regarding inlet matrix temperature and fluid temperature. In all following equations, notations $'$ and $''$ represent heating and cooling periods respectively. Linear variation of temperature is assumed along the regenerator length.

$$\left[T'_m(1,i)\right]_{initial} = T_h - \frac{(i-1)}{N_z}[T_h - T_c] \tag{3.27}$$

According to present assumptions, inlet fluid boundary temperature is equal to hot end temperature. So mathematically

$$\left(T'(1,1)\ T'(2,1)\ldots T'(N_t,1)\right)^T_i = T_h \tag{3.28}$$

$T^*_m = T'_m(\lambda_n, \varsigma)$ By using above boundary conditions, outlet temperatures $\left[T'(1,1)\right]_o$ and $\left[T_m'(1,1)\right]_o$ are calculated. After completing calculations for heating period, flow reversal conditions occurred, so the final matrix temperature and fluid temperature is used as initial condition for cooling period, where $\varsigma = \left[N_z - (i-1)\right]$. Outlet temperatures are computed by setting the first nodes of inlet fluid temperature equal to heating period boundary temperature.

$$\left(T''(1,1)\ T''(2,1)\ldots..T''(N_t,1)\right)^T_i = T_c \tag{3.29}$$

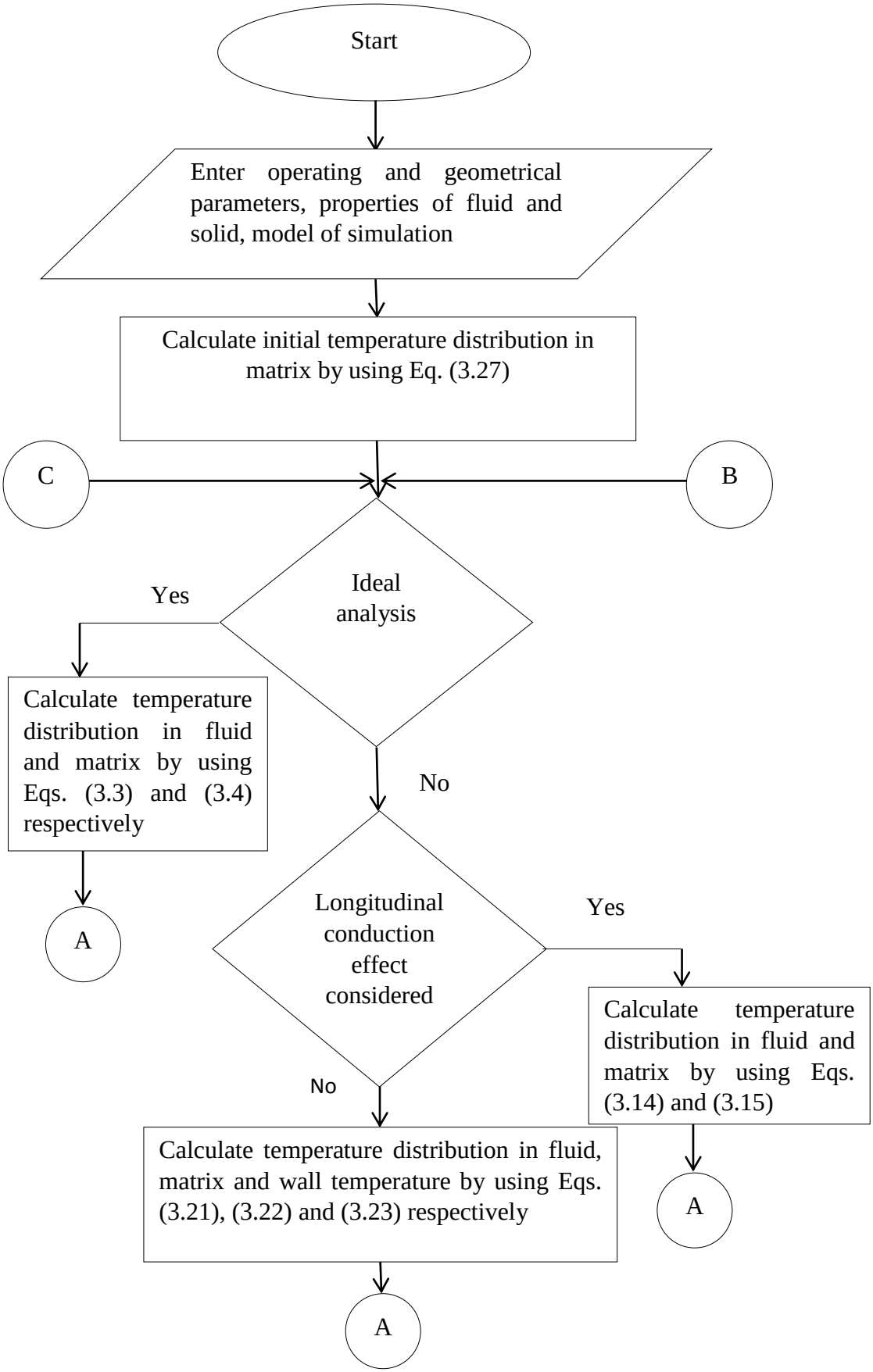
Start
Enter operating and geometrical parameters, properties of fluid and solid, model of simulation
Calculate initial temperature distribution in matrix by using Eq. (3.27)
C
B
Ideal analysis
Yes
No
Calculate temperature distribution in fluid and matrix by using Eqs. (3.3) and (3.4) respectively
A
Longitudinal conduction effect considered
Yes
No
Calculate temperature distribution in fluid and matrix by using Eqs. (3.14) and (3.15)
A
Calculate temperature distribution in fluid, matrix and wall temperature by using Eqs. (3.21), (3.22) and (3.23) respectively
A

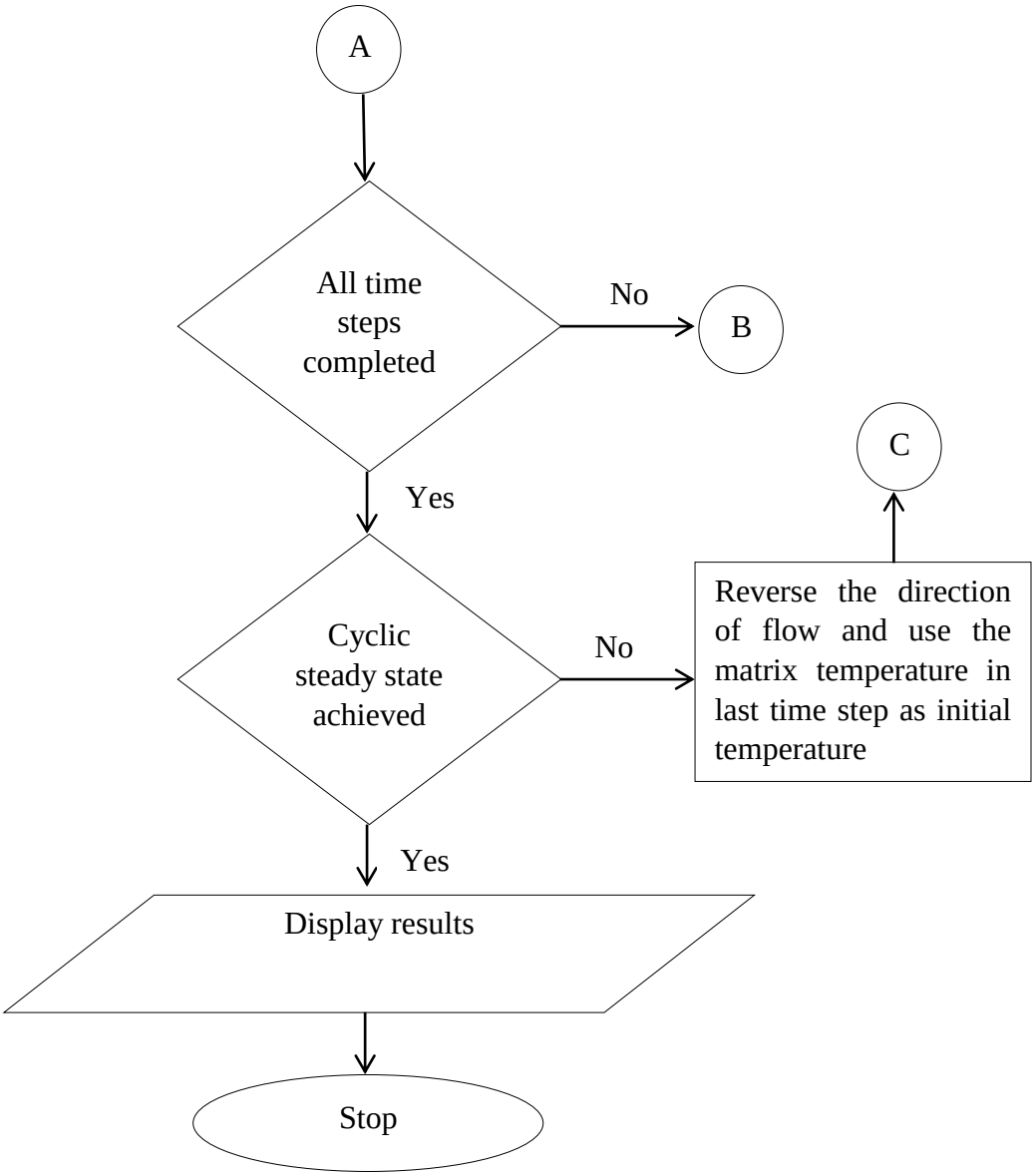

Figure 3.2: Flow chart of CRESP-REGEN package.

3.2 CRESP-REGEN software overview

This section explains the design of software interfaces in detail. A software package has been developed by using the above mathematical model which can be used to predict the performance of a regenerator by the end-user. The main input screen of CRESP-REGEN software is shown in Fig. 3.3. The main screen accepts various input geometrical and operating

parameters. Also, it allows the user to choose the solid and fluid materials from list box. After providing the parameters, the user can choose the desired model: the ideal, the model including longitudinal conduction effect or both longitudinal and wall conduction effects. Then by clicking "*run*", CRESP-REGEN will solve the equations and produce results, which will be displayed after user clicks "*results*".

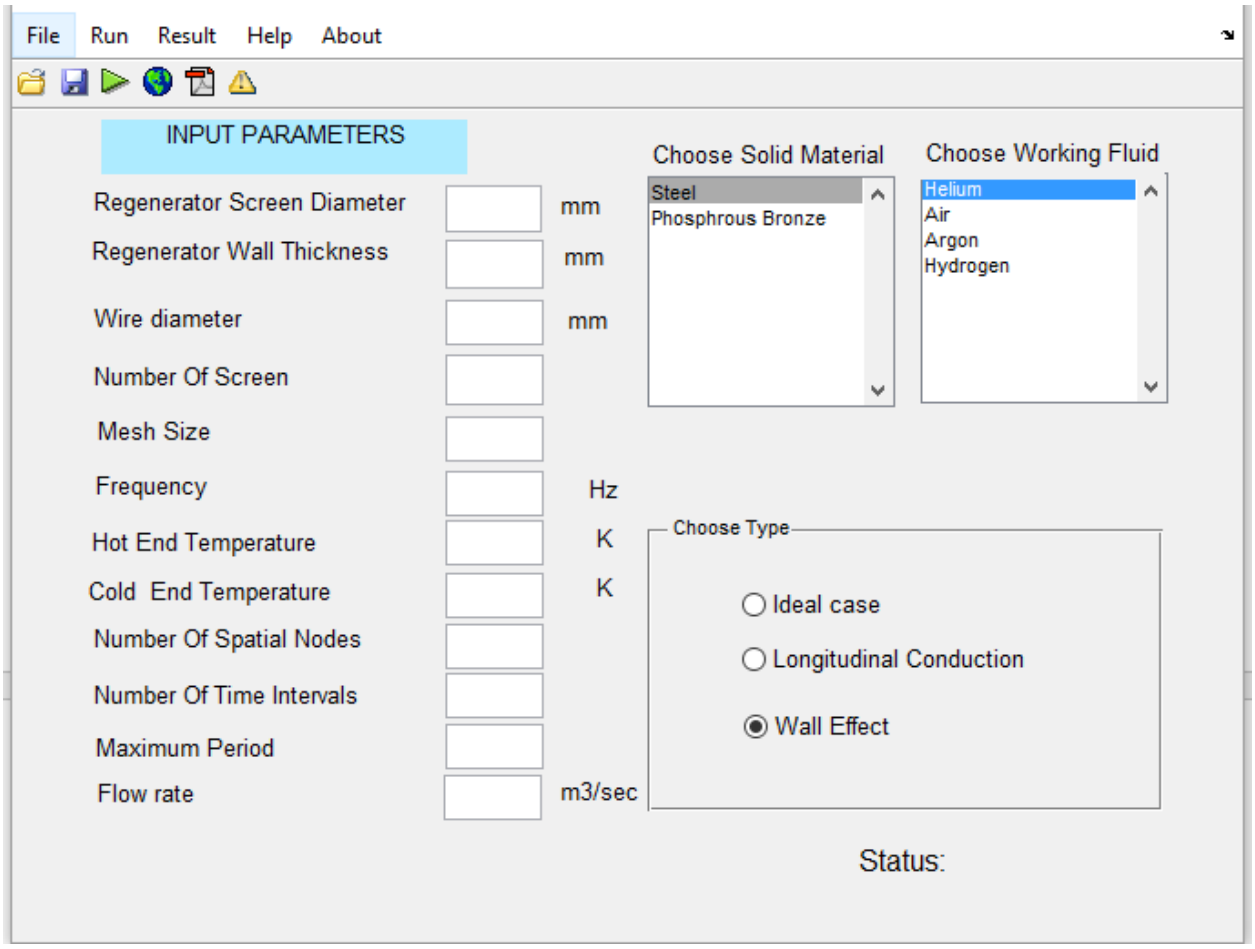

Figure 3.3: Input screen of CRESP-REGEN software.

The descriptions of various menu and toolbar icons are explained in Figs 3.4 and 3.5.

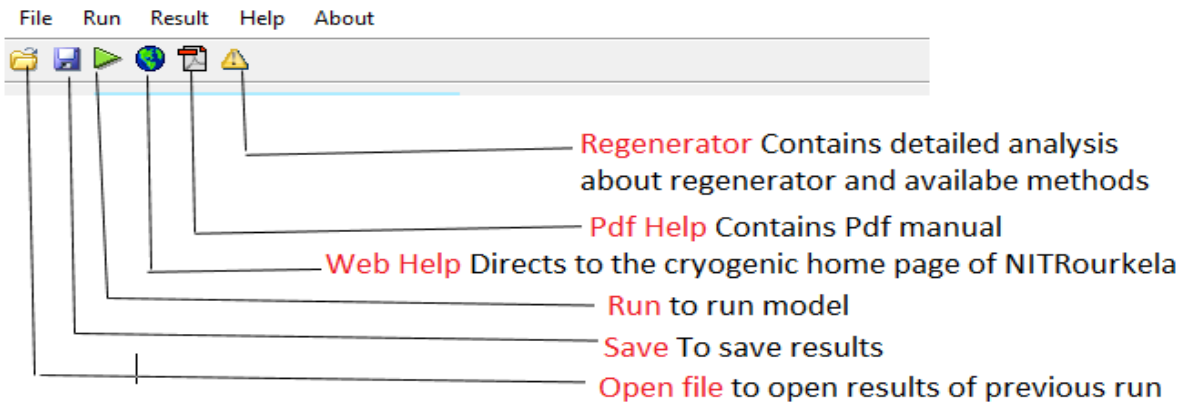

Figure 3.4: Toolbar icons of CRESP-REGEN package.

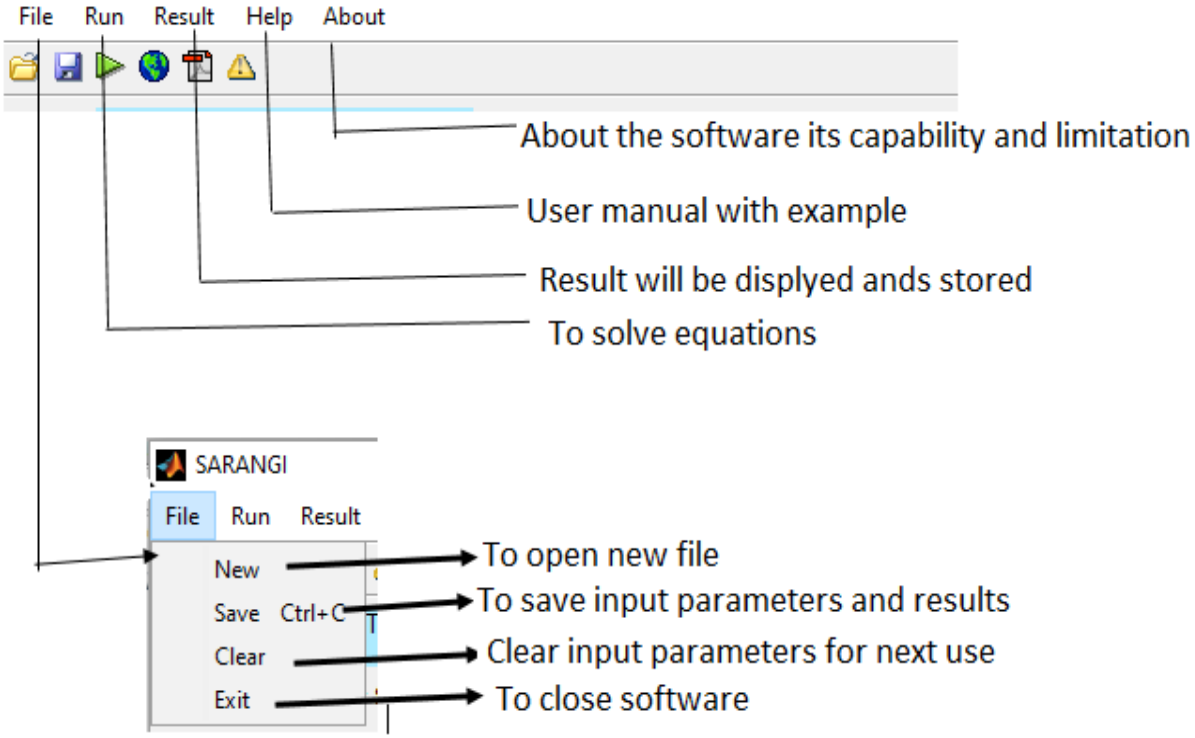

Figure 3.5: Menu items of CRESP-REGEN package.

3.3 Validation of CRESP-REGEN software

3.3.1 Input parameters

Screen diameter = 19.05 mm
Regenerator thickness = 0.152 mm
Mesh size = #150 phosphorous bronze
Cold end temperature = 80 K
Frequency = 50 Hz
Wire diameter = 0.069 mm
Number of screens = 640, 480, 320, 220
Flow rate = 0.00661 m^3/s
Hot end temperature = 300 K

3.3.2 Output parameters for various mesh sizes

Table 3.1: Comparison of CRESP-REGEN software with published results (640 mesh number)

Parameter		Ackerman et al.	Present result	Relative error (%)
Length(cm)		10.16	10.14	-0.19
Heat transfer area(m^2)		0.44	0.48	8.33
Reynolds number		53	53.77	1.43
NTU		192	210	8.57
Stanton number		-	0.16	-
Mass of regenerator		0.1	0.14	28.5
Ineffectivenes	Ideal (%)	0.62	0.68	8.82
	Longitudinal conduction effect (%)	.71	0.79	10.12
	Longitudinal conduction + wall effect (%)	0.99	1.02	2.94

Table 3.2: Comparison of CRESP-REGEN software with published results (480 mesh number).

Parameter		Ackerman et al.	Present	Relative error (%)
Length(cm)		7.62	7.60	-0.263
Heat transfer area(m^2)		0.33	0.36	8.33
Reynolds number		53	53.78	1.45
NTU		144	158	8.86
Stanton number		-	0.16	-
Mass of regenerator		-	0.54	-
Ineffectivenes	Ideal (%)	-	1.20	-
	Longitudinal conduction effect (%)	-	1.48	-
	Longitudinal conduction + wall effect (%)	-	2.50	-

Table 3.3: Comparison of CRESP-REGEN software with published results (320 mesh number).

Parameter		Ackerman et al.	Present	Relative error (%)
Length(cm)		5.08	5.07	-0.197
Heat transfer area(m^2)		0.22	0.24	8.33
Reynolds number		-	53.78	-
NTU		96	105.50	9
Stanton number		-	0.16	-
Mass of regenerator		-	0.03	-
Ineffectivenes	Ideal (%)	1.58	1.69	6.50
	Longitudinal conduction effect (%)	1.76	2.01	12.4
	Longitudinal conduction + wall effect (%)	3.08	3.19	3.44

Table 3.4: Comparison of CRESP-REGEN software with published results (220 mesh number).

Parameter		Ackerman et al.	Present	Relative error (%)
Length(cm)		3.4	3.45	1.44
Heat transfer area(m^2)		0.15	0.17	11.76
Reynolds number		47.80	53.70	10.98
NTU		65	72.57	10.43
Stanton number		-	0.16	-
Mass of regenerator		-	0.02	-
Ineffectivenes	Ideal (%)	-	1.79	-
	Longitudinal conduction effect (%)	-	2.01	-
	Longitudinal conduction + wall effect (%)	-	3.31	-

3.4 Parametric studies

A parametric study has been undertaken to investigate the performance of regenerator (refrigeration power, ineffectiveness, regenerator loss, exergy efficiency, COP etc.) as a function of various input parameters (geometrical and operating parameters) for cryocooler based applications. Here NIST software REGEN 3.3 is used to conduct the parametric studies. The performance of thermal regenerator is obtained in the form of most critical parameters such

as gross refrigeration power, adjusted gross refrigeration power, net cooling power, losses of acoustic power at cold end and hot end of the regenerator. To achieve a steady state, the value of enthalpy flux at the cold end to remain constant and thereby calculation requires a long time in the computational process. A). In order to get a cyclic steady state in the solution procedure, the value of solution depends on upon several user-specified parameters such as number of cycles, number of mesh points along the axial direction and number of time steps used in each cycle.[49]. These parameters have been taken in the present simulation from [49].

NUM_POINTS_X=42, NUM_STEPS_CYC=82, FINAL_CYCLE=5200

Several crucial parameters have been taken into consideration in the present study such as charging pressure, pressure ratio at cold end, area to mass flow ratio, operating frequency, length of the regenerator, phase angle at the cold end of regenerator, porosity of regenerator matrix, temperature at hot end of regenerator and temperature at cold end of regenerator. Temperature-dependent properties of solid and fluid, which is an essential feature of REGEN3.3*, is not available in any other software. The optimum goal of the end user is to change the operating and geometrical parameters in such a manner that losses would be minimum and also the refrigeration power would be maximum. An important parameter is COP, which signifies that minimization of necessary work supply at the hot end of the regenerator to achieve the desired refrigeration power at the hot end. NTCOP=NTCADJ/PVWOKOT.

The acoustic power at the cold end of the regenerator is determined from the integral of the product of dynamic pressure and volumetric flow rate at the cold end of the regenerator in one cycle. The cold end acoustic power is obtained after the subtraction of loss terms ENTFLX (regenerator ineffectiveness loss) and HTFLUX (conduction loss of matrix) from the gross refrigeration power. Some acoustic power loss occurs due to compression and expansion process inside the pulse tube.

---

*Gary, J., O'Gallagher, A., 2006. REGEN 3.3: User Manual. National Institute of Standards and Technology,

Hence in present study, it is assumed that 20% of acoustic power loss occurs due to pressurization in pulse tube. By multiplying this parameter with gross refrigeration power, net refrigeration power has been calculated. PROSS accounts the non-ideal dependence of enthalpy on pressure.

Hot end temperature=300 K	Cold end temperature=80 K
Working fluid Helium 4	Diameter of regenerator=15 mm
Length of regenerator=variable	Mesh size=#653
Frequency = 40 Hz	

3.4.1 Effect of mean pressure

With the increase in charging pressure, the relative heat loss at the cold end starts rising. The rate of heat loss increases consistently, as a result of this refrigeration power increases up to some extent and then it starts decreasing. The magnitude of charging pressure is a function of impedance magnitude on a molar basis which remains constant. However at the same time density may decrease, so impedance magnitude in volumetric flow basis decreases [19]. Hence, there is a degradation in acoustic power due to the increase in friction loss, so the acoustic power ratio decreases, as result COP increases (Fig. 3.7). With increase in mean pressure, refrigeration power increases up to some point, then it starts decreasing and ineffectiveness increases consistently (Fig 3.6). The COP and second law efficiency starts increasing and become maximum at pressure 5 MPa, then it starts decreasing (Fig. 3.7).

3.4.2 Effect of pressure ratio

The effect of pressure ratio at the cold end of regenerator is also having a strong effect on the performance of typical regenerator [133]. From Figs. 3.8 and 3.9, it is evident that with increase in pressure ratio, COP, exergy efficiency and net refrigeration all starts increasing but it is impossible to get a pressure ratio greater than 1.35 at the cold end due to limitations in the pressure wave generator. With increase in pressure ratio, the amplitude of pressure oscillation starts increasing, as a result of this net refrigeration power starts increasing. As COP and exergy efficiency both are directly proportional to net refrigeration power, both starts rising.

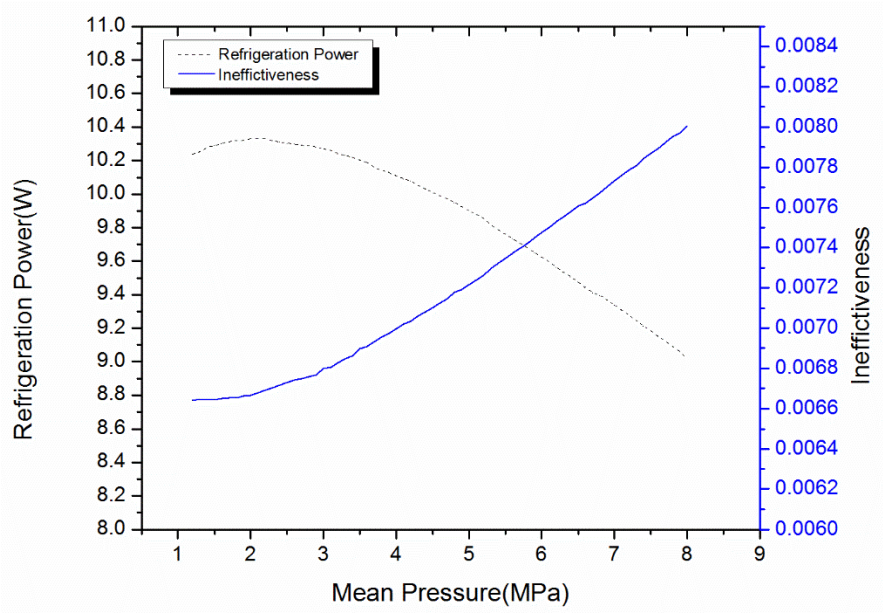

Figure 3.6: Effect of mean pressure on refrigeration power and ineffectiveness.

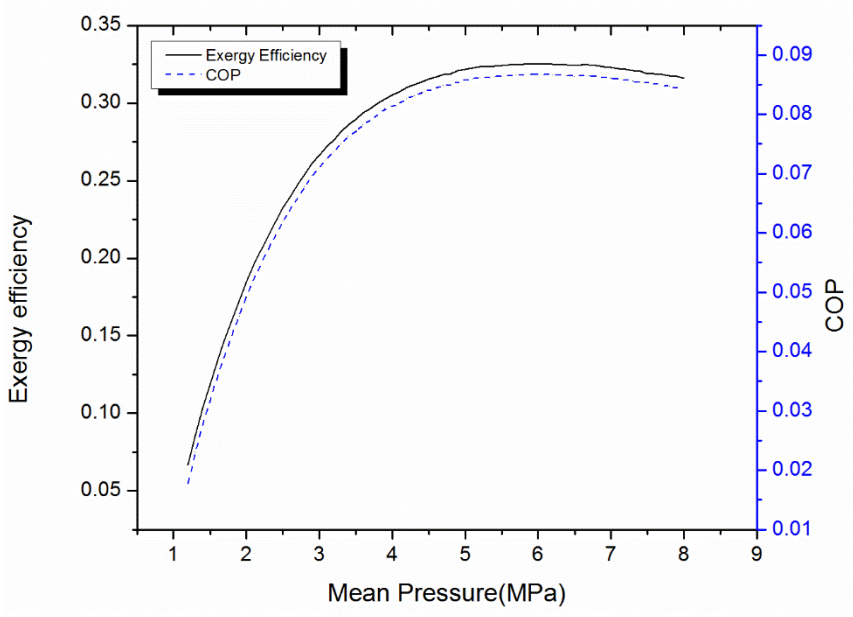

Figure 3.7: Effect of mean pressure on exergy efficiency and COP.

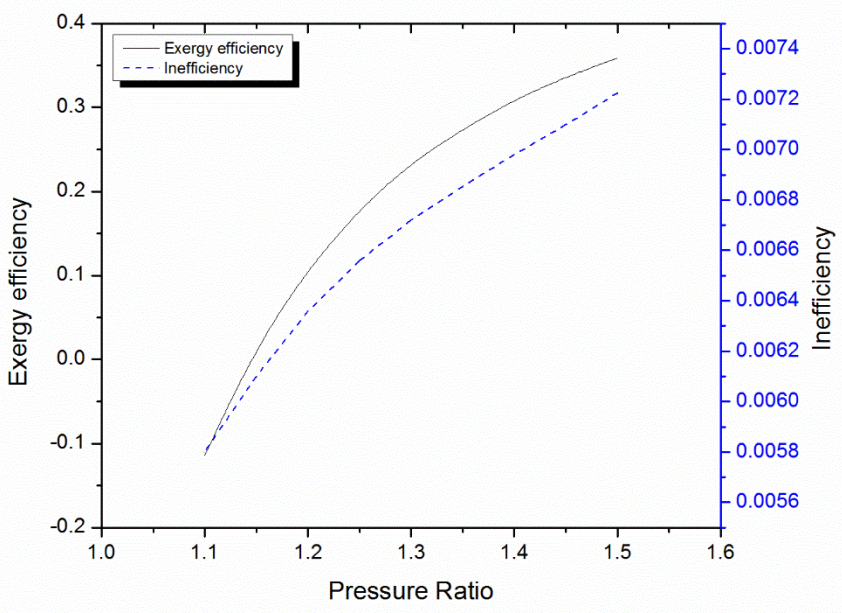

Figure 3.8: Effect of pressure ratio on exergy efficiency and inefficiency.

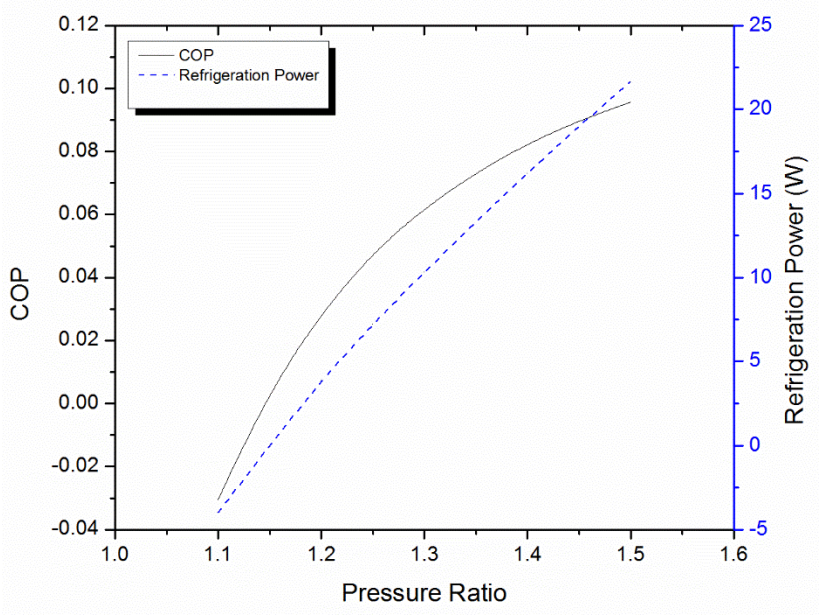

Figure 3.9: Effect of pressure ratio on COP and refrigeration power.

3.4.3 Effect of area to mass flow ratio

With the increase in area to mass flow ratio at cold end of regenerator, COP and exergy efficiency starts increasing up to some extent, then it becomes steady and then starts decreasing in accordance with observations made by [134]. The trend of gross refrigeration power, adjusted gross refrigeration power and net refrigeration power all starts decreasing due to decline in inefficiency loss. The heat loss starts decreasing as a result of decrease in friction loss and refrigeration power [134]. The mass flow rate at the cold end of regenerator has two components: one along the pressure wave known as standing wave, and the other perpendicular to the pressure wave known as a progressive wave. An increase in mass flow rate increases the progressive wave, so refrigerating power decreases, also COP and exergy efficiency related to refrigerating power decreases (Fig. 3.10-3.12).

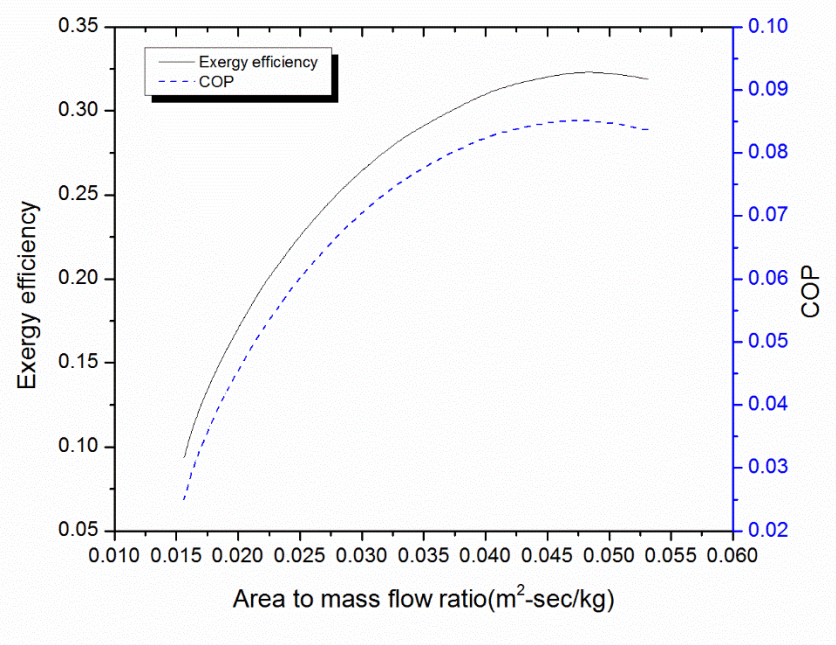

Figure 3.10: Effect of area to mass flow ratio on exergy efficiency and COP.

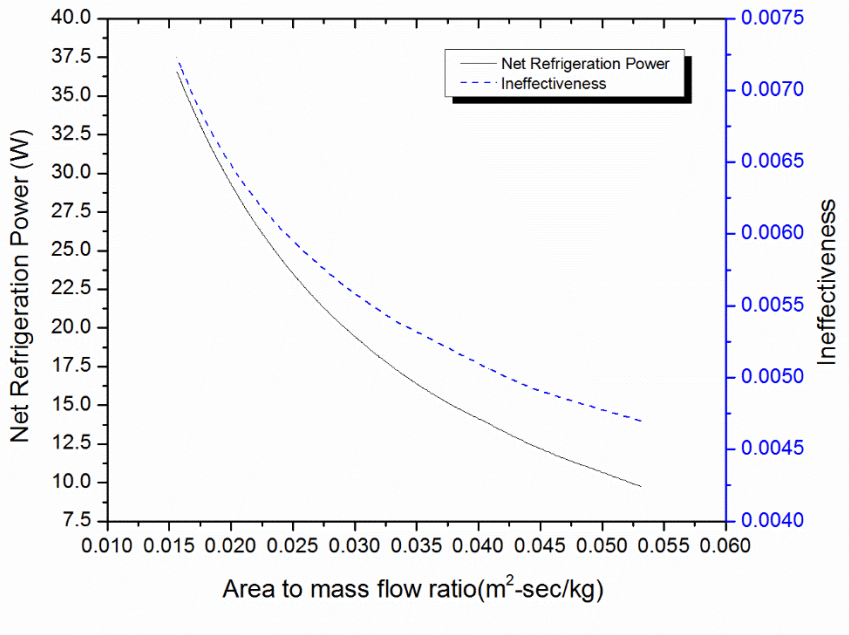

Figure 3.11: Effect of area to mass flow ratio on net refrigeration power and ineffectiveness.

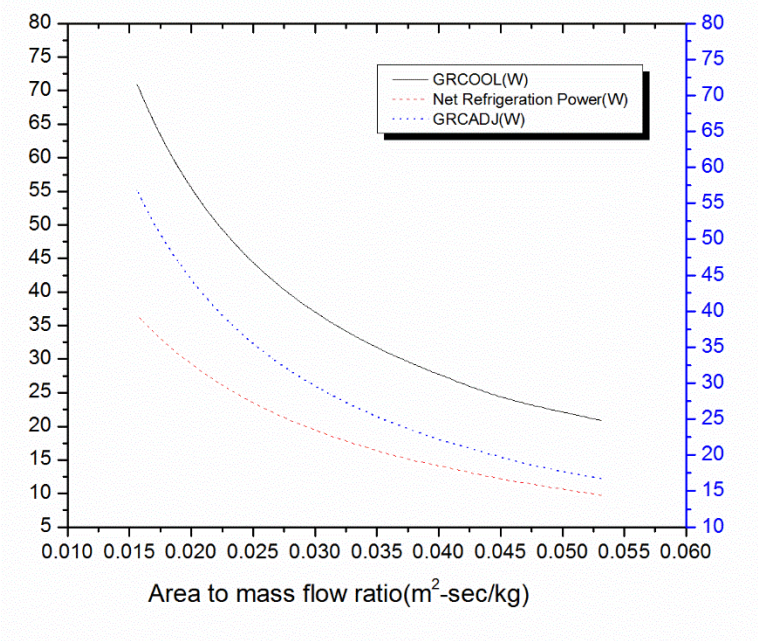

Figure 3.12: Effect of area to mass flow ratio on net refrigeration power and ineffectiveness.

3.4.4 Effect of length of regenerator

With the increase in the length of regenerator, COP starts increasing up to a certain length, after that it starts decreasing (Fig. 3.13) due to increase in viscous losses. So the trend of the curve

is an increasing-decreasing manner. The refrigeration power starts increasing, then after a particular length it becomes steady and then starts decreasing (Fig. 3.14) due to increase in heat loss after a particular length [134]. After a particular length, the heat loss increases due to axial conduction loss thus deteriorates the performance of cryocoolers. There is a generation of entropy inside the matrix, which decreases the exergy flow and reduces the inefficiency of the regenerator in accordance with the observations made by John *et al.* [134].

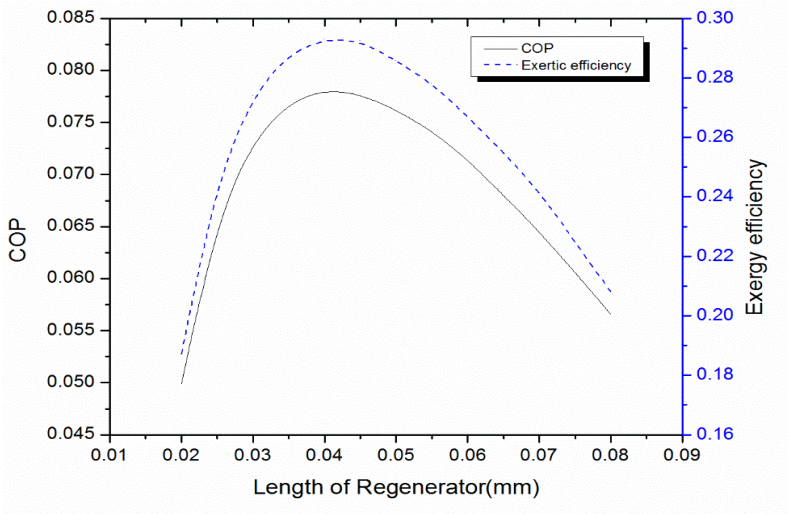

Figure 3.13: Effect of length of regenerator on COP and exergy efficiency.

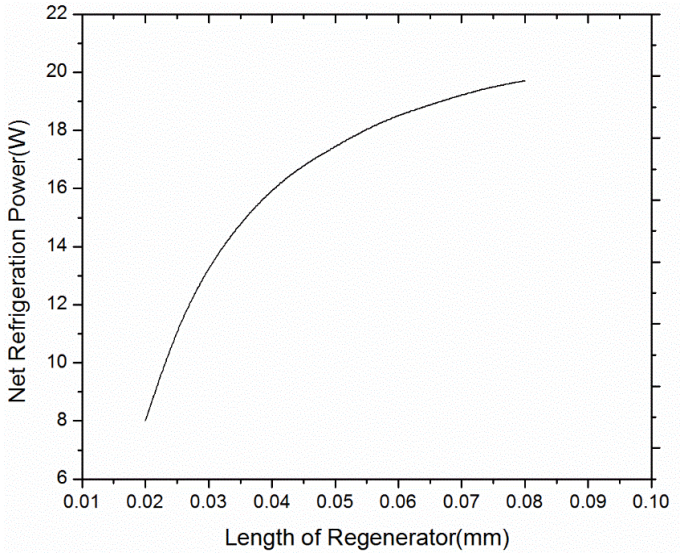

Figure 3.14: Effect of length of regenerator on net refrigeration power.

3.4.5 Effect of operating frequency

The refrigerating power of cryocooler is an active function of the inertance effect, which is generated by the inertance tube, is a function of operating frequency. The rate of heat transfer in regenerator and phase shift both are a strong function of operating frequency. The increase in operating frequency enhances the impedance of phase shifter but decreases its compliance. Also, the rate of heat loss increases in the regenerator. So there must be an optimal balance between them to get an optimum operating frequency. With the increase in operating frequency refrigeration power increases (Fig. 3.15), however, COP and second law efficiency increases up to some point and then starts decreasing (Figs. 3.15-3.16). As the rate of heat loss starts decreasing, inefficiency decreases as shown in Fig. 3.16 in accordance with [19].

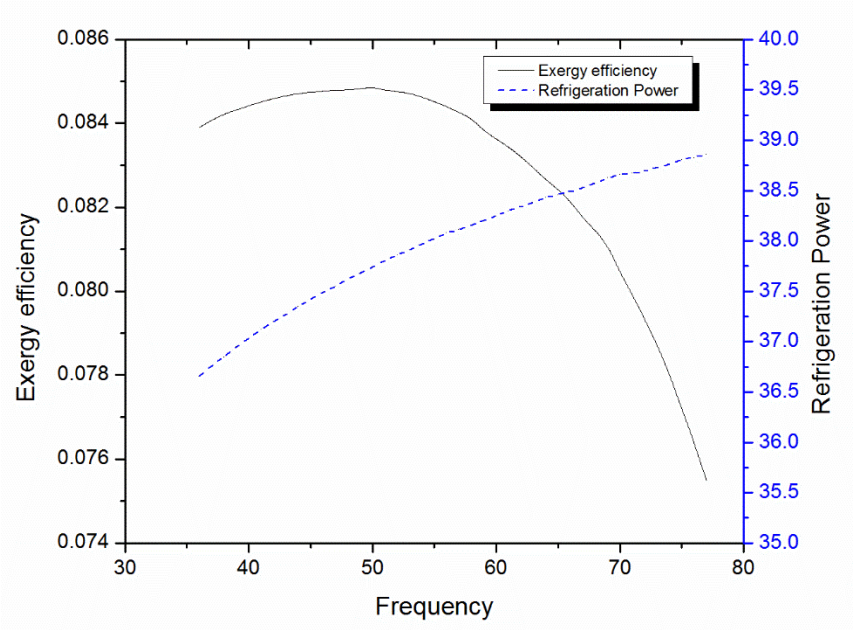

Figure 3.15: Effect of frequency on exergy efficiency and refrigeration power.

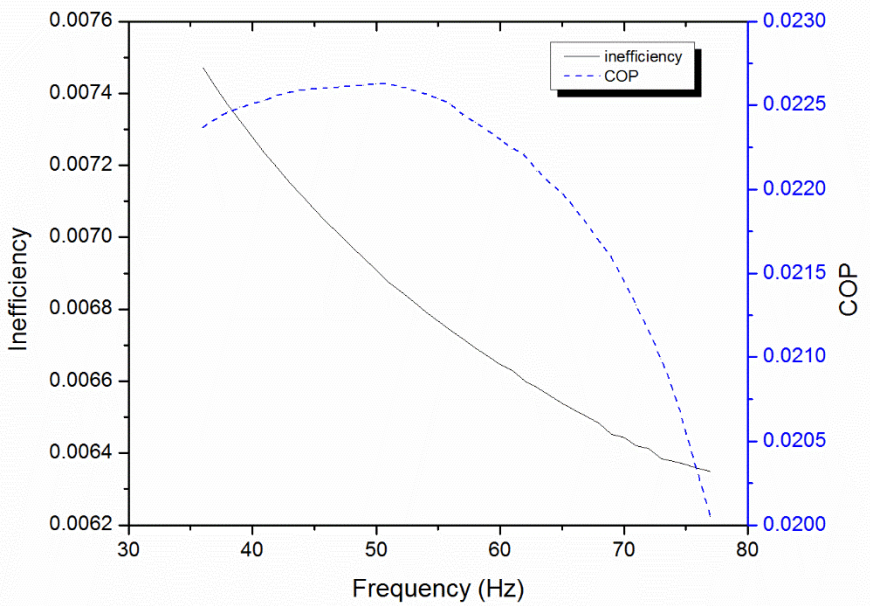

Figure 3.16: Effect of frequency on inefficiency and COP.

3.4.6 Effect of phase angle at cold end of regenerator

The phase angle at the cold end of regenerator is having a significant effect on the performance of cryocoolers. The phase angle is related to the calculation of standing wave and a progressive wave of mass flow rate. Standing wave is the sine angle of the mass flow rate at the cold end, whereas the progressive wave is cosine angle of the mass flow rate. With decrease in phase angle at cold end, cosine angle decreases and progressive wave decreases, thus the inertance effect becomes stronger and its performance is optimum. In standing wave however sine angle is used, which increases with decrease in phase angle and hence its performance increases. The coefficient of performance is maximum at -30 degrees (Fig. 3.18) [133]. COP and exergy efficiency is maximum at this temperature (Fig. 3.17). COP is the ratio between net refrigeration capacities to acoustic power at the warm end of the regenerator. Exergy efficiency is related to COP with the product of hot end temperature to cold end temperature. The isothermal refrigeration power decreases from gross refrigeration power after removing the loss encountered in pulse tube or displacer due to pressurisation in pulse tube (Fig. 3.18). The ineffectiveness is maximum when the phase angle is zero, then it starts decreasing (Fig. 3.19). Figure 3.20 shows the variation of regenerator loss with phase angle.

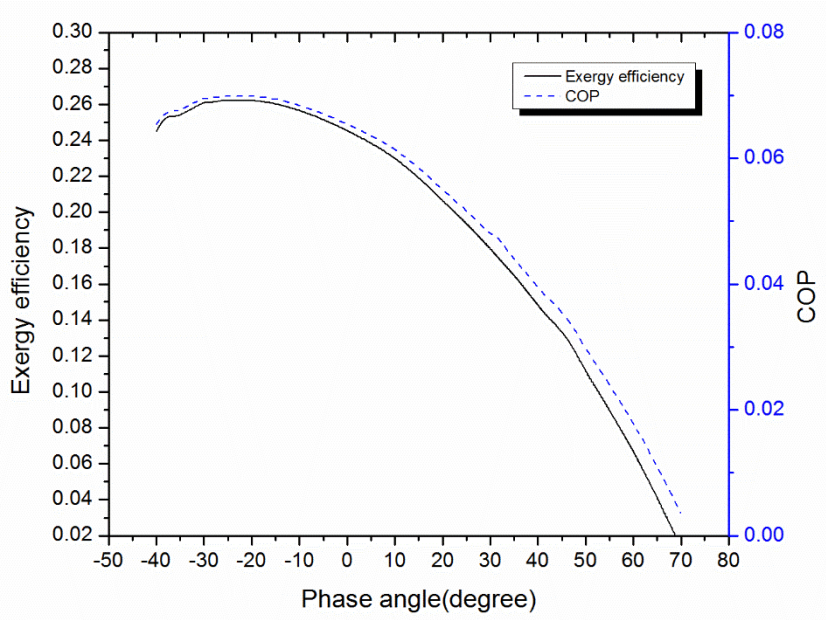

Figure 3.17: Effect of phase angle on exergy efficiency and COP.

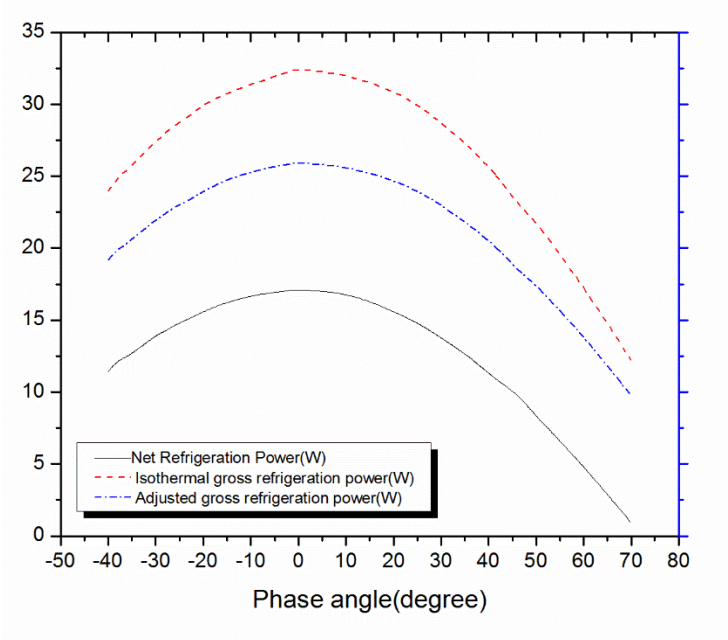

Figure 3.18: Effect of phase angle on refrigeration powers.

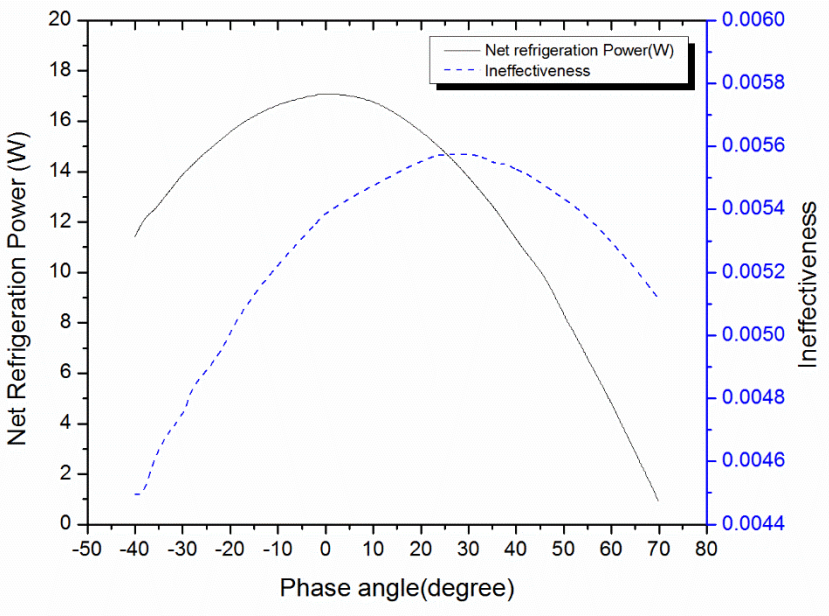

Figure 3.19: Effect of phase angle on net refrigeration power and ineffectiveness.

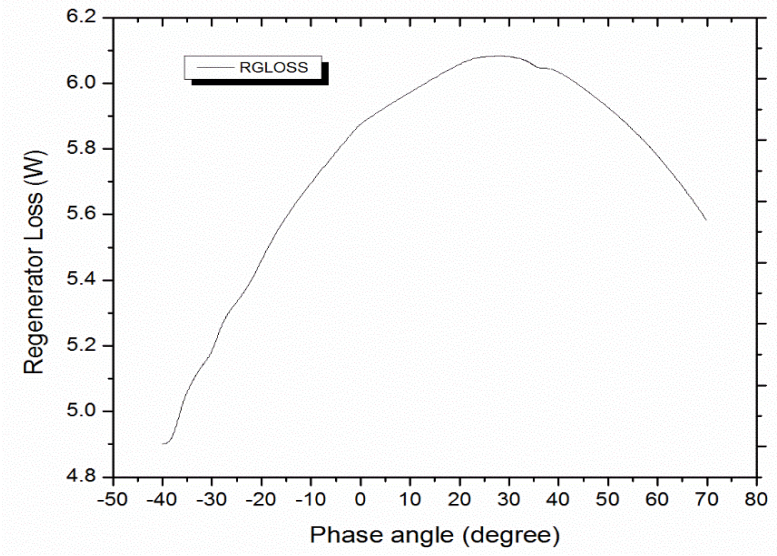

Figure 3.20: Effect of phase angle on regenerator loss.

3.4.7 Effect of hot end temperature of regenerator

With the increase in temperature at the hot end of regenerator, the axial conduction loss increases as a result of this net refrigeration power. As a result, the coefficient of performance and exergy efficiency starts decreasing (Figs. 3.21-23). Thus, an aftercooler may be very much essential to remove the heat of compression, which is placed after pressure wave generator to get better performance.

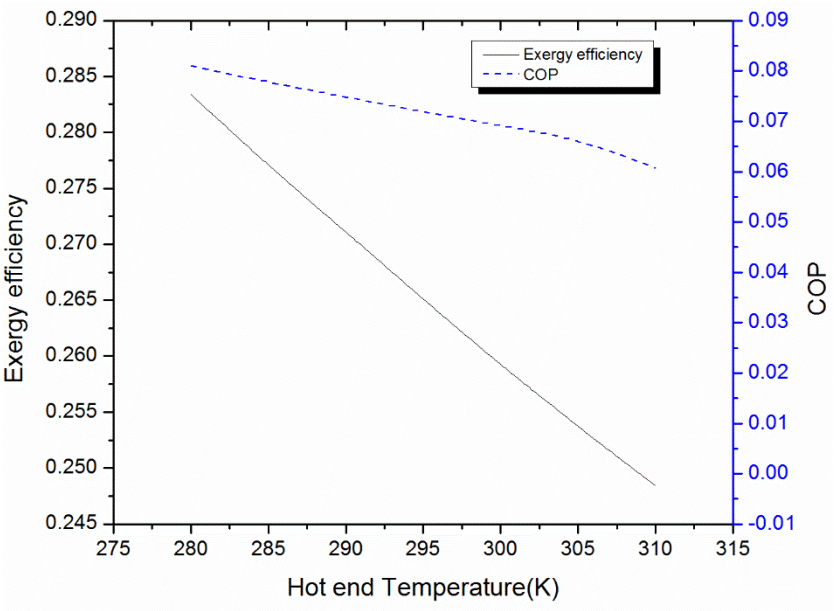

Figure 3.21: Effect of hot end temperature on exergy efficiency and COP.

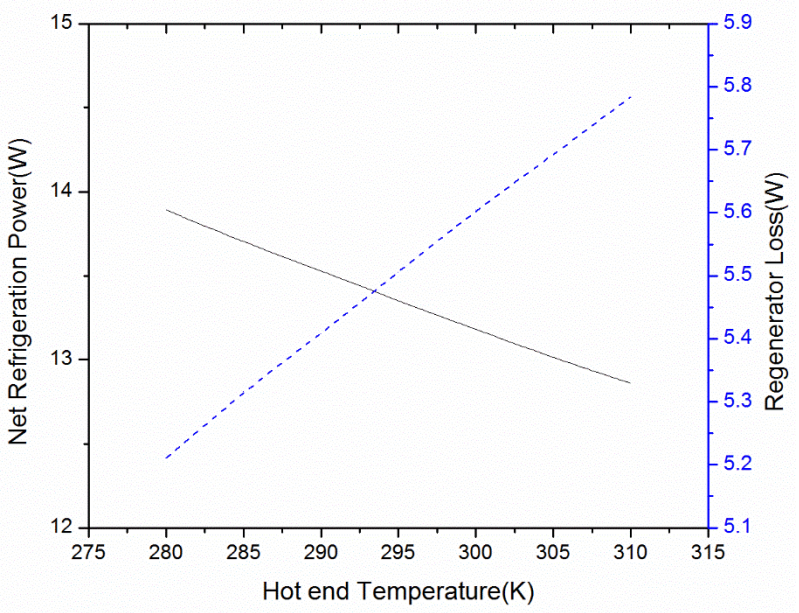

Figure 3.22: Effect of hot end temperature on net refrigeration power and regenerator loss.

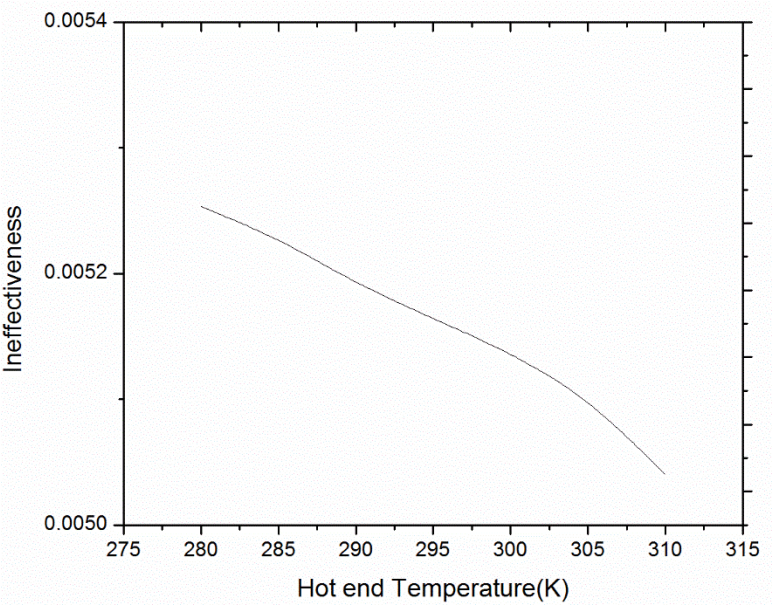

Figure 3.23: Effect of hot end temperature on ineffectiveness

3.4.8 Effect of cold end temperature of regenerator

With the increase in refrigeration temperature/cooling temperature/temperature at the cold end of regenerator, exergy efficiency, COP and net refrigeration capacity starts growing (Figs. 3.24-3.26). The isothermal cooling power is lower than the value of adjusted refrigeration power after removing the loss due to the pressurisation of gases (loss of acoustic power) in pulse tube and displacer. The ineffectiveness of regenerator and regenerator loss start decreasing with increase in refrigerating capacity.

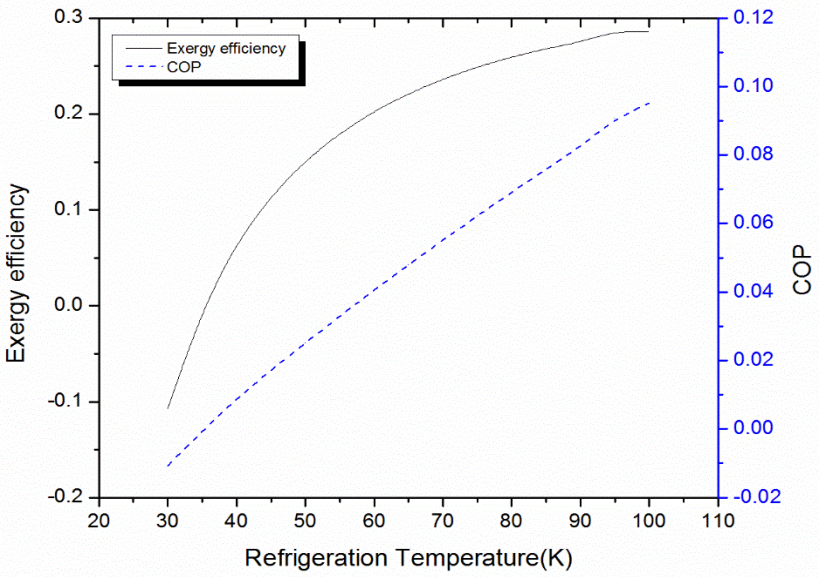

Figure 3.24: Effect of refrigeration temperature on exergy efficiency and COP.

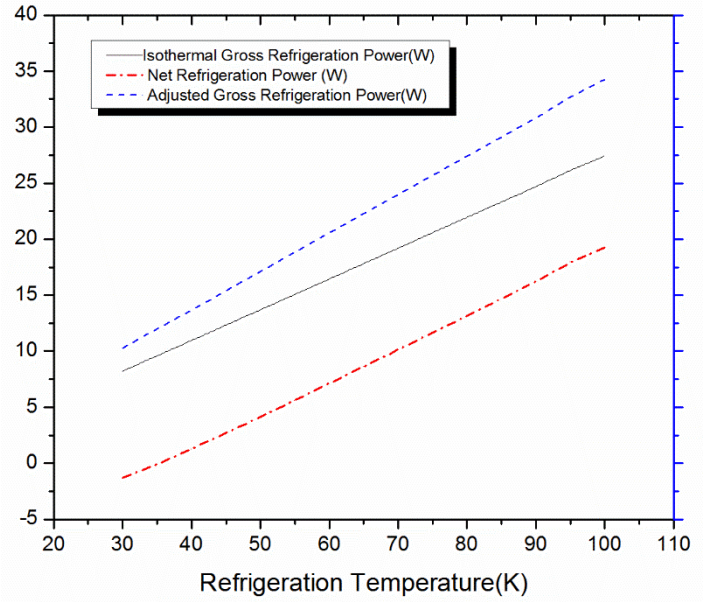

Figure 3.25: Effect of refrigeration temperature on refrigeration powers.

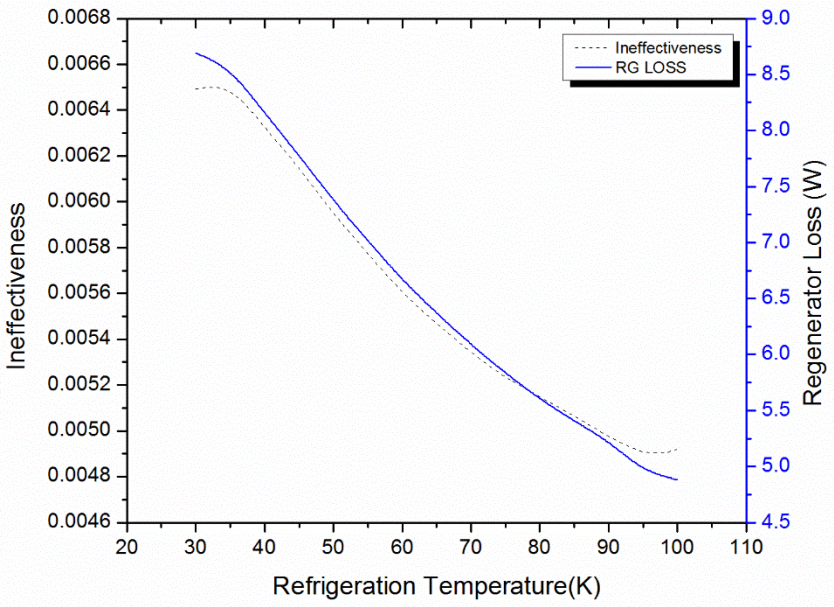

Figure 3.26: Effect of refrigeration temperature on ineffectiveness and regenerator loss.

3.4.9 Effect of thickness of regenerator wall

With an increase in thickness of regenerator net refrigeration power, COP and exergy efficiency of regenerator starts decreasing (Figs. 3.27-3.28) due to increasing in heat loss due to wall conduction.

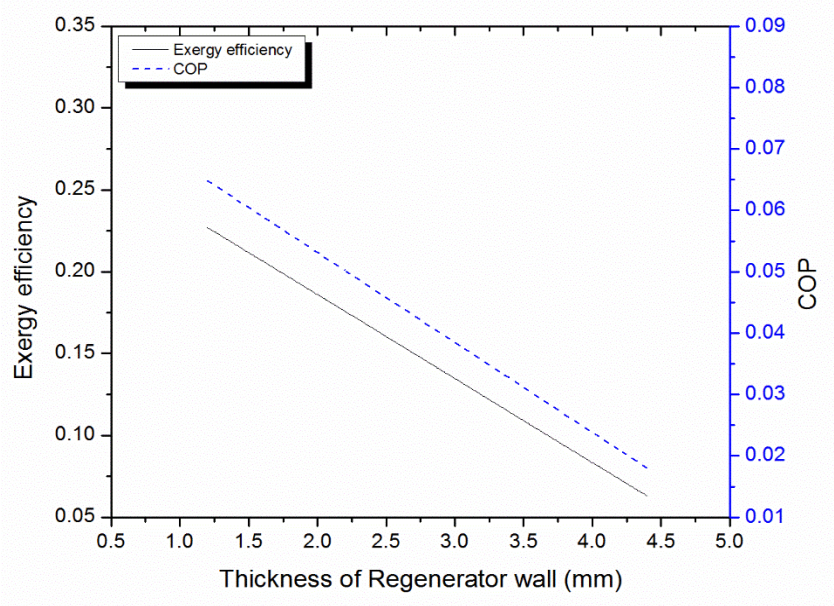

Figure 3.27: Effect of thickness of regenerator wall on exergy efficiency and COP.

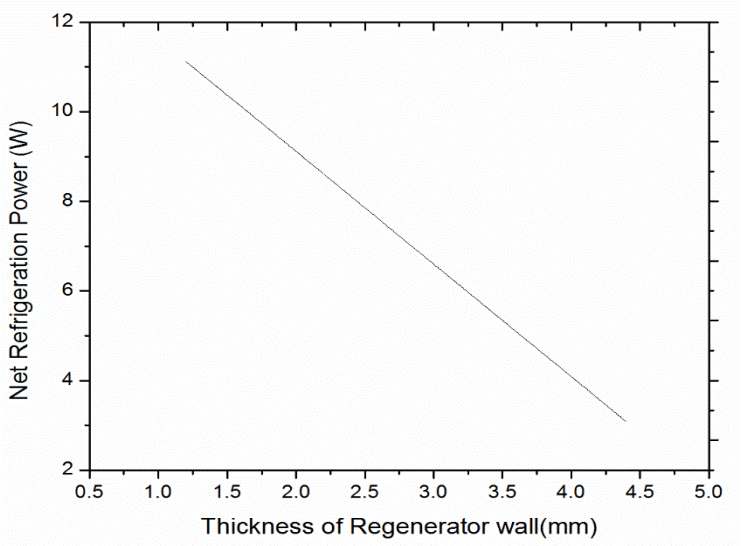

Figure 3.28: Effect of thickness of regenerator wall on net refrigeration power.

3.4.10 Effect of porosity of regenerator

Porosity of regenerator must be an order of thermal penetration depth of fluid intending to achieve better heat transfer between fluid and matrix. With increase in porosity, exergy efficiency and COP starts increasing and become optimum at 0.7, then starts decreasing. Net refrigeration power is also maximum when porosity is 0.7 (Figs. 3.29-31).

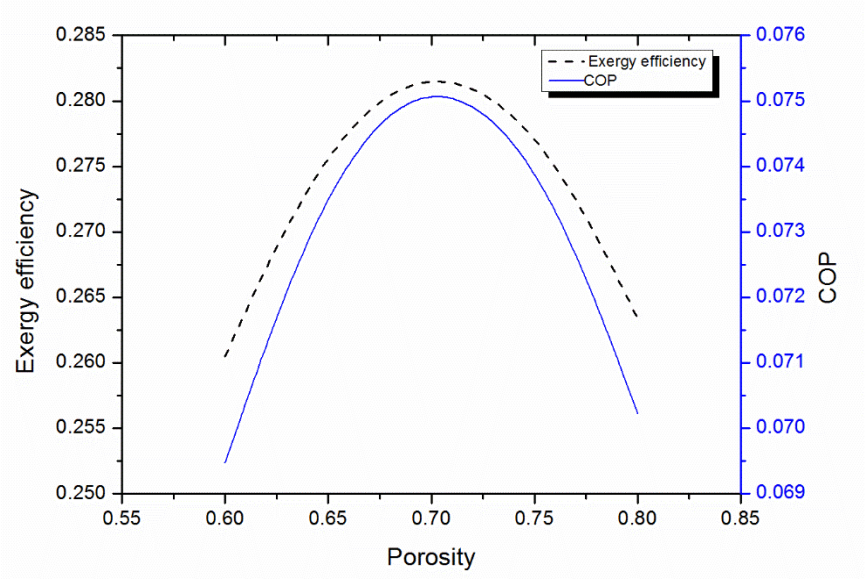

Figure 3.29: Effect of porosity of regenerator on COP and exergy efficiency.

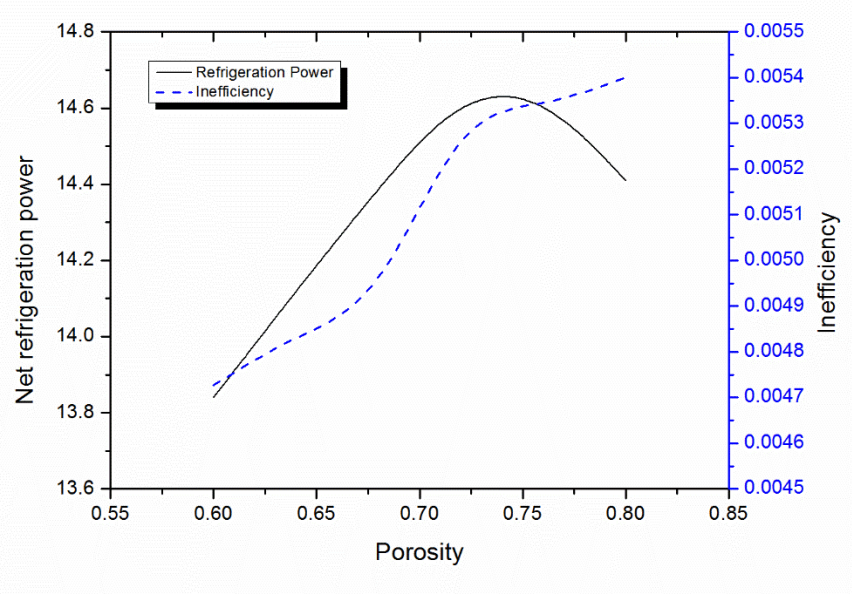

Figure 3.30: Effect of porosity on net refrigeration power and ineffectiveness.

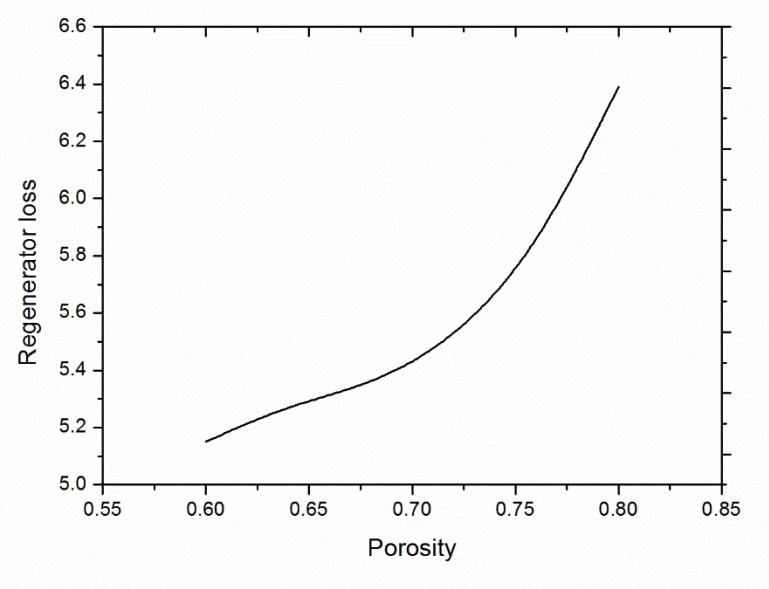

Figure 3.31: Effect of porosity on regenerator loss.

3.5 Summary

In this chapter, detailed mathematical analysis is performed and, by using the mathematical model, a general purpose simulation software is developed to predict the performance of a regenerator for typical cryogenic applications. The software is validated with previously published results. In addition, parametric study is also performed using the NIST software

package REGEN 3.3 to identify the effect of various operating and geometrical parameters and its effect on performance. The main criteria chosen for performance are net refrigeration power, COP and exergy efficiency.

Chapter 4

Mathematical Analysis and Design Software for Pulse Tube Refrigerator

4.1 Isothermal model

Isothermal model is a second order mathematical model developed by Zhu *et al.* [52] and further improved by Atrey *et al.* [52, 131]. It is the simplest analytical model used to predict cooling power and refrigeration temperature of a pulse tube refrigerator. Isothermal model is based on following assumptions:

a. Working fluid behaves as an ideal gas.

b. Pressure variation is a trapezoidal function of time in pulse tube (Fig. 4.2).

c. Unlike previous works, a small pressure drop inside the cold and hot end heat exchangers is taken into account. Pressure variation within the system is constant with respect to time. It is further assumed that the pressure drops in the heat exchangers are proportional to flow rates.

d. Flow is fully developed within the pulse tube.

Based upon above assumptions, the pulse tube refrigerator is divided in to number of control volume as shown in Fig. 4.1.

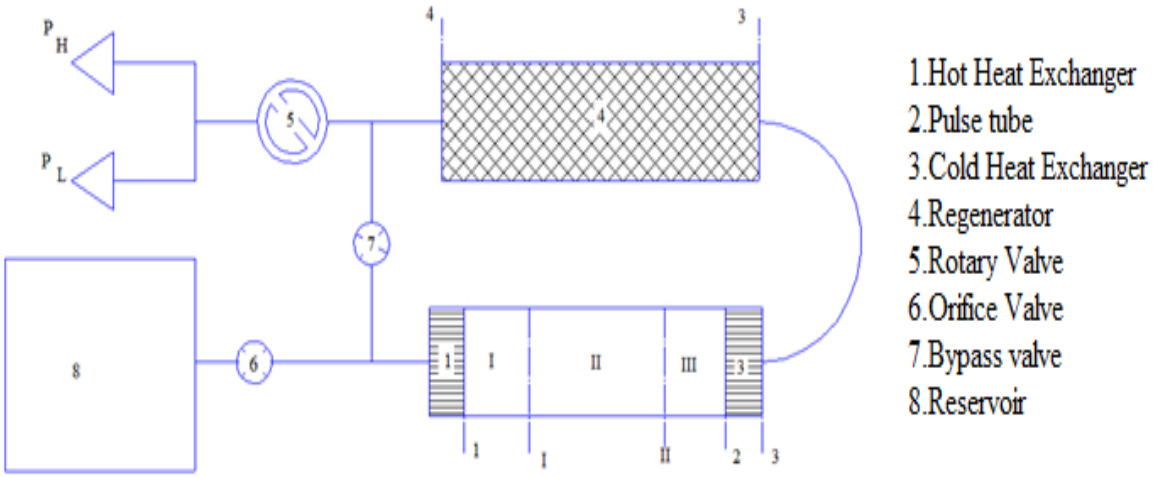

Figure 4.1: Schematic diagram of the GM-type pulse tube refrigerator.

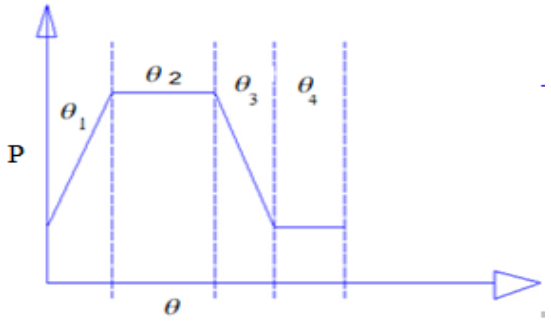

Figure 4.2: Variation of pressure in pulse tube.

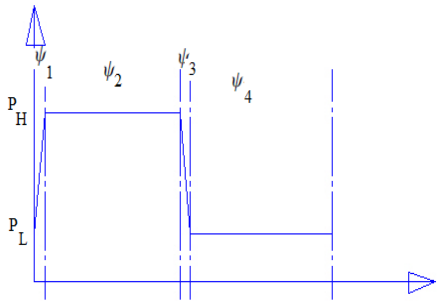

Figure 4.3: Variation of pressure in rotary valve.

4.1.1 Governing equations for isothermal model

Pressure variation within the rotary valve

$$P_r = \begin{cases} P_H \left[0 < t \le \tau/2 \right] \\ P_L \left[\tau/2 < t \le \tau \right] \end{cases} \tag{4.1}$$

Pressure variation within the pulse tube

$$P_{pt}(t) = \begin{cases} P_L + \left(\dfrac{(P_H - P_L)}{\theta_1} \right) \times t \left[0 < t \le \theta_1 \right] \\ P_H \left[\theta_1 < t \le \theta_2 \right] \\ P_H - \left(\dfrac{(P_H - P_L)}{\theta_3 - \theta_2} \right) \times (t - \theta_2) \left[\theta_2 < t \le \theta_3 \right] \\ P_L \left[\theta_3 < t \le \theta_4 \right] \end{cases} \tag{4.2}$$

Mass flow rate through the orifice valve

$$\dot{m}_o = \begin{cases} C_{do} A_o \left(\dfrac{2 \times \gamma}{(\gamma - 1)} \dfrac{{P_{pt}}^2}{R T_h} \left[\left(\dfrac{P_{res}}{P_{pt}} \right)^{2/\gamma} - \left(\dfrac{P_{res}}{P_{pt}} \right)^{\frac{\gamma+1}{\gamma}} \right] \right)^{0.5} & P_{pt} > P_{res} \\ -C_{do} A_o \left(\dfrac{2 \times \gamma}{(\gamma - 1)} \dfrac{{P_{res}}^2}{R T_h} \left[\left(\dfrac{P_{pt}}{P_{res}} \right)^{2/\gamma} - \left(\dfrac{P_{pt}}{P_{res}} \right)^{\frac{\gamma+1}{\gamma}} \right] \right)^{0.5} & P_{pt} < P_{res} \end{cases} \tag{4.3}$$

Mass flow rate through the bypass valve

$$\dot{m}_{di} = \begin{cases} C_{di} A_{di} \left(\dfrac{2 \times \gamma}{(\gamma - 1)} \dfrac{{P_{pt}}^2}{R T_h} \left[\left(\dfrac{P_L}{P_{pt}} \right)^{2/\gamma} - \left(\dfrac{P_L}{P_{pt}} \right)^{\frac{\gamma+1}{\gamma}} \right] \right)^{0.5} & P_{pt} > P_L \\ -C_{di} A_{di} \left(\dfrac{2 \times \gamma}{(\gamma - 1)} \dfrac{{P_H}^2}{R T_h} \left[\left(\dfrac{P_{pt}}{P_H} \right)^{2/\gamma} - \left(\dfrac{P_{pt}}{P_H} \right)^{\frac{\gamma+1}{\gamma}} \right] \right)^{0.5} & P_{pt} < P_H \end{cases} \tag{4.4}$$

Pressure variation within the reservoir

$$\frac{dP_{res}}{dt} = \frac{\dot{m}_o R T_h}{V_{res}} \tag{4.5}$$

Mass flow rate at section 1 of hot heat exchanger

$$\dot{m}_{hhx} = \dot{m}_o + \dot{m}_{di} + \frac{V_{hhx}}{RT_h}\frac{dP_{pt}}{dt} \tag{4.6}$$

Mass of gas in section I

$$m_I = m_{IO} + \int_0^t (-\dot{m}_{hhx})dt \tag{4.7}$$

where, m_{IO} is a constant determined by applying boundary condition $(m_I)_{\min} = 0$

Volume of gas in section I of pulse tube is

$$V_I = \frac{m_I RT_h}{P_{pt}} \tag{4.8}$$

Volume of gas in section II of pulse tube is

$$V_{II} = C_{IIO} P_{pt}^{(-1/\gamma)} \tag{4.9}$$

Volume of gas in section III of pulse tube is

$$V_{III} = V_2 - V_I - V_{II} \tag{4.10}$$

where, C_{IIO} is a constant which can be determined by using boundary condition $(V_{III})_{\min} = 0$

Mass flow rate at section 2 of pulse tube

$$\dot{m}_{pt} = \dot{m}_{hhx}\frac{T_h}{T_c} + \frac{V_{pt}}{\gamma RT_c}\frac{dP_{pt}}{dt} \tag{4.11}$$

Mass flow rate at section cold heat exchanger

$$\dot{m}_{chx} = \dot{m}_{pt} + \frac{V_{chx}}{RT_c}\frac{dP_{pt}}{dt} \tag{4.12}$$

Mass flow rate of gas at section regenerator

$$\dot{m}_{rg} = \dot{m}_{chx} + \frac{V_{rg}}{RT_{mrg}} \frac{dP_{pt}}{dt} \tag{4.13}$$

where, $T_{mrg} = \frac{T_h - T_c}{\ln\left(T_h / T_c\right)}$ (4.14)

Ideal refrigeration power

$$Q = f \oint P_{pt} V_{III} \tag{4.15}$$

4.2 Adiabatic Model

Neveu *et al.* [135] proposed an adiabatic model to obtain the cooling capacity of pulse tube refrigerator, which was further extended to two-stage pulse tube refrigerator by Kasthurirengan. The capability of this model is that real gas properties can be used in this model. So results will be more accurate and realistic as compared to other models. Liang *et al.* [136, 137] tried to simulate the working mechanism of the single stage PTR based on the thermodynamic behavior of gas elements as an adiabatic process in the pulse tube. In the present model the effect of losses related to regenerator, heat exchanger and pulse tube are taken into consideration.

The assumptions employed to simplify the analysis are listed as follows:

1. Axial heat conduction is neglected.
2. The regenerative material is incompressible and of uniform porosity.
3. The regenerator, heat exchangers at cold end and hot end are assumed to be perfect.
4. There is no heat transfer between elements of gas in the tube or between the gas and the tube wall (gas flow is adiabatic).
5. Linear variation of pressure and temperature in the regenerator and pulse tube.
6. Constant temperature in heat exchangers and aftercooler.

   Like isothermal model, in this case the entire pulse tube refrigerator is subdivided into small number of control volumes (Fig. 4.4).

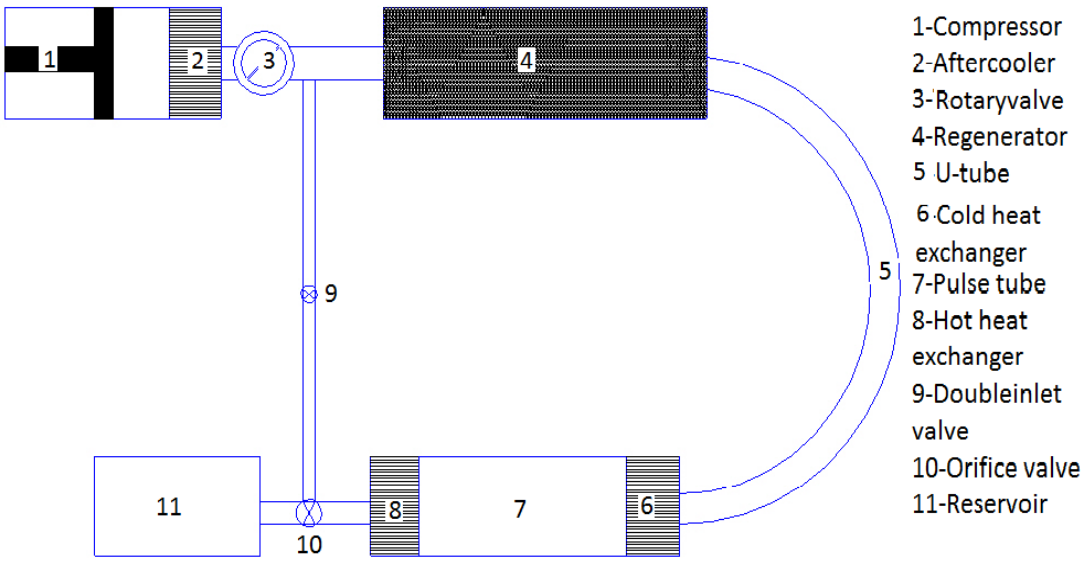

Figure 4.4: Schematic diagram of pulse tube refrigerator with control volume representation.

4.2.1 Governing equations of adiabatic model

Each component is assumed to be a control volume and by applying conservation of energy and mass

From first law of thermodynamics,

$$dq = dW + du + h\,dm \tag{4.16}$$

Since the process is adiabatic,

$$dq = 0 \tag{4.17}$$

Assuming ideal gas yields:

$$\frac{dm}{m} = \frac{dV}{V} + \frac{dP}{P} - \frac{dT}{T} \tag{4.18}$$

$$\text{where } \frac{dT}{T} = \frac{R}{cp}\frac{dP}{P} \tag{4.19}$$

Combining Eqs. (4.16), (4.17), (4.18) and (4.19),

$$PdV + \frac{V}{\gamma} dP = RTdm \tag{4.20}$$

From Eq. (4.18), the variation of mass, pressure, temperature and volume with time can be derived as:

$$\frac{dm}{dt} = \frac{1}{RT}\left[\frac{dV}{dt}P + \frac{V}{\gamma}\frac{dP}{dt}\right] \tag{4.21}$$

$$\frac{dP}{dt} = \frac{\gamma}{V}\left[\dot{m}RT - P\frac{dV}{dt}\right] \tag{4.22}$$

$$\frac{dT}{dt} = \frac{T^2}{P}\left[\frac{1}{T}\frac{dP}{dt} - \frac{\dot{m}R}{V}\right] \tag{4.23}$$

$$\frac{dV}{dt} = \dot{m}RT - \frac{V}{\gamma P}\frac{dP}{dt} \tag{4.24}$$

4.2.1.1 Compressor

Volume variation of compressor is

$$V_{cp}(t) = V_o + \frac{V_s}{2}\left(1 + \sin(2\pi ft)\right) \tag{4.25}$$

Variation of pressure of compressor with respect to time is

$$\frac{dP_{cp}}{dt} = \frac{\gamma}{V_{cp}}\left[-\dot{m}_{cp}RT_{cp} - P_{cp}\frac{dV_{cp}}{dt}\right] \tag{4.26}$$

Mass flow rate of compressor is

$$\dot{m}_{cp} = \dot{m}_{rg} + \dot{m}_{di} + \frac{V_{ac}}{RT_h}\frac{dP_{cp}}{dt} \tag{4.27}$$

In the present work, temperature of compressor is assumed to be constant.

4.2.1.2 Aftercooler

In the case of aftercooler, temperature is assumed to be constant and equal to atmospheric temperature. Variation of pressure with respect to time is equal to pressure variation of the compressor. Mass flow rate at the right side of aftercooler is equal to the algebraic sum of mass flow rate of regenerator and mass flow rate through the double inlet valve. Mass flow rate at the left-hand side is equal to mass flow rate of the compressor, as presented in Eq. (4.27).

4.2.1.3 Regenerator

Variation of temperature is logarithmic mean temperature difference. Linear variation of pressure, gas temperature, and matrix temperature on spatial coordinates:

Variation of temperature on space is

$$T_{mrg} = \frac{T_h - T_c}{\ln\left(T_h / T_c\right)} \tag{4.28}$$

Mass flow rate at the inlet to the regenerator is

$$\dot{m}_{rg} = \frac{\rho \pi d_{rg}^2 d_h^2}{600 L_{rg} \mu} \frac{\alpha^3}{1-\alpha} \left(P_{cp} - P_{pt}\right) \tag{4.29}$$

Mass flow rate at the outlet of the regenerator is equal to mass flow rate of the cold heat exchanger. Pressure drop across regenerator is

$$P_{rg}\left(x,t\right) = \frac{P_{cp}\left(t\right) - P_{pt}\left(t\right)}{L_{rg}} x_{rg} + P_{cp}\left(t\right) \tag{4.30}$$

Variation of matrix temperature is

$$T_m\left(x,t\right) = \frac{T_c - T_h}{L_{rg}} x_{rg} + T_h \tag{4.31}$$

Variation of gas temperature on spatial and temporal direction along length is given as

$$T_{rg}\left(x,t\right)=\varepsilon\frac{T_c-T_h}{L_{rg}}x_{rg}+\varepsilon T_h+T_h\left(1-\varepsilon\right) \tag{4.32}$$

4.2.1.4 Cold heat exchanger

The temperature of the cold heat exchanger is assumed to be refrigeration temperature and a constant. Pressure drop is neglected in the cold heat exchanger. Mass flow rate along cold heat exchanger is given by

$$\dot{m}_{chx}=\dot{m}_{pt}+\frac{V_{chx}}{RT_c}\frac{dP_{pt}}{dt} \tag{4.33}$$

Mass flow rate in the right-hand side of the cold heat exchanger is equal to mass flow rate along pulse tube.

4.2.1.5 Pulse tube

Variation of pressure of pulse tube with time is given by

$$\frac{dP_{pt}}{dt}=\frac{R\left(\dot{m}_{cp}-\dot{m}_{di}\right)-R\left(\dot{m}_o-\dot{m}_{di}\right)\frac{T_h}{T_c}-\frac{V_{ac}}{T_h}\frac{dP_{cp}}{dt}}{\frac{V_{rg}}{T_{mrg}}+\frac{V_{chx}}{T_c}+\frac{V_{pt}}{\gamma T_c}+\frac{V_{hhx}}{T_c}} \tag{4.34}$$

Variation of pressure on spatial coordinate has been neglected. Mass flow rate of pulse tube is given by

$$\dot{m}_{pt}=\dot{m}_{hhx}\frac{T_h}{T_c}+\frac{V_{pt}}{\gamma RT_c}\frac{dP_{pt}}{dt} \tag{4.35}$$

Variation of temperature with respect to temporal step is given by

$$\frac{dT_{pt}}{dt}=\frac{T_{pt}}{P_{pt}}\frac{dP_{pt}}{dt}-\frac{RT_{pt}^2}{P_{pt}V_{pt}}\left(\dot{m}_{pt}-\dot{m}_{hhx}\right) \tag{4.36}$$

Variation of temperature along with space coordinate is assumed to be linear.

4.2.1.6 Hot heat exchanger

Mass flow rate through the hot heat exchanger is

$$\dot{m}_{hhx} = \left(\dot{m}_o - \dot{m}_{di}\right) + \frac{V_{hhx}}{RT_h}\frac{dP_{pt}}{dt} \tag{4.37}$$

Temperature of hot heat exchanger is assumed to be constant. Mass flow rate at the right-hand side of the hot heat exchanger is algebraic sum of mass flow rate of the orifice and double inlet valve.

4.2.1.7 Orifice valve

Mass flow rate through the orifice valve is calculated by

$$\dot{m}_o = C_{do}A_o\sqrt{\frac{2\gamma}{\gamma-1}\frac{P_{pt}^2}{RT_h}\left[\left(\frac{P_{res}}{P_{pt}}\right)^{2/\gamma} - \left(\frac{P_{res}}{P_{pt}}\right)^{\frac{\gamma+1}{\gamma}}\right]} \quad P_{pt} > P_{res} \tag{4.38}$$

$$\dot{m}_o = -C_{do}A_o\sqrt{\frac{2\gamma}{\gamma-1}\frac{P_{res}^2}{RT_h}\left[\left(\frac{P_{pt}}{P_{res}}\right)^{2/\gamma} - \left(\frac{P_{pt}}{P_{res}}\right)^{\frac{\gamma+1}{\gamma}}\right]} \quad P_{pt} < P_{res} \tag{4.39}$$

4.2.1.8 Double inlet valve

Mass flow rate through the double inlet valve is calculated by using

$$\dot{m}_{di} = C_{di}A_{di}\sqrt{\frac{2\gamma}{\gamma-1}\frac{P_{cp}^2}{RT_h}\left[\left(\frac{P_{pt}}{P_{cp}}\right)^{2/\gamma} - \left(\frac{P_{pt}}{P_{cp}}\right)^{\frac{\gamma+1}{\gamma}}\right]} \quad P_{pt} < P_{cp} \tag{4.40}$$

$$\dot{m}_{di} = -C_{di}A_{di}\sqrt{\frac{2\gamma}{\gamma-1}\frac{P_{pt}^2}{RT_h}\left[\left(\frac{P_{cp}}{P_{pt}}\right)^{2/\gamma} - \left(\frac{P_{cp}}{P_{pt}}\right)^{\frac{\gamma+1}{\gamma}}\right]} \quad P_{pt} > P_{cp} \tag{4.41}$$

4.2.1.9 Reservoir

Pressure variation of reservoir is given by

$$\frac{dP_{res}}{dt} = \frac{\dot{m}_o R T_h}{V_{res}} \tag{4.42}$$

The temperature of the reservoir is assumed to be equal to the temperature of the atmosphere.

Cooling power is estimated by using the following relation given by Nika *et al.* [74, 75]:

$$\dot{Q}_c = \frac{V_{chx}}{\gamma - 1}\left[1 - \gamma \frac{T_{rgo}}{T_c}\right]\frac{dP_{pt}}{dt} + C_p\left(T_{rgo} - T_c\right)\dot{m}_{chx} \tag{4.43}$$

Work supplied by the compressor is

$$W = -P_{cp}\frac{dV_{cp}}{dt} + RT_h\dot{m}_{cp} \tag{4.44}$$

The actual refrigeration power differs from ideal refrigeration power due to losses in various components in the pulse tube refrigerator. These losses are discussed in detail as below.

Solution procedure

Table 4.1: Components and parameters declarations.

Component	**Variables**	**Geometrical parameters**	**Constants**
Compressor	$V_{cp}(t), P_{cp}(t),$ $\dot{m}_{cp}(t)$	V_o, V_s	V_o, V_s
Aftercooler	$\dot{m}_{ac}(t)$	Dimensions(V_{ac})	Dimensions(V_{ac})
Regenerator	$\dot{m}_{rg}(t), P_{rg}(x,t)$, $T_s(x,t), T_{rg}(x,t)$	ε,Dimensions	Dimensions
Cold heat exchanger	$\dot{m}_{chx}(t)\ P_t(t)$	Dimensions	Dimensions
Pulse tube	$\dot{m}_{pt}(t)\ P_{pt}(t)\ T_{pt}(t)$	Dimensions	Dimensions
Hot heat exchanger	$\dot{m}_{hhx}(t)\ P_{pt}(t)$	Dimensions	Dimensions

Orifice valve	$\dot{m}_o(t)$	Dimensions	Dimensions
Double inlet valve	$\dot{m}_{di}(t)$	Dimensions	Dimensions
Reservoir	$P_{res}(t)$	Dimensions	Dimensions

In the above, there are 21 numbers of equations.

Operating parameters: $V_o, V_s, f, T_h, T_c, C_{di}, C_o$

Geometrical parameters: $V_{ac}, V_{chx}, V_{hhx}, V_{res}, A_{di}, A_o, V_{rg}, d_h, \varepsilon, \alpha$

Constants: $\gamma, R \ \pi$

Variables: $V_{cp}(t), P_{cp}(t), P_t(t), P_r(t), P_{rg}(x,t), \dot{m}_{cp}(t), \dot{m}_{rg}(t), \dot{m}_c(t),$
$\dot{m}_t(t), \dot{m}_h(t), T_{rg}(x,t), T_s(x,t)$

All the coupled nonlinear differential equations (Eqs. (4.21)-4(.24)) are solved by using numerical methods. In the present case, Runge-Kutta method of order four has been implemented to solve above set of equations. The details of the solution procedure is presented in the Appendix-I. Table4.1 shows different components, variables with associated parameters in tabular form.

4.3 Loss analysis

The actual refrigeration power produced in a pulse tube refrigerator differs from this gross refrigeration power due to loss in the regenerator, heat exchangers, pulse tube and valves. These losses are responsible for reducing the cooling power [130].

4.3.1 Regenerator ineffectiveness loss

The fractional period is the total period of total cycle time during which the steady flow gas enters into the regenerator. If the effect of pressure changes during gas flow through the regenerator taken into consideration then

$$Q_{il} = \left(\frac{\dot{m}_{rg} C_{vg} \left(T_h - T_c \right)}{NSTEP} \right) \frac{2}{2 + NTU} \tag{4.45}$$

This loss is calculated on a cyclic basis, and the total refrigeration power loss due to ineffectiveness is obtained by adding individual losses.

4.3.2 Temperature swing loss

This loss is due to variation of matrix temperature with respect to time. It will be calculated as follows:

$$DELTX = \left(\frac{\dot{m}_{rg}}{NSTEP} \right) \left(T_h - T_c \right) \frac{C_{vg}}{\omega M_m \left(C_p \right)_m} \tag{4.46}$$

This loss is calculated during the pressurization process of the cycle

$$Q_{ts} = \left(\frac{\dot{m}_{rg}}{NSTEP} \right) C_{vg} \frac{DELTX}{2} \tag{4.47}$$

4.3.3 Conduction loss

Conduction loss in pulse tube wall is

$$QC_{pt} = k_{pt} A_{pt} \left(\frac{T_h - T_c}{L_{pt}} \right) \tag{4.48}$$

Conduction loss in regenerator wall is

$$QC_{rg} = k_{rg} A_{rg} \left(\frac{T_h - T_c}{L_{rg}} \right) \tag{4.49}$$

Conduction loss in regenerator matrix is

$$QC_m = k_m A_m \left(\frac{T_h - T_c}{L_{rg}} \right) \tag{4.50}$$

$$k_m = k_g \frac{K_X - (1-\alpha)}{K_X + (1-\alpha)} \tag{4.51}$$

$$K_X = \frac{1 + \left(k_{rg} / k_g \right)}{1 - \left(k_{rg} / k_g \right)} \tag{4.52}$$

Total conduction loss is equal to

$$QC_{total} = QC_{pt} + QC_{rg} + QC_m \tag{4.53}$$

4.3.4 Void volume at cold end

If there is any connecting pipe between the cold regenerator end and cold end heat exchanger some amount of gas remains inside this pipe and does not contribute to the cooling effect. This is termed as void volume loss and given by

$$Q_{vv} = \left(P_H - P_L \right) V_d \tag{4.54}$$

4.3.5 Loss due to pressure drop in regenerator

The loss due to pressure drop in regenerator has been calculated following [138].

$$Q_{pd} = \Delta p \left(\frac{PR + 1}{PR} \right) V_{rg} \tag{4.55}$$

The pressure drop along the regenerator can be computed by using the following formula adopted from [139].

$$\Delta p = \frac{fr}{2} \frac{L_{rg}^{\ 2}}{d_h} \frac{G^2}{\rho} \tag{4.56}$$

4.3.6 Loss due to radiation

Radiation loss takes place due to heat exchange between vacuum chamber and cold heat exchanger of the pulse tube refrigerator, which can be minimized by multi-layered insulation [140].

$$Q_{rd} = \frac{\sigma F A_C \left(T_h^4 - T_c^4\right)}{\frac{1}{e_c} + \frac{1}{e_s} - 1 + \left(N_I - 1\right)\left(\frac{2}{e_s} - 1\right) + \frac{1}{e_h} + \frac{1}{e_s} - 1} \tag{4.57}$$

Net refrigeration power is

$$Q_{net} = Q_{ideal} - \left(Q_{il} + Q_{ts} + QC_{total} + Q_{vv} + Q_{pd} + Q_{rd}\right) \tag{4.58}$$

4.4 Numerical Model

Numerical model followed is a third-order model, that predicts much accurate result in agreement with experimental values but the computational time is little bit longer. The governing equations are continuity, momentum, energy equations of fluid and energy equation of wall as given in [141-144]. It is based on following assumptions:

- Working fluid is ideal.
- Gas is incompressible in regenerator and heat exchangers, whereas compressible in other parts.
- Constant temperature is considered to be isothermal in cold heat exchanger, hot heat exchanger and after coolers.

4.4.1 Governing equations

Continuity equation is

$$\frac{\partial m_i}{\partial t} = \dot{m}\Big|_{i+1}^{i} \tag{4.59}$$

Momentum equation is given by

$$\frac{\partial}{\partial t}\left(mu\right)_{f,i} + \left[\dot{m}u\right]_{cv,i-1}^{cv,i} + A_i\left(P_i - P_{i-1}\right) - \left(\frac{\mu}{\varphi}\alpha u + \frac{C_f \rho}{\sqrt{\varphi}}\alpha^2 u\left|u\right|\right)_{f,i} A_i \delta\xi_i - m_{f,i} g\cos\theta = 0 \tag{4.60}$$

Energy equation of fluid is

$$\frac{\partial}{\partial t}\left(m\frac{u^2}{2}+mc_vT \right)_{cv,i}+h_iA_{L,i}\left(T_i^l-T_{s,i}^l \right)-P_i\frac{dV_i}{dt}=\left(\dot{m}\frac{u^2}{2}+\dot{m}c_pT-kA\frac{\partial T}{\partial x} \right)\Bigg|_{f,i+1}^{f,i} \tag{4.61}$$

Energy equation of solid wall is

$$\frac{\partial}{\partial t}\left(m_sc_sT_s \right)_{cv,i}+h^l{}_iA_{L,i}\left(T_{s,i}^l-T_i^l \right)+\left(\zeta k_s^lA_s^l\frac{\partial T_s}{\partial x} \right)\Bigg|_{f,i+1}^{f,i}=q_cV_{s,cv,i} \tag{4.62}$$

Ideal gas equations

$$P_iV_i=m_iRT_i \tag{4.63}$$

The finite volume discretized mesh is shown in Fig. 4.12. Pressure, temperature, density, mass are calculated at the centre of control volume (red line in Fig. 4.12) whereas mass flow rate, velocity and enthalpy are calculated at faces of control volume (black line in Fig. 4.12). The continuity and momentum equations are converted into single algebraic equation by using ideal gas equation to improve speed of calculation [141].

$$Z_{1,i}\dot{m}_{i-2}^l+Z_{2,i}\dot{m}_{i-1}^l+Z_{3,i}\dot{m}_i^{\,l}+Z_{4,i}\dot{m}_{i+1}^l+Z_{5,i}\dot{m}_{i+2}^l=B_i \tag{4.64}$$

The coefficients for second order time step are

$$Z_{1,i}=\psi_{2,i-1}\max\left(u_{cv,i-1}^l,0 \right) \tag{4.65}$$

$$Z_{2,i}=-\psi_{2,i}\max(u_{cv,i}^l,0)-\psi_{1,i-1}\max\left(u_{cv,i-1}^l,0 \right)-A_i\delta\eta\frac{RT_{i-1}^l}{1.5V_{i-1}} \tag{4.66}$$

$$\begin{aligned}Z_{3,i}=1.5\frac{\delta\xi_i}{\delta\eta}+\psi_{1,i}\max\left(u_{cv,i}^l,0 \right)-\psi_{3,i-1}\min\left(u_{cv,i-1}^l,0 \right)+A_i\delta\eta\frac{R}{1.5}\left(\frac{T_i^l}{V_i}+\frac{T_{i-1}^l}{V_{i-1}} \right)+\\ \left(F_{1,i}\frac{RT_{f,i}^lu_{f,i}^l}{P_{f,i}^l}+F_{2,i}\left| u_i^l \right| \right)\delta\xi_i\end{aligned} \tag{4.67}$$

$$Z_{4,i}=\psi_{3,i}\min\left(u_{cv,i}^l,0 \right)+\psi_{4,i-1}\min\left(u^l{}_{cv,i-1},0 \right)-A_i\delta\eta\frac{RT_i^l}{1.5V_i} \tag{4.68}$$

$$Z_{5,i}=-\psi_{4,i}\min\left(u_{cv,i}^l,0 \right) \tag{4.69}$$

$$B_i = \frac{\delta\xi_i}{\delta\eta}\left(2\dot{m}_i^{l-1} - 0.5m_i^{l-2}\right) - A_i\left(2\frac{P_i^{l-1}}{T_i^{l-1}} - 0.5\frac{P_i^{l-2}}{T_i^{l-2}}\right)\frac{T_i^l}{1.5} + A_i\left(2\frac{P_{i-1}^{l-1}}{T_{i-1}^{l-1}} - 0.5\frac{P_{i-1}^{l-2}}{T_{i-1}^{l-2}}\right)\frac{T_{i-1}^l}{1.5} + \left(\frac{P_{f,i}^l}{RT_{f,i}^l}\right)A_i\delta\xi_i g\cos\theta \tag{4.70}$$

By the similar procedure, the energy equation of fluid is converted into following algebraic equation[141]:

$$Z_{1,i}T^l{}_{i-2} + Z_{2,i}T^l{}_{i-1} + Z_{3,i}T_i^l + Z_{4,i}T^l{}_{i+1} + Z_{5,i}T^l{}_{i+2} = B_i \tag{4.71}$$

In second order time steps, the coefficients are

$$Z_{1,i} = \psi_{6,i}\max\left(\dot{m}_i^l c_{p,f,i}^l, 0\right) \tag{4.72}$$

$$Z_{2,i} = -\psi_{6,i+1}\max\left(\dot{m}_{i+1}^l c_{p,f,i+1}^l, 0\right) - \psi_{5,i}\max\left(\dot{m}_i^l c_{p,f,i}^l, 0\right) - \frac{k_{f,i}^l A_i}{\delta\xi_i} \tag{4.73}$$

$$Z_{3,i} = 1.5\left(\frac{P_i^l V_i}{RT_i^l}\right)\frac{c_{v,i}^l}{\delta\eta} + \psi_{5,i+1}\max\left(\dot{m}_{i+1}^l c_{p,f,i+1}^l, 0\right) - \psi_{7,i}\min\left(\dot{m}_i^l c_{p,f,i}^l, 0\right) + \left(\frac{k_{f,i}^l A_i}{\delta\xi_i} + \frac{k_{f,i+1}^l A_{i+1}}{\delta\xi_{i+1}}\right) + h_i^l A_{L,i} \tag{4.74}$$

$$Z_{4,i} = \psi_{7,i+1}\,min\left(\dot{m}_{i+1}^l c_{p,f,i+1}^l, 0\right) + \psi_{8,i}\,min\left(\dot{m}_i^l c_{p,f,i}^l, 0\right) - \frac{k_{f,i+1}^l A_{i+1}}{\delta\xi_{i+1}} \tag{4.75}$$

$$Z_{5,i} = -\psi_{8,i+1}\min\left(\dot{m}_{i+1}^l c_{p,f,i+1}^l, 0\right) \tag{4.76}$$

$$B_i = \left(2P_i^{l-1}c_{v,i}^{l-1} - 0.5P_i^{l-2}c_{v,i}^{l-2}\right)\frac{V_i}{R\delta\eta} + h_i^l A_{L,i}^l T_{s,i}^l - 0.5\left[\left(1.5\frac{P_i^l\left(u_{cv,i}^l\right)^2}{T_i^l} - 2\frac{P_i^{l-1}\left(u_{cv,i}^{l-1}\right)^2}{T_i^{l-1}} + 0.5\frac{P_i^{l-2}\left(u_{cv,i}^{l-2}\right)^2}{T_i^{l-2}}\right)\frac{V_i}{R\delta\eta} + \dot{m}_{i+1}^l\left(u_{i+1}^l\right)^2 - \dot{m}_i^l\left(u_i^l\right)^2\right] \tag{4.77}$$

Energy equation of solid [141]:

$$Z_{1,i}T_{s,i-1}^l + Z_{2,i}T_{s,i}^l + Z_{3,i}T_{s,i+1}^l = B_i \tag{4.78}$$

In second order time step, coefficients are

$$Z_{1,i} = -\frac{\zeta k_{s,i}^l A_{s,i}}{\delta\xi_i} \tag{4.79}$$

$$Z_{2,i} = 1.5\frac{m_{s,i}c_{s,i}^{l}}{\delta\eta} + \frac{\zeta_i k_{s,i}^{l} A_{s,i}}{\delta\xi_i} + \frac{\zeta_{i+1} k_{s,i+1}^{l} A_{s,i+1}}{\delta\xi_{i+1}} + h_i^{l} A_{L,i} \tag{4.80}$$

$$Z_{3,i} = -\frac{\zeta_{i+1} k_{s,i+1}^{l} A_{s,i+1}}{\delta\xi_{i+1}} \tag{4.81}$$

$$B_i = \left[\frac{2m_{s,i}c_{s,i}^{l-1}T_{s,i}^{l-1} - 0.5m_{s,i}c_{s,i}^{l-2}T_{s,i}^{l-2}}{\delta\eta}\right] + h_i^{l} A_{L,i} T_i^{l} \tag{4.82}$$

The pressure and temperature at the interface of the control volume are estimated as [141]

$$P_{f,i}^{l} = \frac{\Delta\xi_{i-1}P_i^{l} + \Delta\xi_i P_{i-1}^{l}}{\Delta\xi_{i-1} + \Delta\xi_i} \tag{4.83}$$

$$T_{f,i}^{l} = \begin{cases} \psi_{5,i}T_{i-1}^{l} - \psi_{6,i}T_{i-2}^{l} & m_i^{l} \geq 0 \\ \psi_{7,i}T_i^{l} - \psi_{8,i}T_{i+1}^{l} & m_i^{l} < 0 \end{cases} \tag{4.84}$$

The various geometrical parameters are explained as follows: [141]

Geometrical parameters are

$$\psi_{1,i} = \frac{\Delta\xi_i + 2\Delta\xi_{i-1}}{2\Delta\xi_{i-1}} \qquad \psi_{2,i} = \frac{\Delta\xi_i}{2\Delta\xi_{i-1}}$$

$$\psi_{3,i} = \frac{\Delta\xi_i + 2\xi_{i+1}}{2\Delta\xi_{i+1}} \qquad \psi_{4,i} = \frac{\Delta\xi_i}{2\xi_{i+1}} \tag{4.85}$$

$$\psi_{5,i} = \frac{\Delta\xi_{i-1} + 2\delta\xi_{i-1}}{2\delta\xi_{i-1}} \qquad \psi_{6,i} = \frac{\Delta\xi_{i-1}}{2\delta\xi_{i-1}}$$

$$\psi_{7,i} = \frac{2\delta\xi_{i+1} + \Delta\xi_i}{2\delta\xi_{i+1}} \qquad \psi_{8,i} = \frac{\Delta\xi_i}{2\delta\xi_{i+1}}$$

4.4.2 Initial conditions and boundary conditions

Since it is a transient problem, initial conditions are essential to solve the equations [141].

$$\dot{m}(x,0) = 0 \tag{4.86}$$

$$P(x,0) = P_{charging} \tag{4.87}$$

$$T(x,0) = T_s(x,0) = given\ \ by\ user \tag{4.88}$$

Boundary conditions are

$$P_i^l \frac{dV_i^l}{dt} = \frac{\dot{m}_{comp}^l RT_i^l}{V_i^l}\left[-V_s \pi f \cos(\omega t)\right] \tag{4.89}$$

No slip conditions are given as velocity boundary conditions at the walls, mass flow rate is zero at the wall and temperature as surface temperature.

The friction factor terms are [141]:

$$fr_{f,i}^l = \begin{cases} \dfrac{64}{Re_{f,i}^l} & Re_{f,i}^l < 2\times10^3 \\ \dfrac{124}{Re_{f,i}^l} + 0.0143 & 2\times10^3 \le Re_{f,i}^l \le 5\times10^5 \end{cases} \tag{4.90}$$

$$fr^l{}_{f,i} = \begin{cases} 0.316\,Re^{-0.25} & 3500 < Re < 2\times10^4 \\ 0.184\,Re^{-0.2} & Re > 2\times10^4 \end{cases} \tag{4.91}$$

where, Reynolds Number become

$$Re_{f,i}^l = \frac{\rho_{f,i}^l \left|u_i^l\right| d_{h,i}}{\mu^l{}_{f,i}} = \frac{u_i^l d_{h,i}}{\nu^l{}_{f,i}} \tag{4.92}$$

Hydraulic diameter related to wire diameter is

$$d_{h,i} = \frac{\alpha}{1-\alpha} d_{w,i} \tag{4.93}$$

Nusselt number for transfer of heat between regenerator, aftercooler and heat exchanger [145]

$$Nu_i^l = \left[1 + 0.99\left(Re_i^l\, Pr_i\right)^{0.66}\right]\alpha_i^{1.79} \tag{4.94}$$

Nusselt number for transfer of pipe sections is [146]

$$Nu_i^l = 1.86\left(Re_i^l\, Pr_i^l \frac{d_h}{\Delta\xi_i}\right)^{0.332}\left(\frac{\mu}{\mu_{s,w}}\right)^{1.14} \tag{4.95}$$

$$Pr_i^l = \frac{\mu_i^l c_{p,i}^l}{k_i^l} \tag{4.96}$$

For turbulent flow inside the pipe, the following correlations are used:

$$Nu_i^l = 0.023\left(Re_i^l\right)^{0.8}\left(Pr_i^l\right)^{0.4} \tag{4.97}$$

The solution procedure is explained in detailed in the Appendix-II.

4.5 CRESP-PTR software descriptions

This section describes the detailed interface design of CRESP-PTR software. It consists of a main interface that accepts input information's from the user. A plot screen displays interactive plots and graphs. An output screen displays results. Figure 4.5 shows the input interface that accepts geometrical parameters related to various components of pulse tube refrigerator and operating parameters. Toolbar and menu icons are also included in the software to improve its reliability. The user has the freedom to choose the material of solid from drop down list. Then after clicking "*enter*" button or hitting "*run*" icon in toolbar, it will solve the equations described above. After the solution converges, results will be displayed in the output screen and may be stored for future references. Plot screen shown in Fig. 4.6 will appear once the user will call it. Interactive plots will be generated after user chooses it from dropdown popup list.

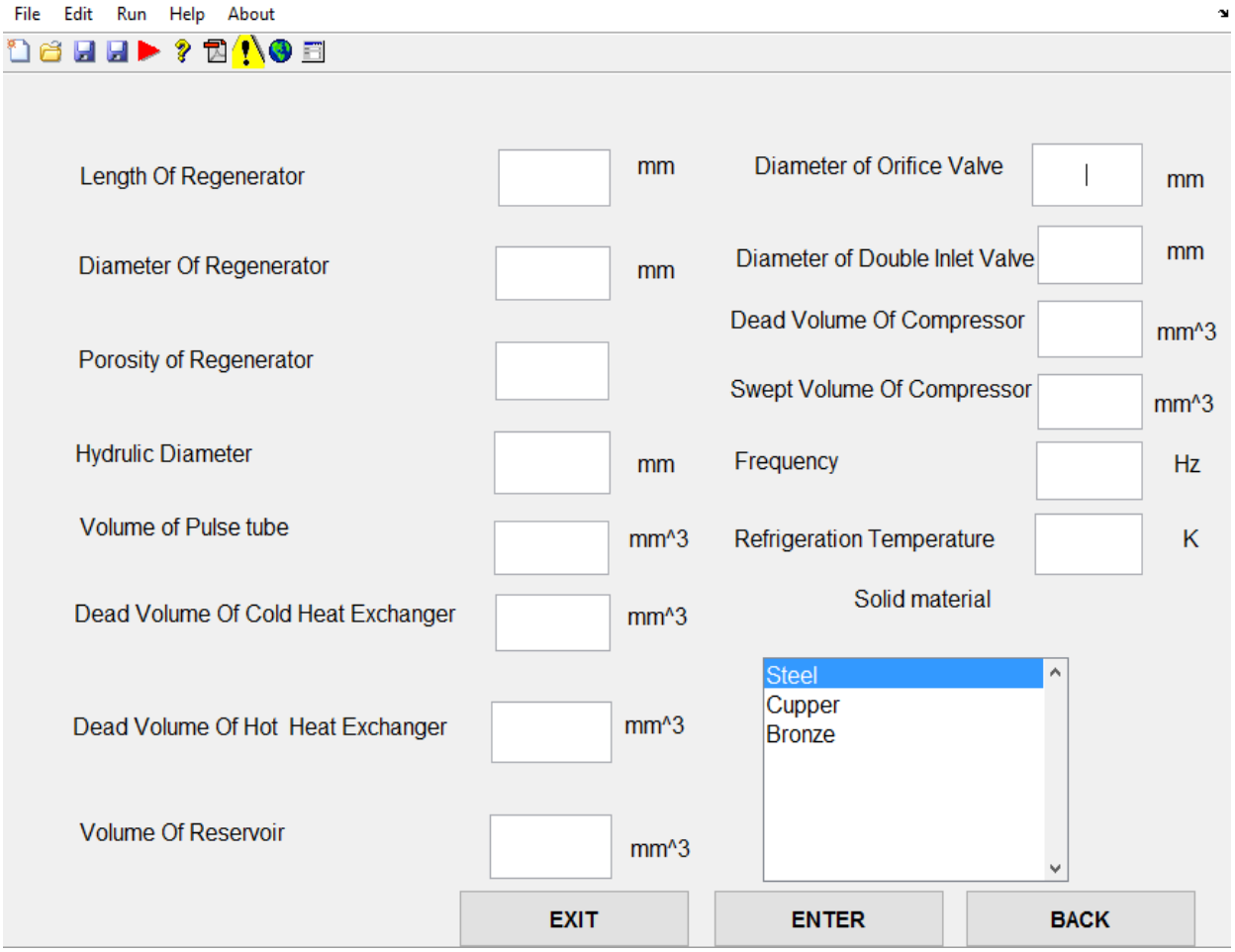

Figure 4.5: Input screen for CRESP-PTR pulse tube model.

The various kinds of plots presented in the popup menu are described in Fig. 4.7. The variation of various important variables such as pressure, temperature, density, mass flow rate at each and every locations at the inlet and outlet of components can be plotted both in spatial and temporal directions. Figure 4.8 shows the detail descriptions of various menu items of the software.

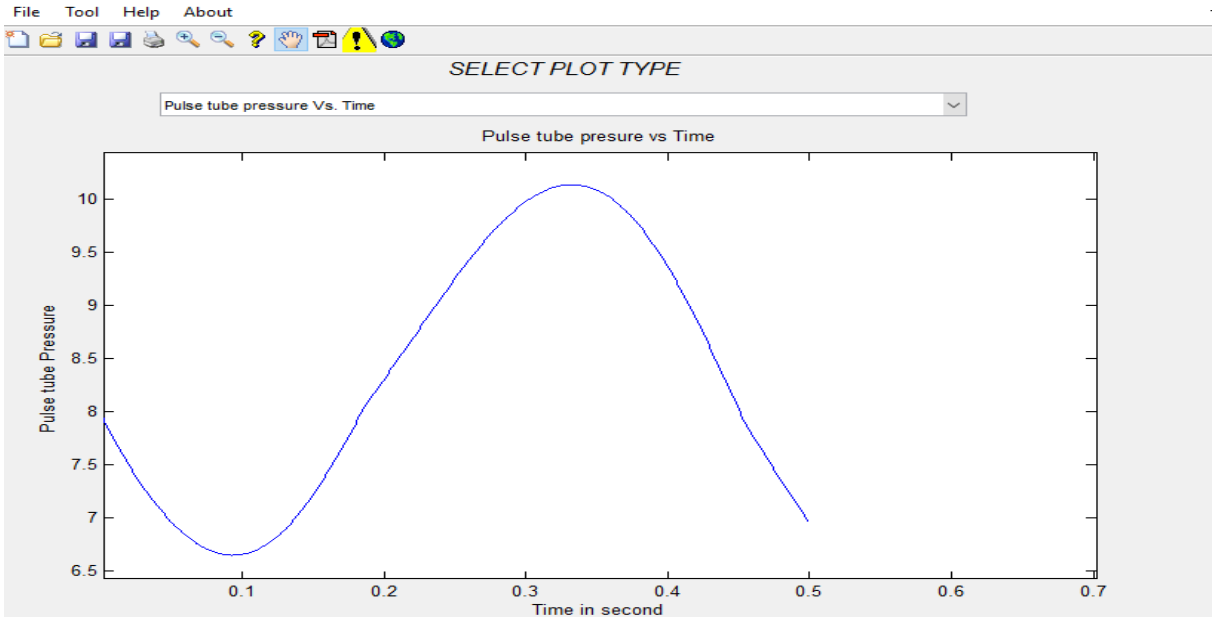

Figure 4.6: Plot screen for CRESP-PTR pulse tube model.

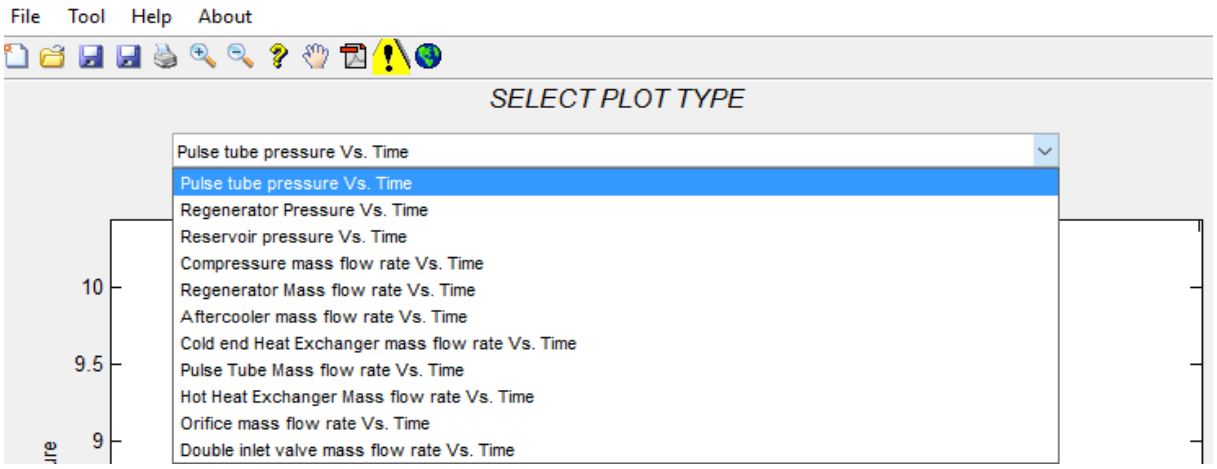

Figure 4.7: Various plot options in CRESP-PTR pulse tube model plot screen.

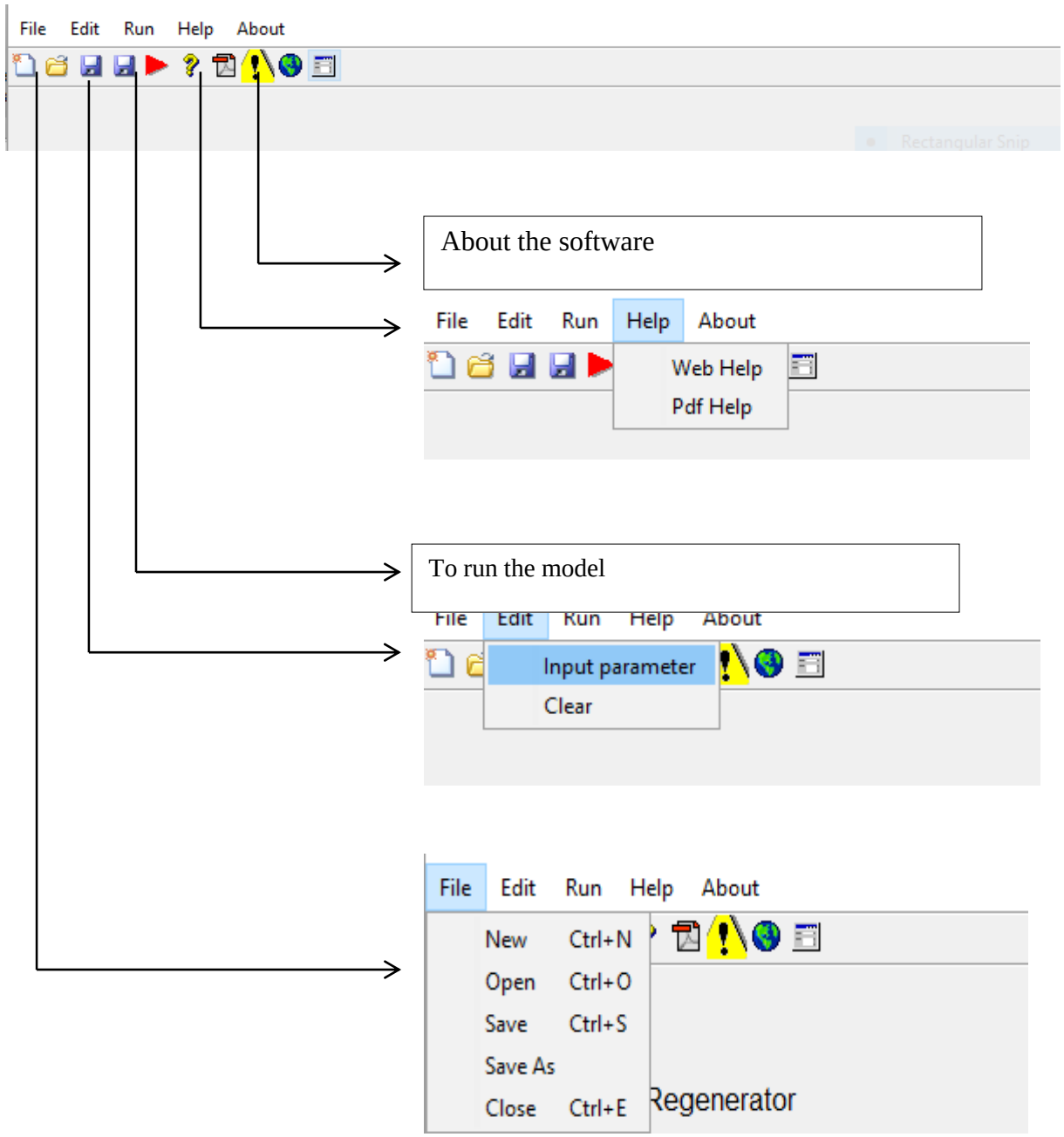

Figure 4.8: Various menu items in CRESP-PTR pulse tube model input screen.

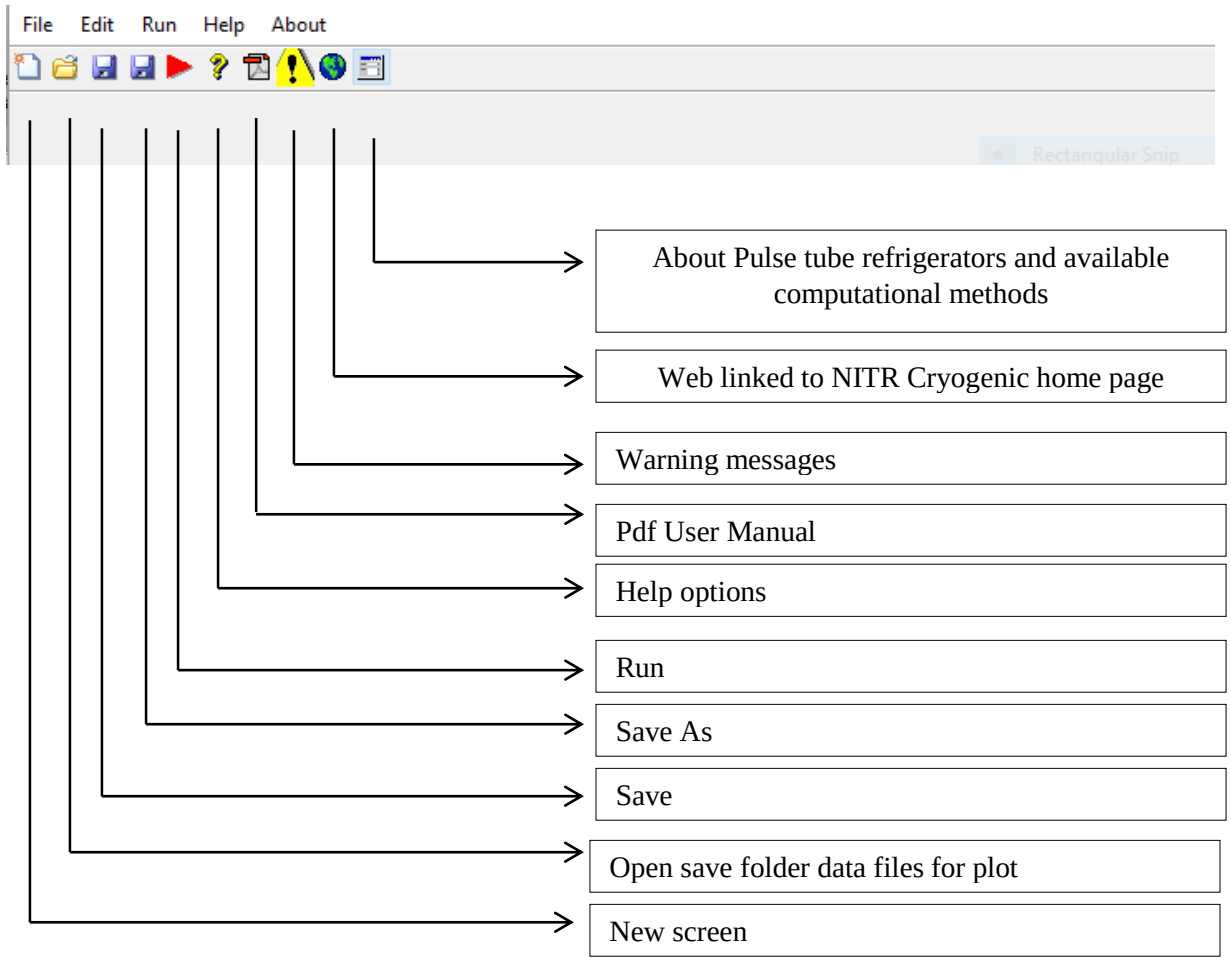

Figure 4.9: Various toolbar items in CRESP-PTR pulse tube model input screen.

Various menu items of input screens are described in Fig. 4.8. The detailed descriptions of toolbar icons of input screen are shown in Fig. 4.9. The menu items plot screens are explained in Fig. 4.10.

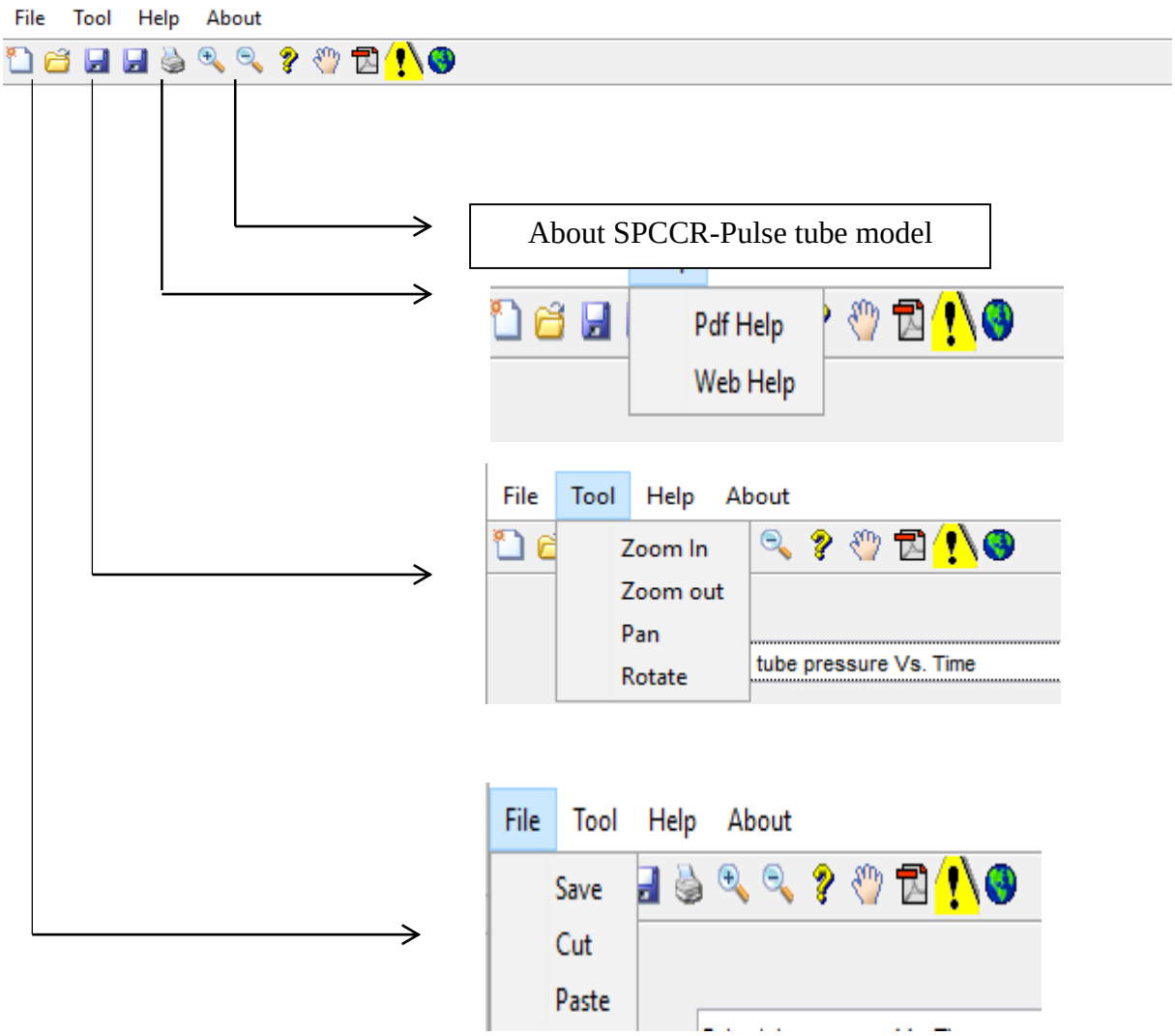

Figure 4.10: Various menu items in CRESP-PTR pulse tube model plot screen.

Different toolbar icons of plot screens are well explained in Fig. 4.11.

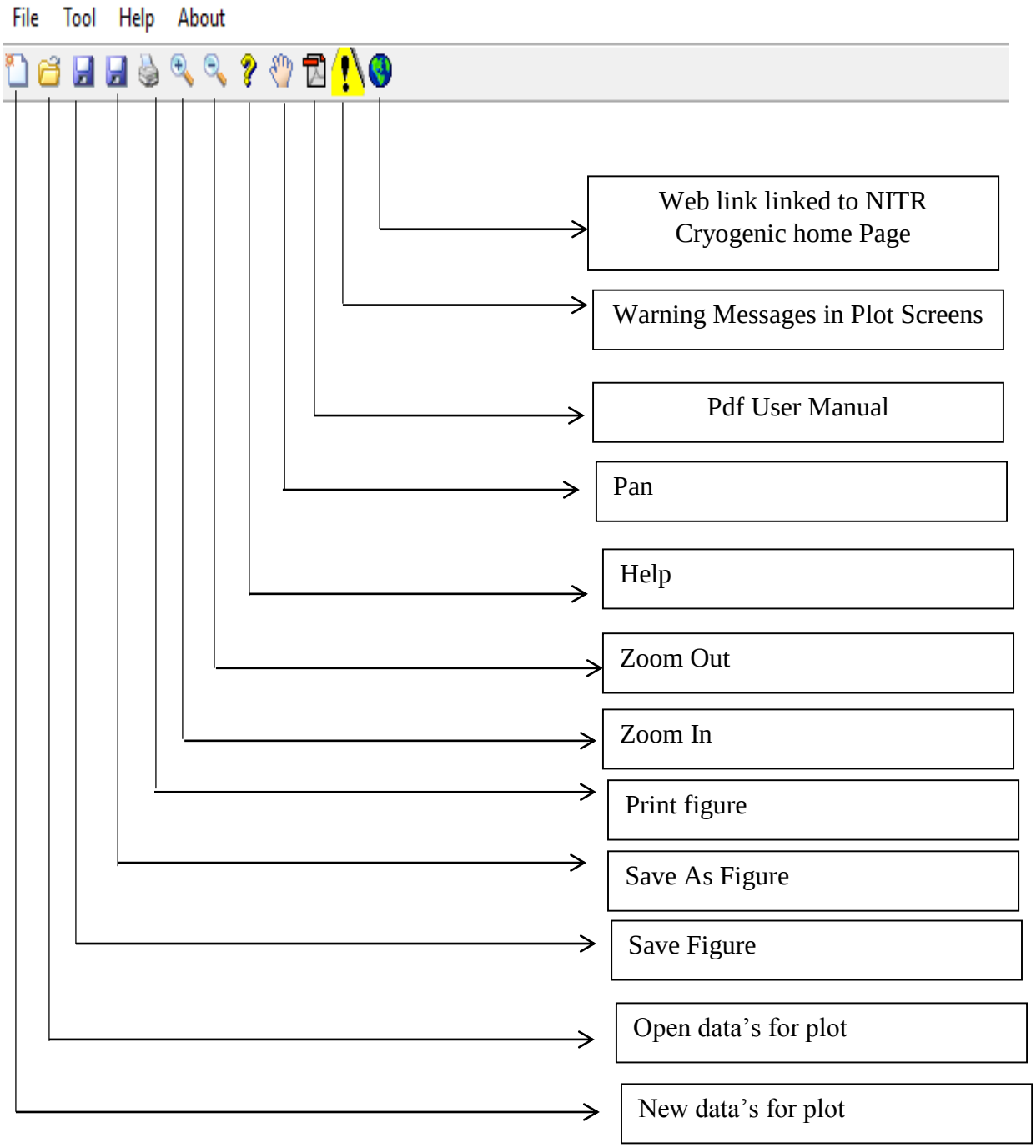

Figure 4.11: Various toolbar items in CRESP-PTR pulse tube model plot screen.

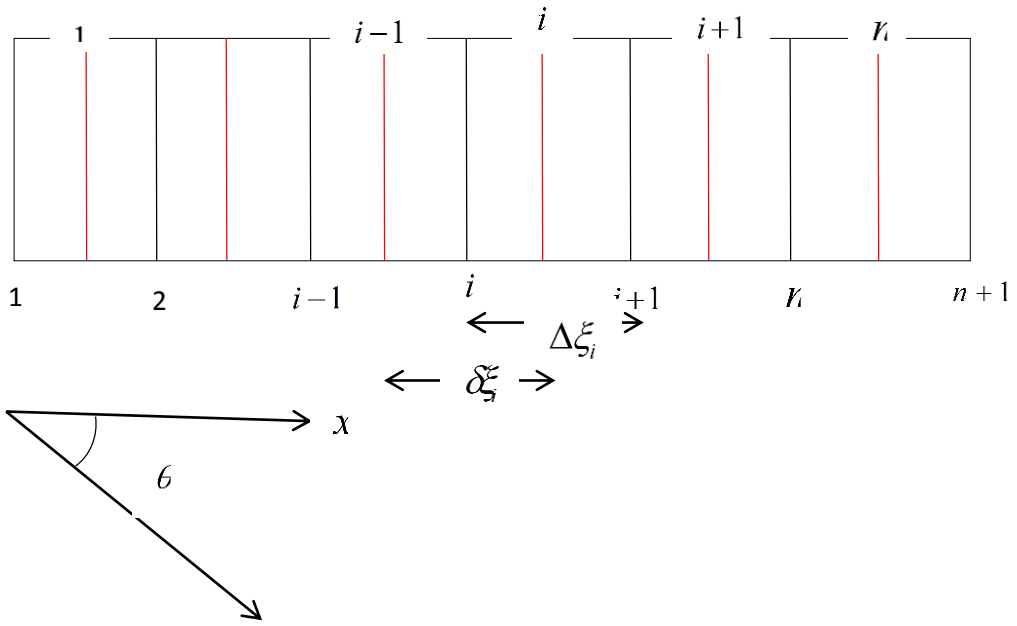

Figure 4.12: Discretization of control volume.

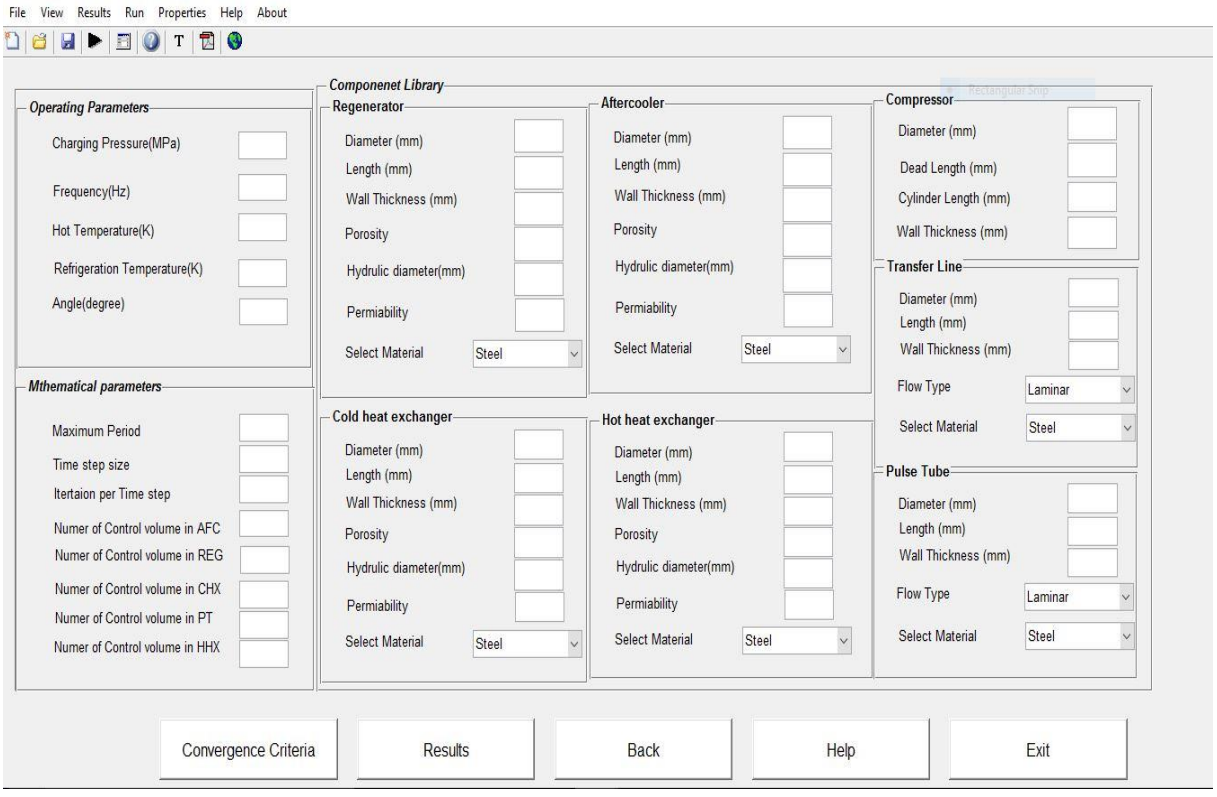

Figure 4.13: Input interface of CRESP-SPTR BPTR module.

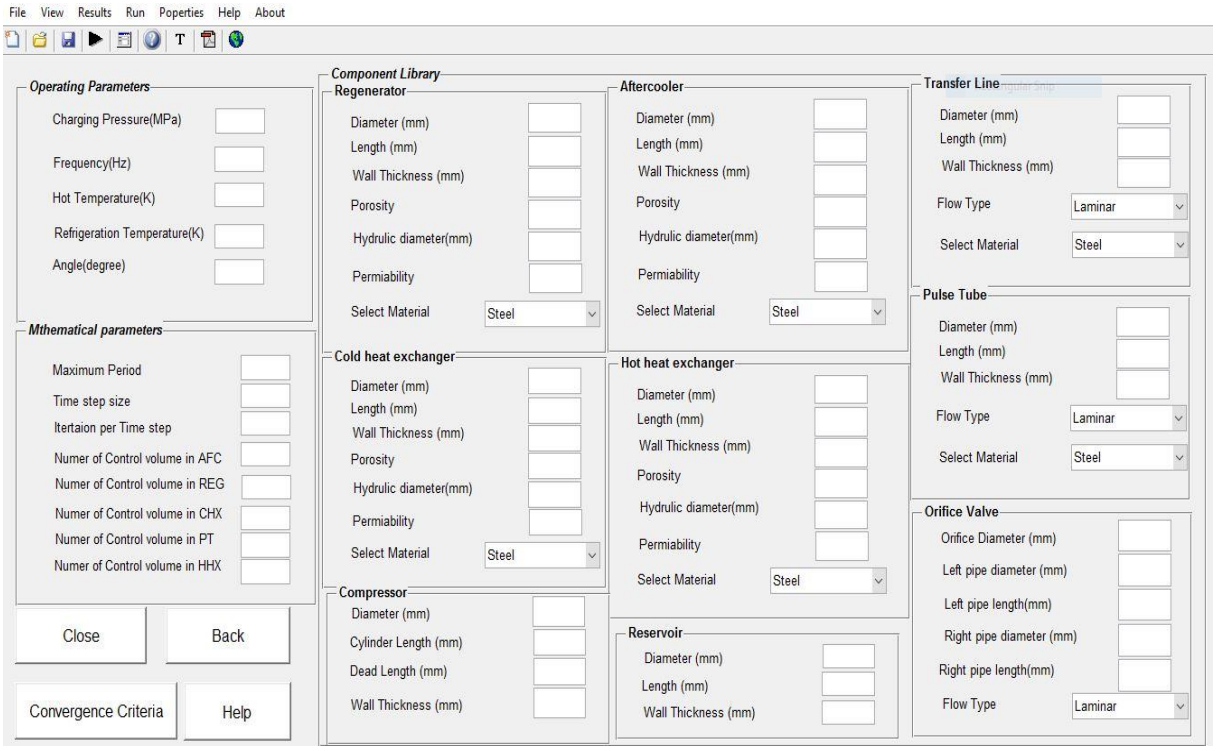

Figure 4.14: Input interface of CRESP-SPTR OPTR module.

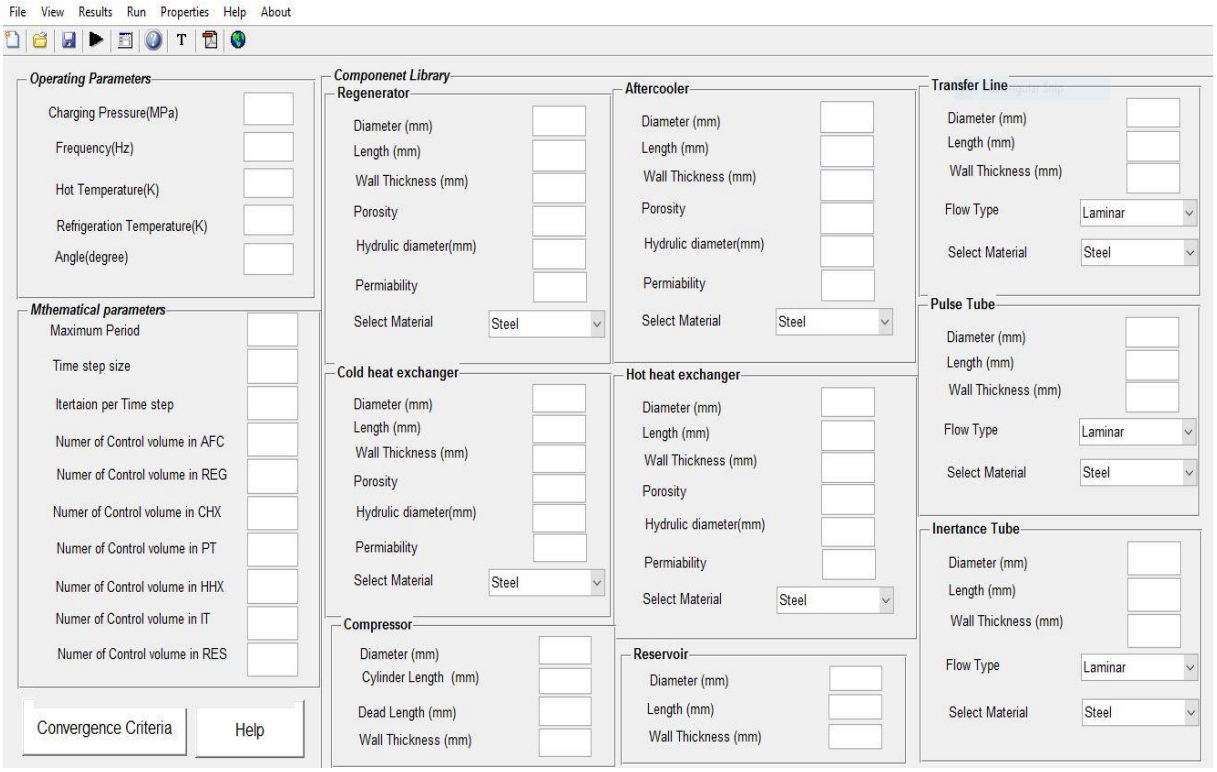

Figure 4.15: Input interface of CRESP-SPTR IPTR module.

4.6 Validation of CRESP-SPTR software

The developed program is first validated with previously published results to ensure the accuracy of the model. Figs. 4.16 and 4.17 present the validations for IPTR and OPTR respectively. Fig. 4.16 shows the relations of COP with different lengths of inertance tube (Validated with the results of Zhu *et al.* [96], Boroujerdi *et al.*[141], Arablu *et al.*[142]), whereas Fig. 4.17 shows the variations of orifice opening with COP (Boroujerdi *et al.* [141]).

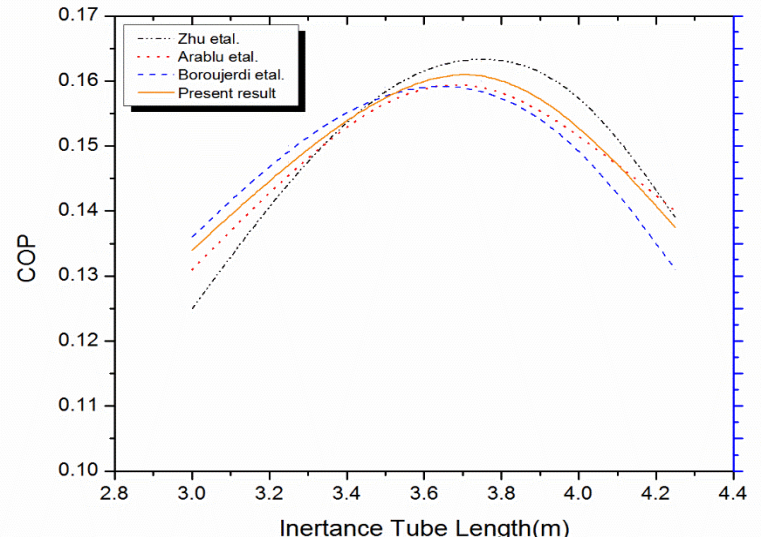

Figure 4.16: Validation of CRESP-SPTR with published results.

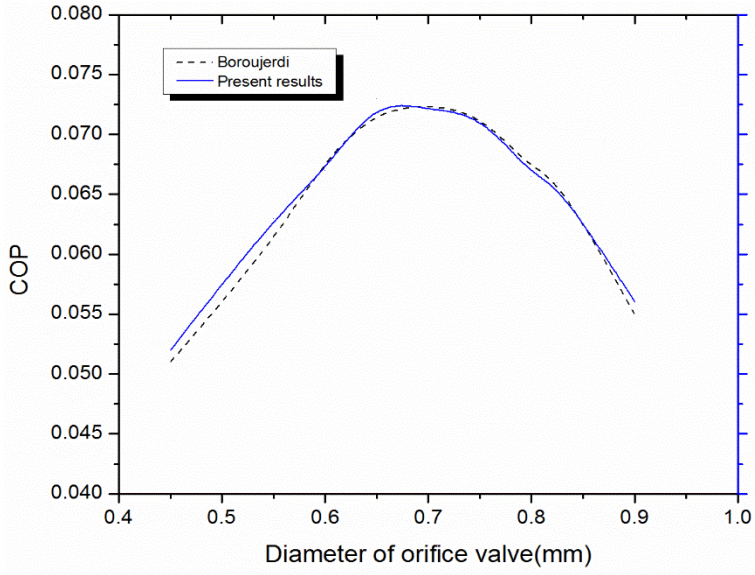

Figure 4.17: Validation of CRESP-SPTR with published results.

4.7 Results and Discussion

The dimensions of important componenets of pulse tube cryocooler used for simulation in CRESP-PTR are presented in Table 4.2.

Table 4.2 : Dimensions of different component's used for simulation in CRESP-SPTR.

Componenet	Diameter (mm)	Length (mm)
Regenerator	20	50
Pulse tube	16	48
Aftercooler	20	12
CHX	16	8
HHX	16	10
Inertance tube	1	1200

Table 4.3 : Colour code of CRESP-SPTR software.

Colour	Component name (from left hand side)
Red	Compressor
Black	Transfer line
Blue	Aftercooler
Magenta	Regenerator
Green	CHX
Red	Pulse tube
Green	HHX
Blue	Inertance tube
Cyan	Buffer

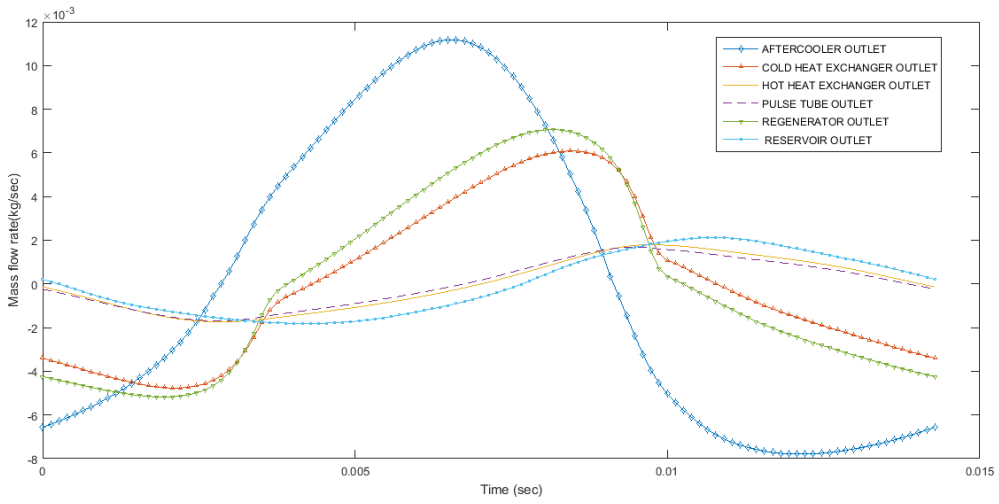

Figure 4.18: Variation of mass flow rate with respect to time.

Figure 4.18 shows that there is a decrease in amplitude of mass flow rate when it passes gradually from compressor to the buffer. Due to viscous resistance and inertial resistance, there is a gradual drop in pressure amplitude in the porous media (e.g. regenerator, aftercooler, cold heat exchanger, hot heat exchanger) as shown in Figs. 4.19, 4.20 and Fig. 4.21. Fig. 4.22 shows that drop of pressure amplitude is more in regenerator. From Fig. 4.22, it is revealed that principal source of pressure drop is regenerator due to viscous and inertial resistance. In Fig. 4.21 top line represents maximum pressure, middle line represents mean pressure and bottom line represents minimum pressure.

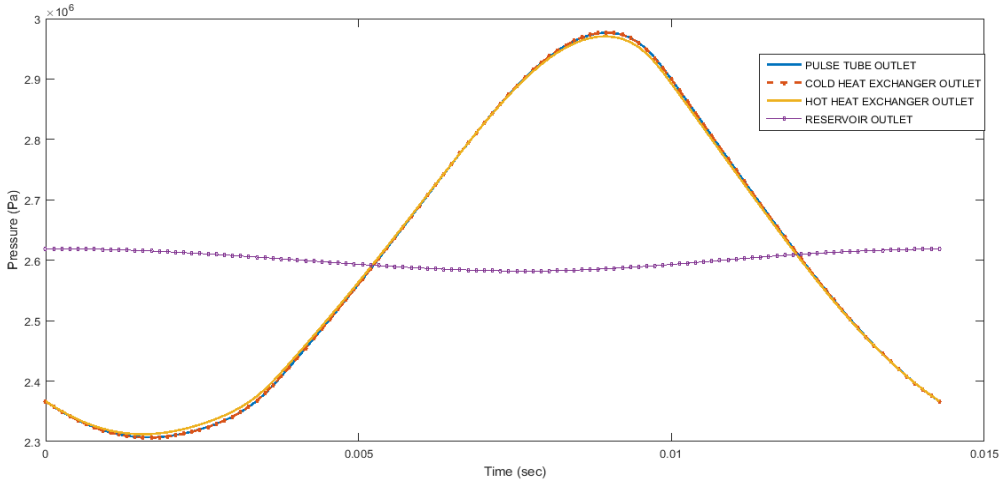

Figure 4.19: Variations of pressure of pulse tube, CHX, HHX, buffer with time.

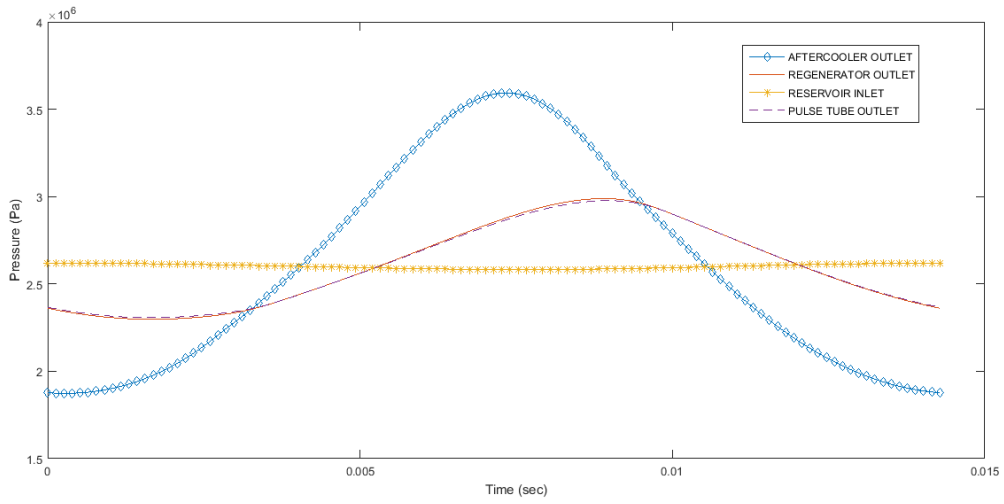

Figure 4.20: Variations of pressure in aftercooler, regenerator, pulse tube, reservoir.

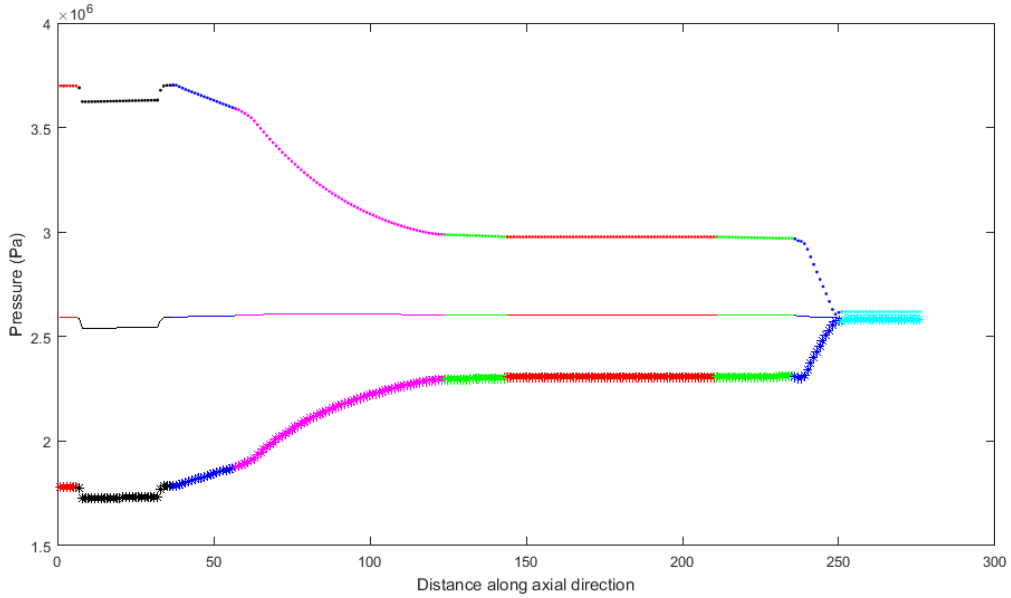

Figure 4.21: Variations of pressure along axial direction. (Colours are in Table 4.3)

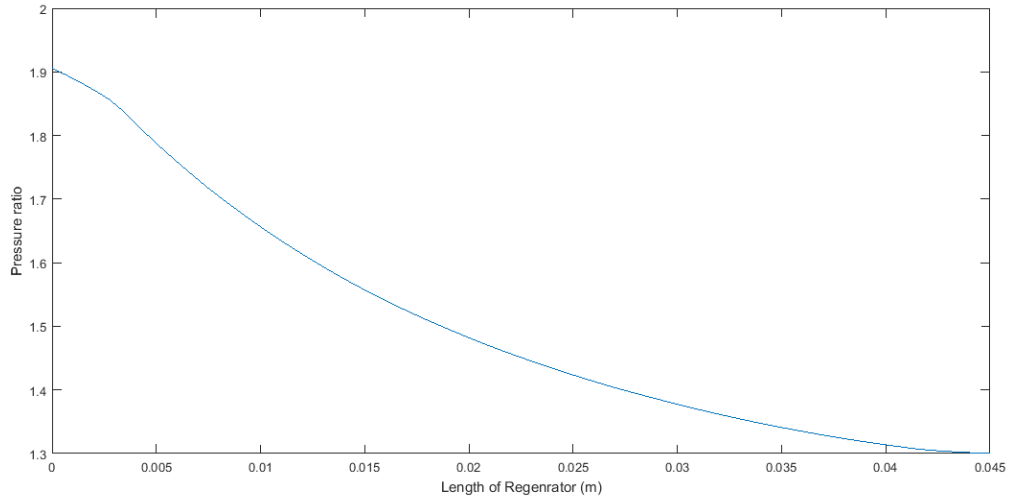

Figure 4.22: Variation of pressure ratio along regenerator.

Figure 4.22 shows that the variations of pressure ratio along axial direction. It is concluded that pressure ratio decreases in regenerator and increases in pulse tube.

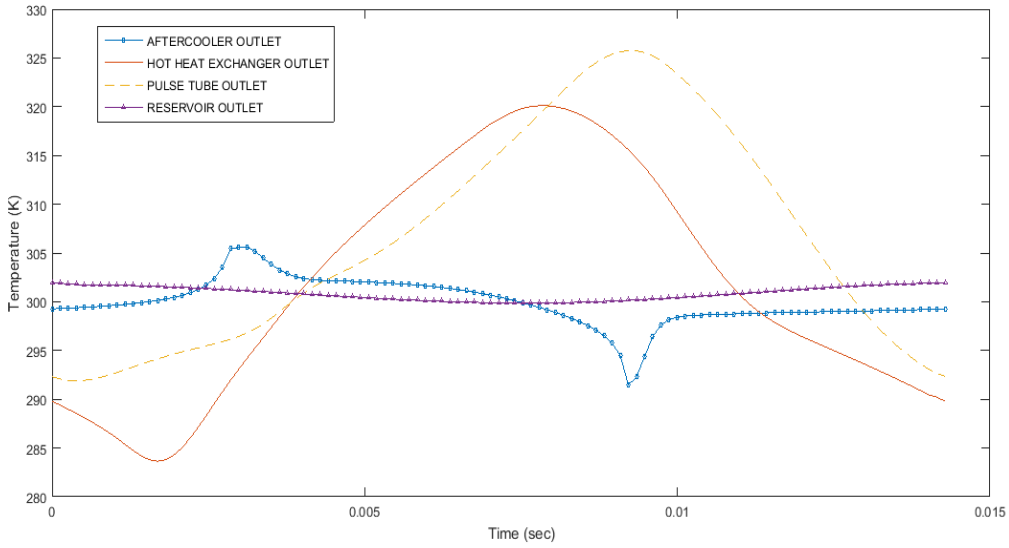

Figure 4.23: Variations of temperature with time.

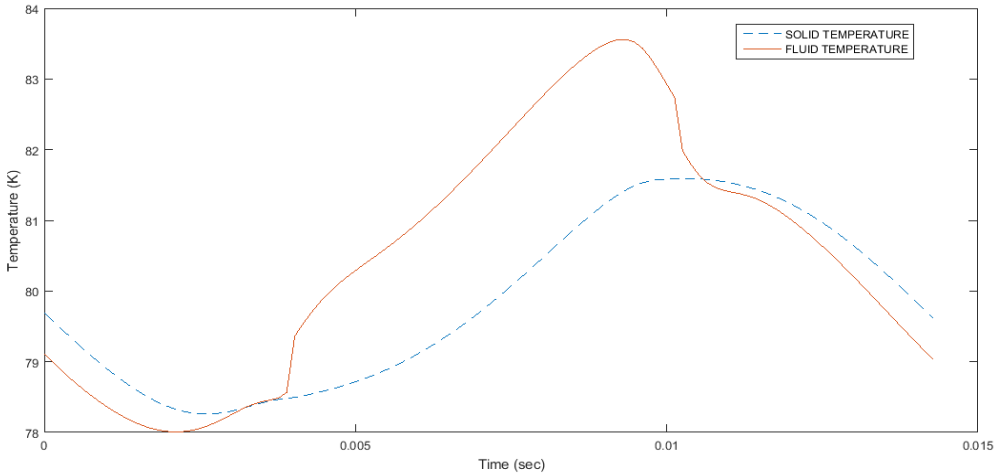

Figure 4.24: Variations of solid temperature and fluid temperature with time.

Figure 4.23 shows the variations of temperature with respect to time. It is observed that the amplitude of temperature oscillation is more in pulse tube and hot heat exchanger as compared to aftercooler and buffer. Figure 4.24 signifies that amplitude of fluid temperature oscillation is more in regenerator outlet with respect to solid temperature, the difference is nearly about 2 K. In Fig. 4.25 top line represents maximum temperature, middle line represents mean temperature and bottom line represents minimum temperature.

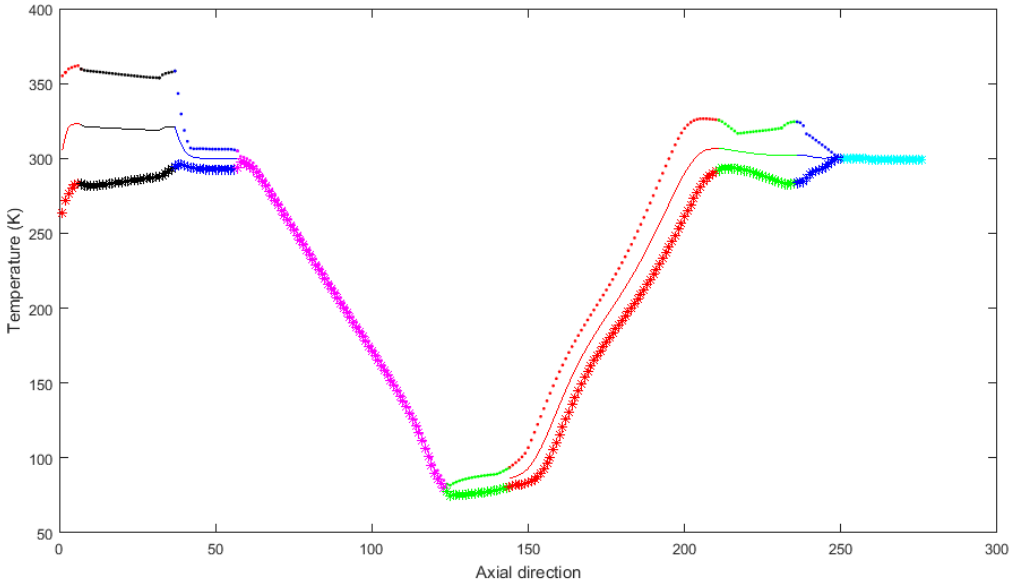

Figure 4.25: Variations of temperature along axial direction. (Colours are in Table 4.3)

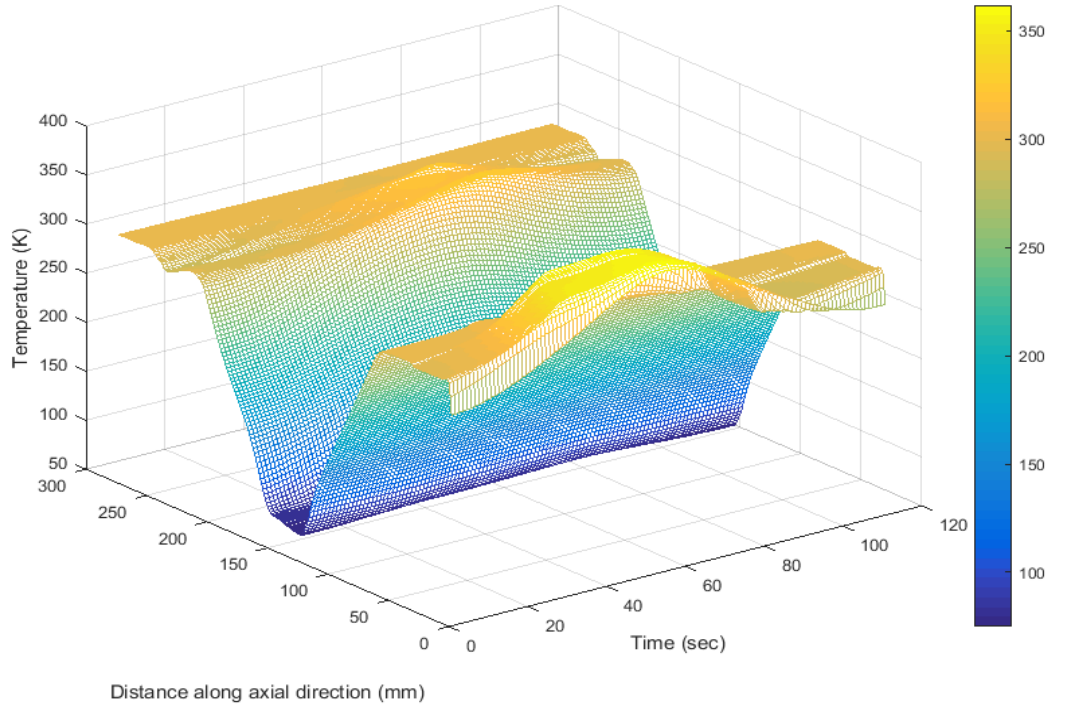

Figure 4.26: Variations of temperature with space and time.

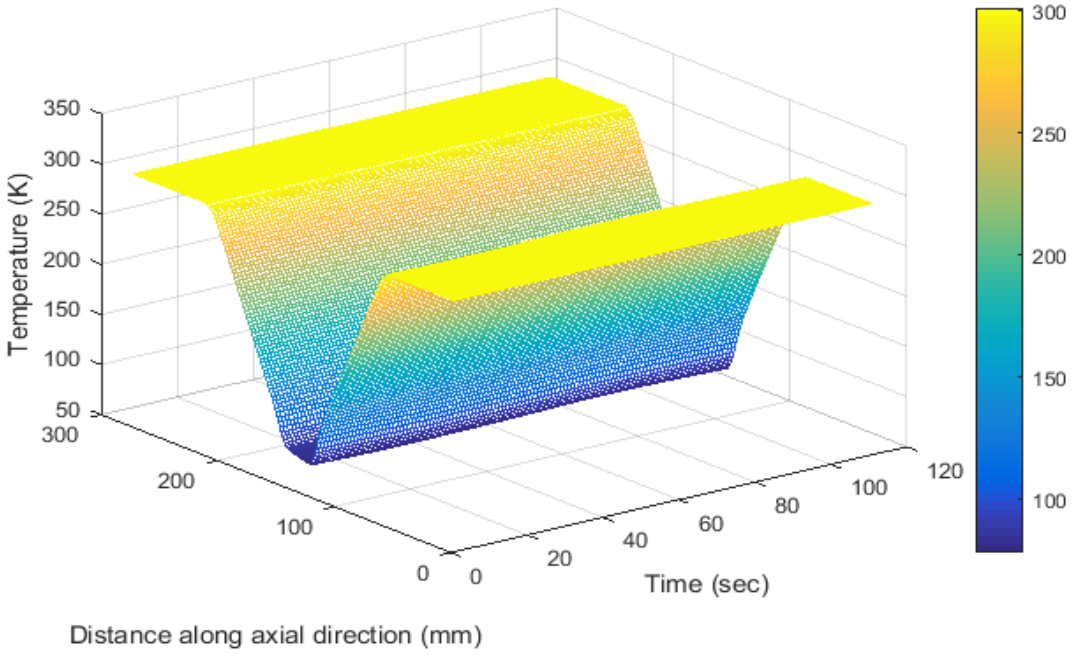

Figure 4.27: Variations of solid temperature with respect to both space and time.

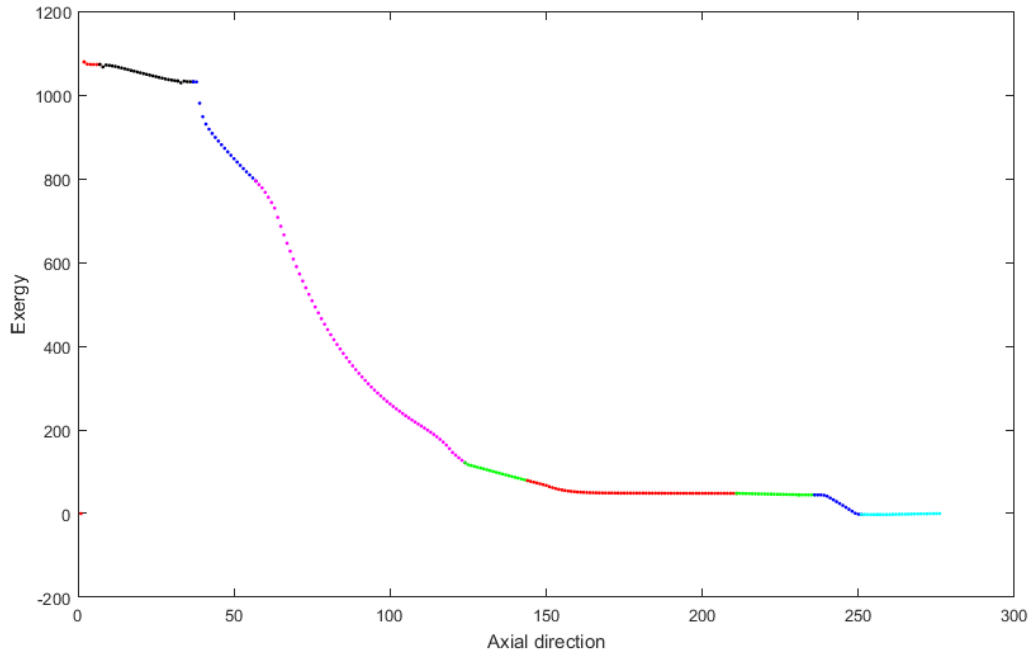

Figure 4.28: Variation of exergy along axial direction. (Colours are in Table 4.3)

Figure 4.28 shows that maximum amount of exergy drop occurs at regenerator due to irreversibility and generation of entropy, whereas considerable of exergy drop occurs at aftercooler, cold heat exchanger and inertance tube. As shown in Fig. 4.28, there is no drop of exergy in pulse tube and reservoir. Variation of energy along axial direction is presented in Fig. 4.29. As compressor is the main source of energy production, its value is maximum in pressure wave generator, however it decreases gradually as it flows towards buffer.

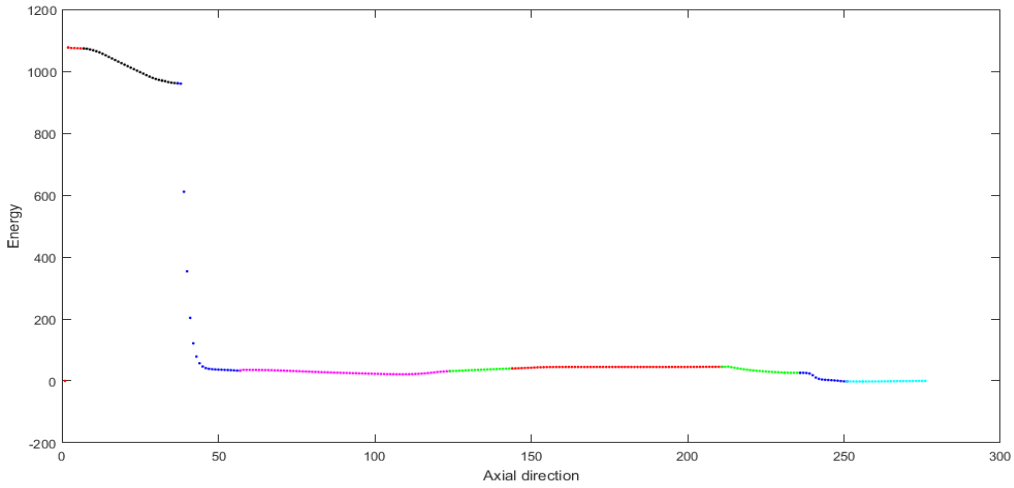

Figure 4.29: Variation of energy along axial direction. (Colours are in Table 4.3)

4.8 Summary

In this chapter detailed mathematical modeling of pulse tube refrigerator is presented. By using isothermal model, adiabatic model and numerical model, the software package CRESP-PTR has been developed and validated with existing results. Detailed description of various interface is also explained in detail. A typical example of an IPTR is presented. From the simulation results of inertance type pulse tube refrigerator, it is obvious that regenerator is the main source of loss of acoustic power due to pressure drop. Also, main source of exergy destruction is regenerator due to entropy generation. Pressure ratio decreases mainly within the regenerator hence, in order to increase performance of cryocoolers, it may be necessary to decrease the pressure ratio.

Chapter 5

CFD Analysis of Pulse Tube Refrigerator

CFD techniques are widely used for analysis of systems involving fluid flow, heat transfer and associated phenomena involving chemical reaction and multiphase flow by using numerical simulation. So it is mostly used by various industries and research centres as well as institutes for defining the problem and solving it to get reasonable accurate results. There are many commercial packages available for CFD analysis such as CFX, FLUENT, ICEM CFD, CFD-STAR+ etc. Computational fluid dynamics is a very useful and valuable technique to predict the mechanism of cold production in pulse tube refrigerators. Many investigators have used it to understand the mechanism of fluid flow and heat transfer. Here, an attempt has been made to conduct the CFD analysis by using the commercial software FLUENT because of its capability to solve complex heat and fluid flow situations in complex geometries. The FLUENT software provides the capability of modelling the compressor by using dynamic meshing with proper "user defined functions", modelling of regenerator and heat exchangers involving porous media.

The analysis of the complete system includes geometry creation, mesh generation, and setup the problem with proper boundary conditions and user defined functions. To study the effect of heat transfer and cold production, energy equation has been checked in, also to consider the effect of turbulence kinetic energy, standard $k-\varepsilon$ turbulence model has been checked in.

5.1 Governing equations of ANSYS FLUENT

Main governing equations used are continuity equation, momentum equations, energy equation and turbulence equation. These equations must be satisfied when the fluid is flowing from one component to another component in the pulse tube refrigerator [147].

5.1.1 Equation of conservation of mass or continuity equation

$$\frac{\partial \rho}{\partial t} + \nabla.(\rho \vec{v}) = S_m \tag{5.1}$$

The first term in left-hand side is the unsteady term; the second term is a change of mass along space coordinate and the term in right-hand side represent the source term.

5.1.2 Conservation of momentum equation

$$\frac{\partial}{\partial t}(\rho \vec{v}) + \nabla.(\rho \vec{v}\vec{v}) = -\nabla p + \nabla.(\bar{\bar{\tau}}) + \rho \vec{g} + \vec{F} \tag{5.2}$$

Stress tensors can be defined as:

$$\bar{\bar{\tau}} = \mu\left[(\nabla \vec{v} + \nabla \vec{v}^T) - \frac{2}{3}\nabla.\vec{v}I\right] \tag{5.3}$$

The first term on the left-hand side of Eq. (5.2) represents the unsteady term while the second term is the inertia term. In right-hand side, the first term represents the pressure gradient, the second term represents the viscous term; the third term represents the body force, and the fourth term represents external body force.

5.1.3 Conservation of Energy

$$\frac{\partial}{\partial t}(\rho E) + \nabla.(\vec{v}(\rho E + p)) = \nabla.(k_{eff}\nabla T - \sum_j h_j \vec{J}_j + (\bar{\bar{\tau}}_{eff}.\vec{v})) + S_h \tag{5.4}$$

$$E = h - \frac{p}{\rho} + \frac{v^2}{2}$$

$$h = \int_{T_{ref}}^{T} C_P dT$$

$$k_{eff} = k + k_t$$

5.1.4 Turbulent kinetic energy equations

Turbulence kinetic energy (k) and its rate of dissipation (ε) have been calculated from the following equations:

$$\frac{\partial}{\partial t}(\rho k) + \frac{\partial}{\partial x_i}(\rho k u_i) = \frac{\partial}{\partial x_j}\left[\left(\mu + \frac{\mu_t}{\sigma_k}\right)\frac{\partial k}{\partial x_j}\right] + G_k + G_b - \rho\varepsilon - Y_M + S_k \tag{5.5}$$

$$\frac{\partial}{\partial t}(\rho \varepsilon) + \frac{\partial}{\partial x_i}(\rho \varepsilon u_i) = \frac{\partial}{\partial x_j}\left[\left(\mu + \frac{\mu_t}{\sigma_\varepsilon}\right)\frac{\partial \varepsilon}{\partial x_j}\right] + C_{1\varepsilon}\frac{\varepsilon}{k}(G_k + C_{3\varepsilon}G_b) - C_{2\varepsilon}\frac{\varepsilon^2}{k} + S_\varepsilon \tag{5.6}$$

In the present case, an inertance type pulse tube refrigerator has been modeled by using FLUENT. To save computational time, axisymmetric modeling has been carried out in the present analysis. So the governing equations for 2D axisymmetric geometry have been governed by the following sets of the equations.

5.1.5 Continuity equation

$$\frac{\partial \rho}{\partial t} + \frac{\partial}{\partial x}(\rho v_x) + \frac{1}{r}\frac{\partial}{\partial r}(r \rho v_r) = S_m \tag{5.7}$$

The first term in left-hand side represents the unsteady term; the second term accounts for a change in mass along the axial direction, the third term represent a shift in mass along the radial direction. The term on the right-hand side represents the source term.

5.1.6 Momentum equation in axial direction

$$\begin{aligned}&\frac{\partial}{\partial t}(\rho v_x) + \frac{1}{r}\frac{\partial}{\partial x}(r \rho v_x v_x) + \frac{1}{r}\frac{\partial}{\partial r}(r \rho v_r v_x) = -\frac{\partial p}{\partial x} \\ &+ \frac{1}{r}\frac{\partial}{\partial x}\left[r\mu\left(2\frac{\partial v_x}{\partial x} - \frac{2}{3}(\nabla.\vec{v})\right)\right] + \frac{1}{r}\frac{\partial}{\partial r}\left[r\mu\left(\frac{\partial v_x}{\partial r} + \frac{\partial v_r}{\partial x}\right)\right] + S_x\end{aligned} \tag{5.8}$$

5.1.7 Momentum equation in radial direction

$$\frac{\partial}{\partial t}(\rho v_r)+\frac{1}{r}\frac{\partial}{\partial x}(r\rho v_x v_r)+\frac{1}{r}\frac{\partial}{\partial r}(r\rho v_r v_r)=-\frac{\partial p}{\partial r}$$
$$+\frac{1}{r}\frac{\partial}{\partial r}\left[r\mu\left(2\frac{\partial v_r}{\partial r}-\frac{2}{3}(\nabla.\vec{v})\right)\right]+\frac{1}{r}\frac{\partial}{\partial x}\left[r\mu\left(\frac{\partial v_r}{\partial x}+\frac{\partial v_x}{\partial r}\right)\right] \quad (5.9)$$
$$-2\mu\frac{v_r}{r^2}+\frac{2}{3}\frac{\mu}{r}(\nabla.\vec{v})+\rho\frac{v_z^2}{r}+S_r$$

Gradient of velocity is represented as

$$\nabla.\vec{v}=\frac{\partial v_x}{\partial x}+\frac{\partial v_r}{\partial r}+\frac{v_r}{r} \quad (5.10)$$

where, S_x and S_r are represents two source terms in the axial and radial directions respectively, whose values are equal to zero for the nonporous zone. For the porous zone, the momentum equation can be defined by adding two extra terms to the volume averaged momentum equation: the Darcy term and the Forchheimer term, which are responsible for flow resistance through the porous media. The Darcy term is liable for the pressure drop, directly proportional to flow velocity whereas the Forchheimer term, is responsible the pressure drop, commensurate with the square of the flow velocity. Assuming the solid matrix homogeneous and isotropic, the following momentum source terms are included in the *x* and *r* volume averaged momentum equations:

$$S_x=-\left(\frac{\mu}{\kappa}v_x+\frac{1}{2}C\rho|\vec{v}|v_x\right) \quad (5.11)$$

$$S_r=-\left(\frac{\mu}{\kappa}v_r+\frac{1}{2}C\rho|\vec{v}|v_r\right) \quad (5.12)$$

The first term in the above equation represents the Darcy term and Forchheimer term. Both these terms represent the flow inside porous zone due to pressure drop. In the present studies, thermal equilibrium model has been assumed for porous zones, since FLUENT V15 thermal non-equilibrium model may not work properly [147, 148]. In the porous zone, there are two different models in FLUENT such as thermal equilibrium model and thermal non-equilibrium model. In thermal equilibrium model, FLUENT assumes single equation for gas, on the other

hand, in thermal non-equilibrium model fluent solves two different equations for gas and matrix. The energy equation assuming thermal equilibrium model in porous zone is given below.

5.1.8 Energy Equation

$$\frac{\partial}{\partial t}(\alpha\rho_f E_f + (1-\alpha)\rho_s E_s) + \nabla.(\vec{v}(\rho_f E_f + P)) = \nabla.(k_{eff}\nabla T + \tau.\vec{v}) \tag{5.13}$$

where, $k = \alpha k_f + (1-\alpha)k_s$

$E_f = h - p/\rho_f + v^2/2$

k_s = Solid medium thermal conductivity

k_f =Fluid thermal conductivity

5.1.9 Heat transfer coefficient between solid regenerator matrix and working fluid

Tanaka *et al.* [87] introduced a correlation to calculate the heat transfer coefficient for oscillating gas flow in a regenerator.

$$h = 0.33\frac{k_f}{d_h}\left(\frac{\rho d_h 2V_s\rho}{\mu A_s \alpha}\right)^{0.67} \tag{5.14}$$

where, k_f is the thermal conductivity of working fluid,

d_h is the equivalent hydraulic diameter,

V_s is the piston swept volume,

A_s is the total surface area.

5.1.10 Thermal conductivity of porous matrix

Koh and Fortini formula is used for the calculation of thermal conductivity of regenerator solid matrix

$$k_s = \frac{1-\zeta}{1+11\zeta}k \tag{5.15}$$

where k is thermal conductivity of solid matrix used in porous zone.

k_s is defined as the effective thermal conductivity of the solid matrix while considering the porosity ζ.

5.1.11 Compressor input power

Input power supplied by the pressure wave generator is calculated by using

$$W_{comp} = f \oint P_{Vavg} \frac{dV}{dt} \tag{5.16}$$

where, P_{Vavg} is, the volume averaged pressure inside the swept volume of the compressor. Some other variables used for analysis are computed by the following [147]:

- The **Area** of a surface is calculated by adding the areas of the faces that define the surface. Faces on a surface are either triangular or quadrilateral in shape.

$$A = \int dA \sum_{i=1}^{n} |A_i| \tag{5.17}$$

In the above expression the index 'i' denotes a face and the summation extends over all the '*n*' faces.

- The integral on a surface is computed by summing the product of the facet area and the selected field variable. If the face is on a boundary surface, an interpolated face value is used for the integration instead of the cell value. This is done to improve the accuracy of the calculation and to ensure that the result matches the boundary conditions specified on the boundary and the fluxes prescribed on the boundary.

$$\varsigma_{i1} = \int \varsigma dA = \sum_{i=1}^{n} \varsigma_i |A_i| \tag{5.18}$$

The **Area-Weighted Average** of a quantity is computed by dividing the summation of the product of the selected field variable and face area by the total area of the surface:

$$\varsigma_{aw} = \frac{1}{A} \int \varsigma dA = \frac{1}{A} \sum_{i=1}^{n} \varsigma_i |A_i| \tag{5.19}$$

- The **Flow Rate** of a quantity through a surface is computed by summing the product of density and the selected field variable with the dot product of the face area vector and the face velocity vector.

$$\varsigma_{fr} = \int \varsigma \rho \vec{v} d\vec{A} = \sum_{i=1}^{n} \varsigma_i \rho_i \vec{v}_i \left| d\vec{A}_i \right| \tag{5.20}$$

- The **Mass Flow Rate** through a surface is computed by summing the product of density with the dot product of the face area vector and the face velocity vector.

$$\varsigma_{mf} = \int \rho \vec{v} d\vec{A} = \sum_{i=1}^{n} \rho_i \vec{v}_i . \left| d\vec{A}_i \right| \tag{5.21}$$

- The **Mass-Weighted Average** of a quantity is computed by dividing the summation of the product of the selected field variable and the absolute value of the dot product of the facet area and momentum vectors by the summation of the absolute value of the dot product of the facet area and momentum vectors.

$$\varsigma_{mw} = \frac{\int \varsigma \rho \left| \vec{v} d\vec{A} \right|}{\int \rho \left| \vec{v} d\vec{A} \right|} = \frac{\sum_{i=1}^{n} \varsigma_i \rho_i \left| \vec{v}_i . d\vec{A}_i \right|}{\sum_{i=1}^{n} \rho_i \left| \vec{v}_i . d\vec{A}_i \right|} \tag{5.22}$$

The sum of a specified field variable on a surface is computed by summing the value of the selected variable at each facet

$$\varsigma_{sm} = \sum_{i=1}^{n} \varsigma_i \tag{5.23}$$

The **Facet Average** of a specified field variable on a surface is calculated by dividing the summation of the facet values of the chosen variable by the total number of faces.

$$\varsigma_{fa} = \frac{\sum_{i=1}^{n} \varsigma_i}{n} \tag{5.24}$$

- ❖ The **Volume Flow Rate** through a surface is computed by summing the dot product of the face area vector and the face velocity vector

$$\varsigma_{vf} = \vec{v} . d\vec{A} = \sum_{i=1}^{n} \vec{v}_i . d\vec{A}_i \tag{5.25}$$

- ❖ The **Facet Minimum** of a specified field variable on a surface is the minimum facet value of the selected variable on the surface.
- ❖ The **Facet Maximum** of a specified field variable on a surface is the maximum facet value of the selected variable on the surface.

5.2 Details of geometry creation and meshing

Table 5.1 : Dimensions of geometry and boundary conditions.

Components	Diameter (m)		Length (m)		Boundary condition
	Cha et al.	Present model	Cha et al.	Present model	
Compressor	0.02	0.02	0.0075	0.008	Adiabatic
Transfer line	0.0031	0.0033	0.101	0.1	Adiabatic
After cooler	0.008	0.008	0.02	0.02	298 K
Regenerator	0.008	0.008	0.058	0.06	Adiabatic
Cold heat exchanger	0.008	0.008	0.0057	0.006	Adiabatic
Pulse tube	0.005	0.005	0.06	.01	Adiabatic
Hot heat exchanger	0.008	0.008	0.012	0.012	298 K
Inertance tube	0.00085	0.0009	0.684	0.7	Adiabatic
Reservoir	0.026	0.025	0.13	0.12	Adiabatic

By using the above dimensions, geometry has been created in the ANSYS. Dual opposed configuration of the pressure wave generator has been modelled by using dynamic meshing function assuming sinusoidal motion of the piston. Regenerator, aftercooler, cold heat exchanger and hot heat exchanger are modelled by using porous zone. Value of porosity, inertial resistance and viscous resistance have been calculated by using formulae from relevant literature [97]. The UDF for dynamic meshing function is

```
#include "udf.h"
DEFINE_CG_MOTION (vel_comp, dt,vel,omega,time,dtime)
{
real freq = 40.0;
real w = 2.0 * M_PI * freq;
real Xcomp = 0.004511;
NV_S(vel, = ,0.0);
```

```
NV_S(omega, = ,0.0);
vel[0] = w * Xcomp * cos (w * time);
}
```

Variation of density is calculated by ideal gas assumption. Temperature dependent properties of viscosity and thermal conductivity have been modelled from NIST data base. Suitable UDF have been written and attached in the FLUENT compiler [149].

```
#include "udf.h"
DEFINE_PROPERTY(cell_viscosity, c, t)
{
 real mu_lam;
 real temp = C_T(c, t);
 if (temp < 300.)
  mu_lam = (29.0*pow(temp,-1.27)+0.52*pow(temp,0.64))*1.e-6;
 else
 mu_lam = ((-5.7e-6*pow(temp,2.))+(4.4393e-2*temp)+7.5665)*1.e-6;
return mu_lam;
}
DEFINE_PROPERTY(knew,c,t)
{
real ktc;
real temp = C_T(c,t);
 if (temp < 300.)
 ktc = (0.0038*pow(temp,0.65))+(0.0172*exp(-0.025*pow((temp-6),2)));
 else
 ktc = (-4.74e-5*pow(temp,2))+(0.35044*temp)+(60.848)*1e-3;
  return ktc;
}
```

The axisymmetric geometry generated is shown in the following figure:

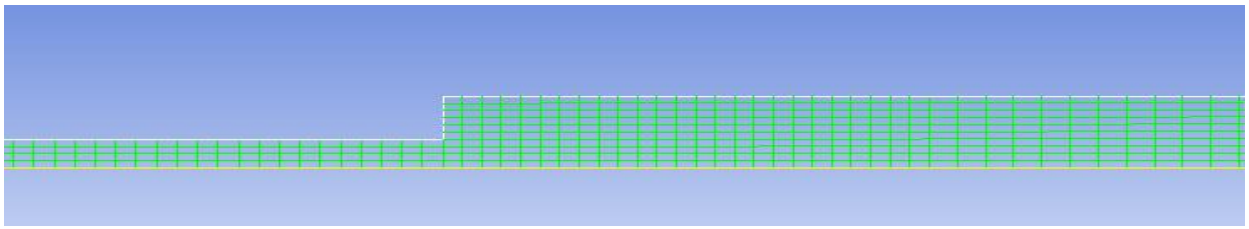

Figure 5.1: Mesh of transfer line and regenerator.

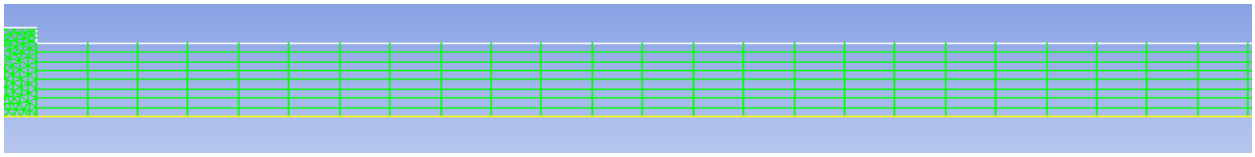

Figure 5.2: Mesh of cold heat exchanger and pulse tube.

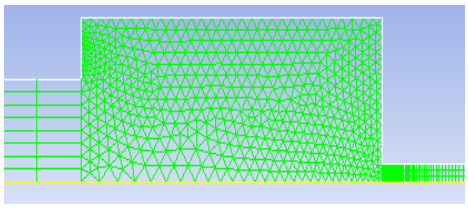

Figure 5.3: Mesh of pulse tube, hot heat exchanger, and inertance tube.

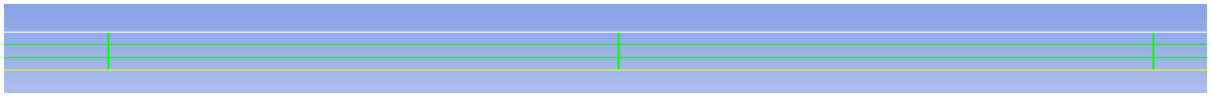

Figure 5.4: Mesh of inertance tube.

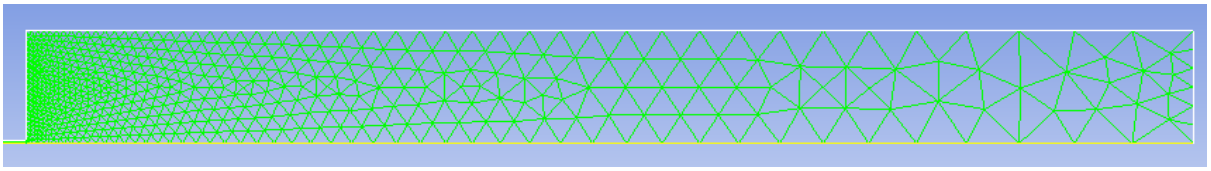

Figure 5.5: Mesh of reservoir

Dynamic meshing parameters are presented here.

Table 5.2: Dynamic meshing parameters.

Smoothing	Yes
Layering	Yes
Remeshing	Yes

Under "Smoothing" various parameters are assigned.

Table 5.3: Smoothing parameters.

Method	Spring/Laplace/Boundary layer
Spring constant factor	1
Convergence Tolerance	0.001
Number of iteration	20
Elements	Tri in Tri Zones
Laplace node Relaxation	1

For "Layering", the following values are assigned.

Table 5.4: Layering parameters.

Split factor	0.4
Collapse factor	0.2

For "Remeshing", the following values are assigned.

Table 5.5: Remeshing parameters.

Minimum Length Scale	0
Maximum length scale	1000
Size Remeshing Interval	5

5.3 Setup declaration

5.3.1 Initial condition

As the present case involves an unsteady state, so initial conditions must be provided to start the simulation. The initial pressure is assumed as mean pressure, and the temperature is assumed as the ambient temperature in the present simulation purpose and various boundary conditions are given in the above tables (Table 5.1).

5.3.2 Solution algorithm

After defining initial conditions and boundary conditions, proper solution algorithm and convergence tolerance must be provided for solution purposes. Axisymmetric, unsteady, cell-based second order implicit time, physical velocity with segregated solver is considered for the present analysis. For solving the discretized governing equations, unsteady pressure based segregated solver with implicit formulation is used. Due to dynamic meshing, first order method is used. Various dynamic meshing parameters are explained in Table 5.2 to Table 5.5. The governing equations are formulated assuming two-dimensional, axis-symmetric, turbulent flow in cylindrical coordinates along with boundary conditions representing a set of non-linear, coupled differential equations, which are solved iteratively using the finite volume method. The PRESTO scheme uses the discrete continuity balance for a "staggered" control volume about the face to compute the "staggered" (i.e., face) pressure (Table 5.6). This procedure is similar in spirit to the staggered meshes; comparable accuracy is obtained using a similar algorithm. For unsteady problems, it is an efficient method to solve the momentum equations. Suitable under-relaxation factors (Table 5.8) for momentum, pressure, and energy have been used to improve the rate of convergence. Quadrilateral as well as triangular cells are utilized for the computational domain. For all equations, convergence of the discretized equations have been achieved when the whole field residual is kept at 10^{-6} (Table 5.7). A line-by-line solver based on TDMA (Tridiagonal matrix algorithm) is used to solve iteratively the algebraic equations obtained after discretization. Details of the numerical method and solution procedures may be found in the work of Versteeg and Malalasekera [150] and Patankar [151]. Proper under

relaxation factors are used for the settlement of the pressure correction equation, momentum equations and the energy equation.

5.3.3 Spatial discretization

Table 5.6: Spatial discretization schemes.

Gradient	Least square Cell Based
Pressure	Second order, PRESTO
Density	Second order upwind
Momentum	Second order upwind
Turbulent Kinetic Energy	First order upwind
Turbulent formulation	First order implicit
Transient formulation	First order implicit

5.3.4 Convergence criteria

Table 5.7: Convergence criteria used in simulation.

Continuity	1e−6
X-Velocity	1e−6
Y-Velocity	1e−6
Energy	1e−7
k	0.001
epsilon	0.001

To improve the speed of calculation several under-relaxation factors have been choosen.

Table 5.8: Under relaxation factors.

Pressure	0.3
Density	1
Body Force	1
Momentum	0.7
Turbulent kinetic energy	0.8

5.4 Mesh independence test

In CFD analysis, the geometry is divided into a number of control volumes. The governing equations need to be solved in each control volumes. If the number of grids within the solution domain increases, the accuracy of the results will be more, on the other hand, computational time will also increases. So it is important to make a comfortable balance between the number of grids and results. In the solution domain, number of mesh sizes has been varied, and corresponding results are noted. Finally after a certain number of meshes, there is little change in output is observed and this mesh size has been selected. Figure 5.6 shows the variation of cold end temperature with mesh number. The following figure (Fig. 5.6) shows the variation of cold end temperature with mesh number. Finally, a mesh size of 4950 is found to be good enough for the present simulation purpose, as there is no change in results. Hence, a grid size of 4950 has been used in all cases.

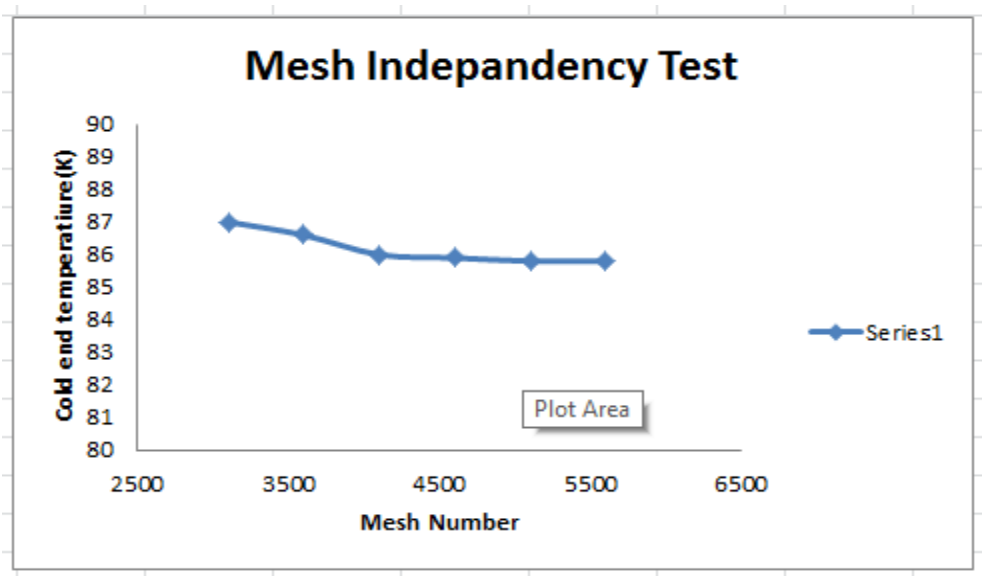

Figure 5.6: Mesh independence test.

5.5 Validation of present results

To ensure the accuracy of the solution, the present model has been validated with previously published results. Figure 5.7 shows the comparison of the present results with those of Cha [97] result.

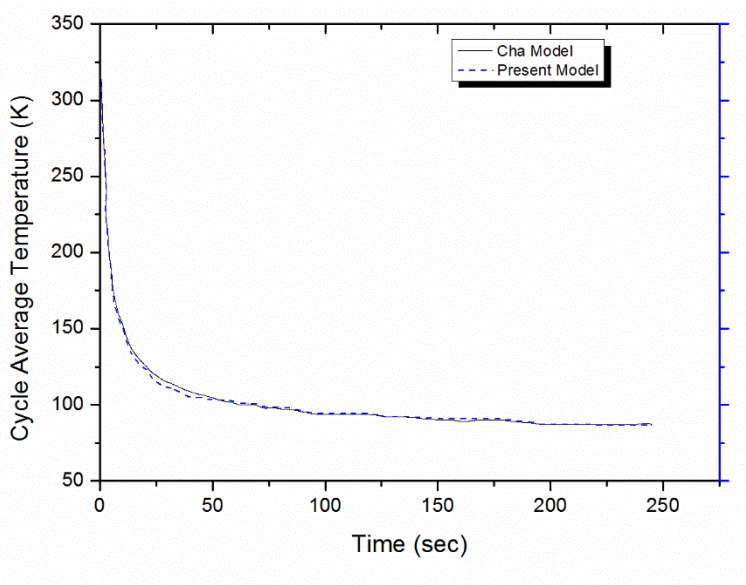

Figure 5.7: Validation of present result with published data.

5.6 Results and Discussion

After validating the present results with previously published results, the effect of operating frequency on the mechanism of cold production has been investigated. It is observed that, with an increase in frequency, cold end temperature decreases and the rate of cooling is faster (Fig. 5.8).

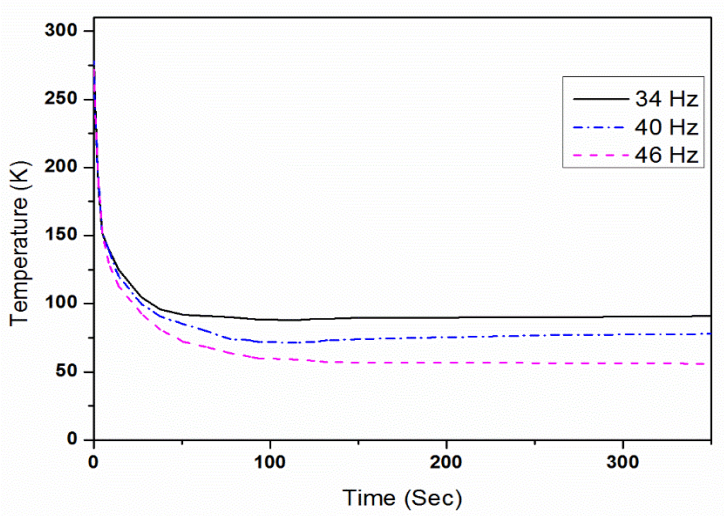

Figure 5.8: Effect of operating frequency.

The plots of various contours obtained from FLUENT are shown in following pages. Since it is a transient problem, the various parameters such as temperature, pressure, density, etc. at any location changes with time. Here, all contours are shown at a particular time (Figs. 5.12-5.15). Temperature near the cold end of the pulse tube is nearer to cold end temperature and near to the hot end of the pulse tube is hot end temperature. The variation of temperature along the regenerator and pulse tube is nearly linear due to a temperature gradient (Fig. 5.16). The change of temperature in pulse tube is the point of interest, as temperature variation is almost like three segments as in isothermal model by Zhu *et al.* [52] Since ideal gas equation has been used, it is important to study the effect of density. The density contour has been shown in the Fig. 5.13.

The variation of density shows nearly a linear trend near the cold heat exchanger. It is observed that density increses along the axial direction upto a certain value, then it starts decreasing and approaches to a lower value near the hot heat exchanger (Fig. 5.17). The phase angle between mass flow rate and pressure is a very critical parameter to improve the performance of pulse tube refrigerator (Fig. 5.9). In both aftercooler and hot end heat exchanger, the temperature is assumed to be isothermal, so the temperature variation is nearly linear. On the other hand, an excellent temperature gradient has been established along the regenerator and the pulse tube.

In the present analysis, the effect of turbulence has been considered by using turbulent kinetic energy dissipation equation. It is evident that there is no turbulence in aftercooler, regenerator, pulse tube, cold heat exchanger and hot heat exchanger. However, turbulence dissipation rate is more in transfer line and inertance tube. Velocity is nearly zero in pulse tube, so there is no development in any boundary layer (Fig. 5.14 and Fig. 5.15). The variation of skin friction coefficient is also presented in Fig. 5.18. The jet effect is shown in the Fig. 5.15 and the effect of variation of pressure with respect to time is illustrated in Fig. 5.10 and 5.11 during the beginning and after steady state achieved respectivly.

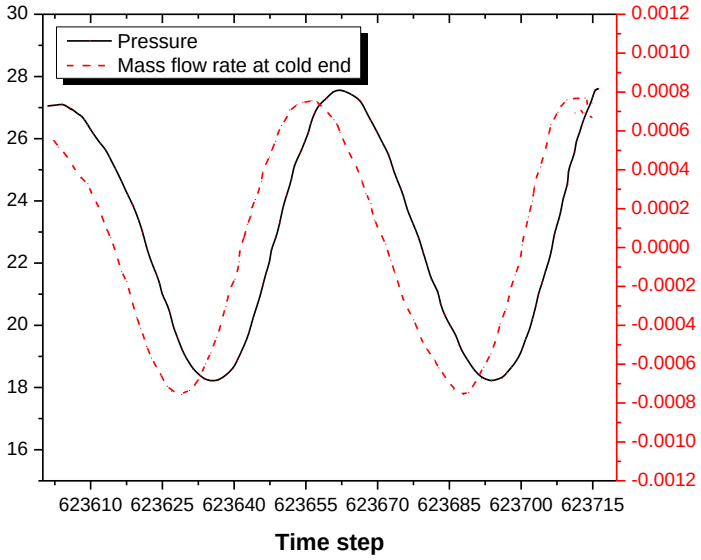

Figure 5.9: Effect of frequency on refrigeration temperature.

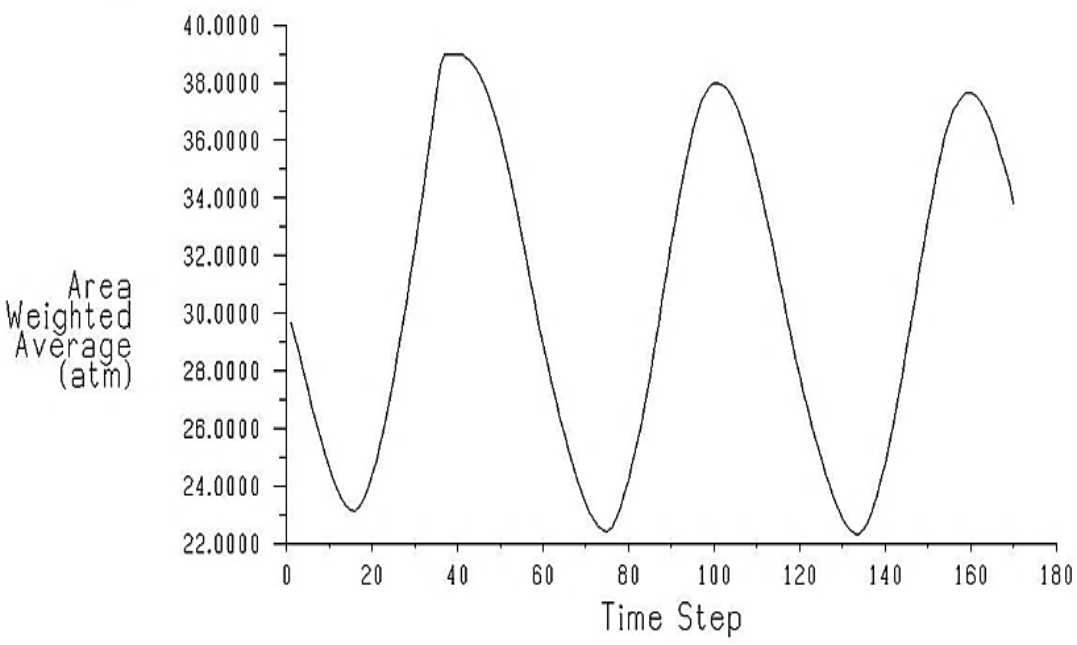

Figure 5.10: Pressure variation in pulse tube at the beginning of simulation.

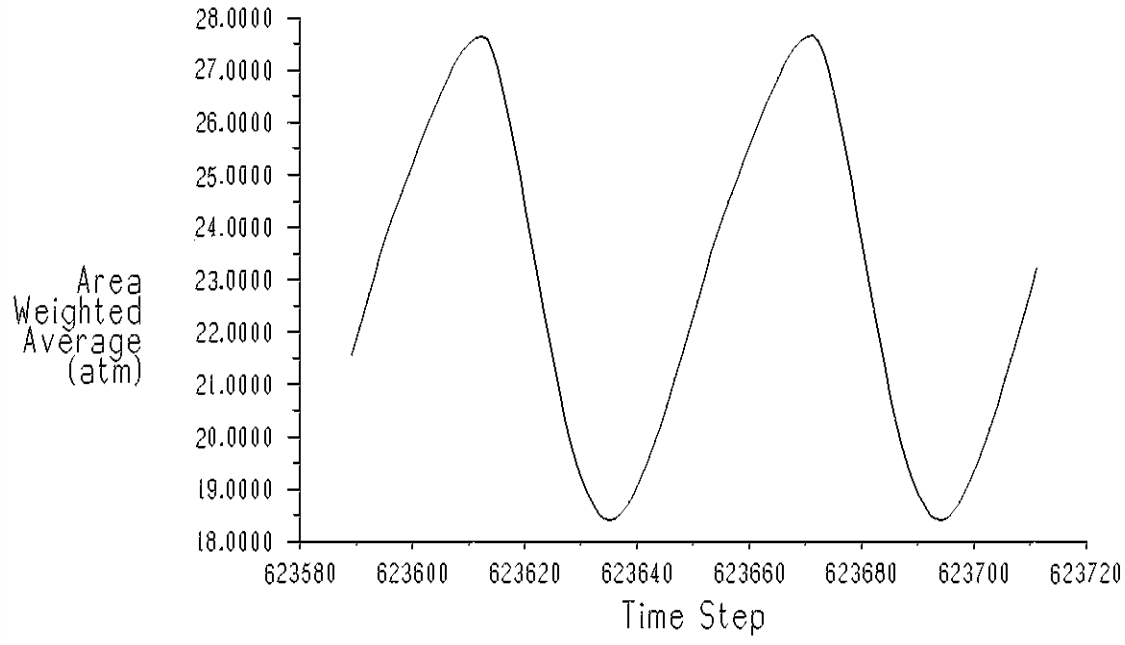

Figure 5.11: Pressure variation in pulse tube after quasi steady state.

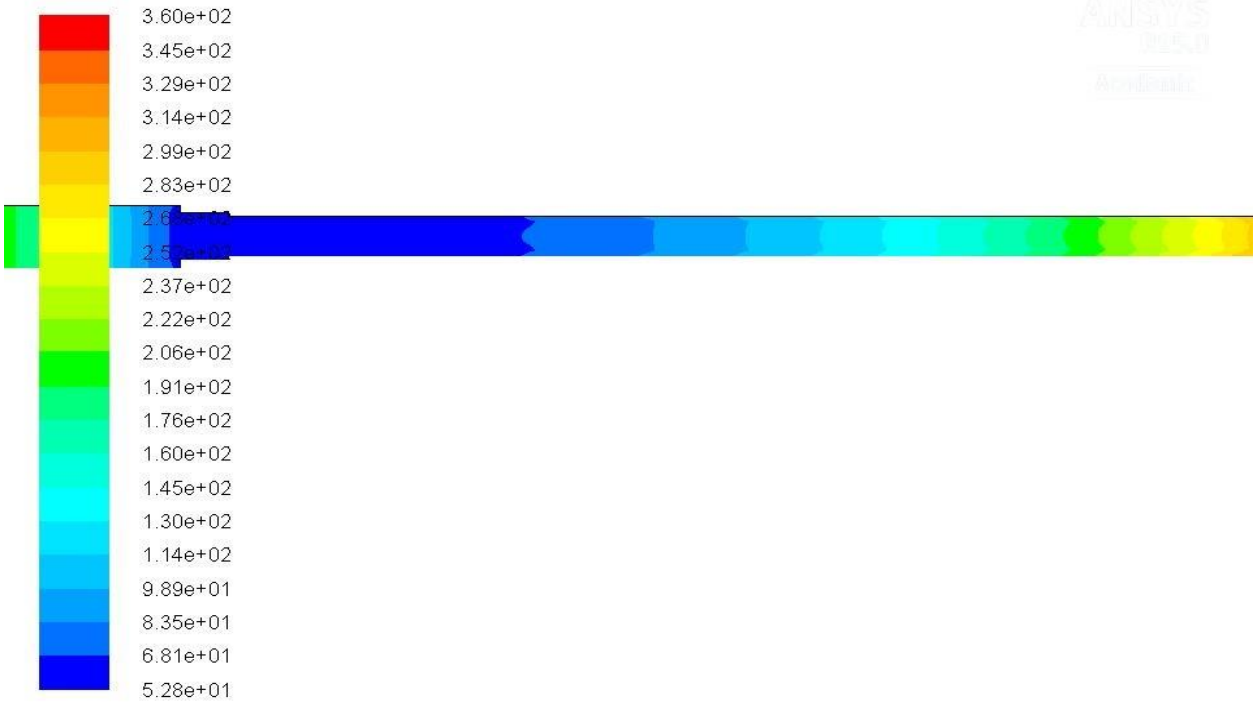

Figure 5.12: Static temperature contour in pulse tube.

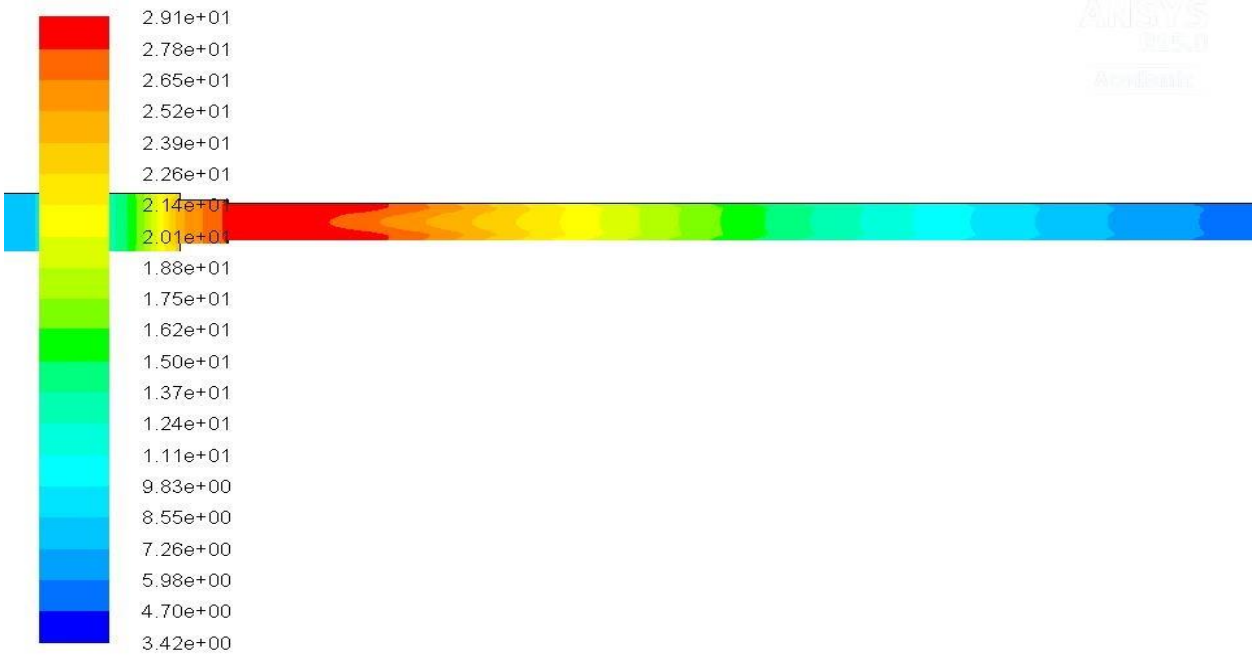

Figure 5.13: Density contour for pulse tube.

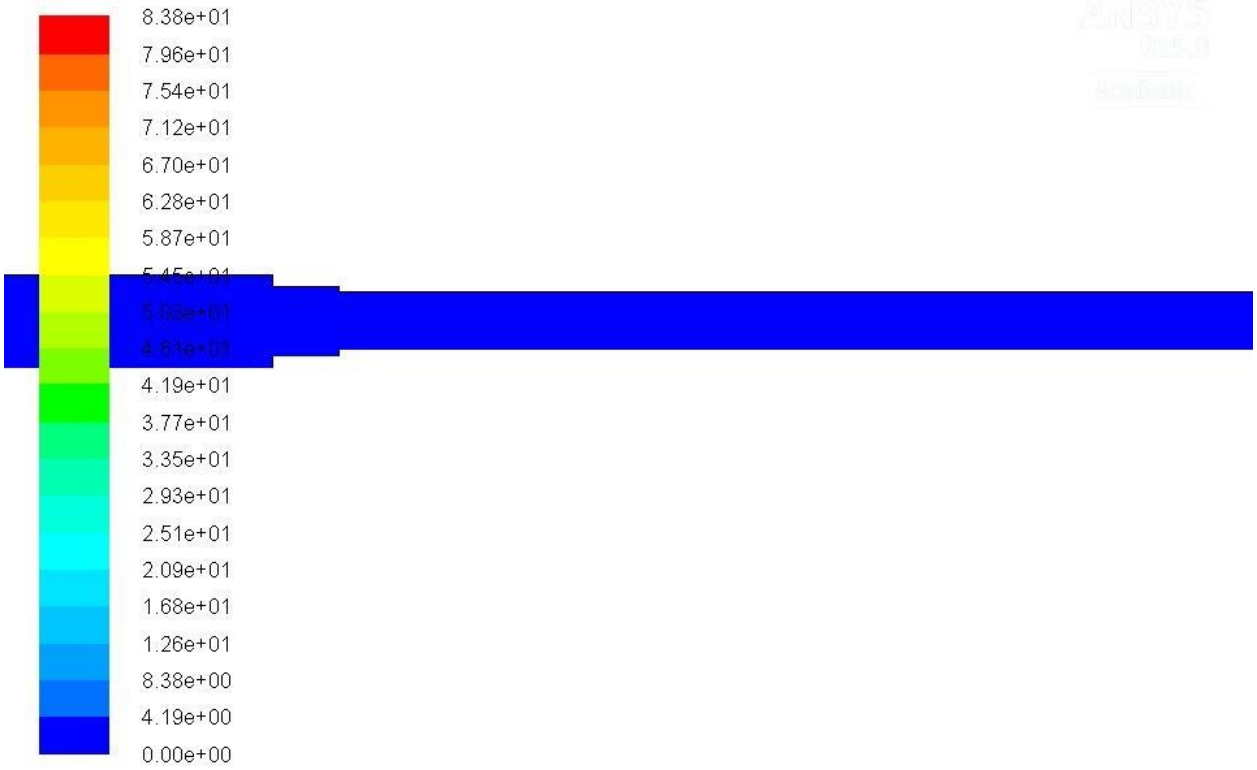

Figure 5.14: Velocity contour for pulse tube.

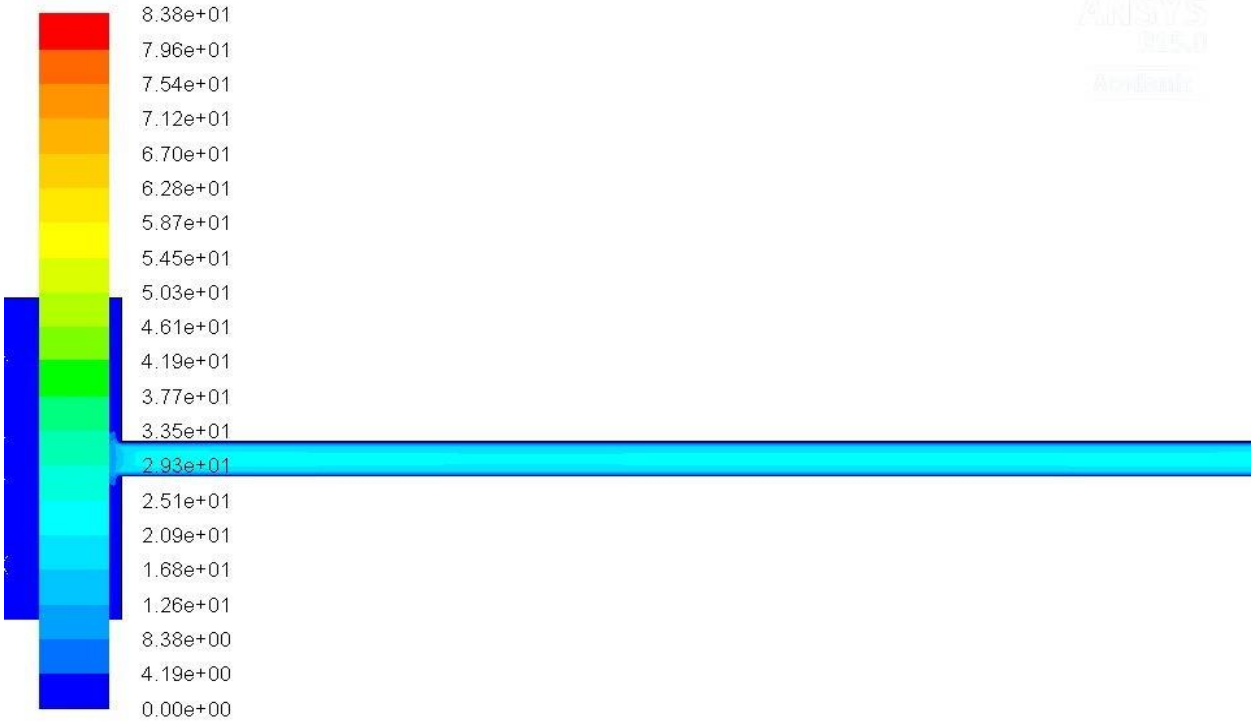

Figure 5.15: Velocity contour for inertance tube.

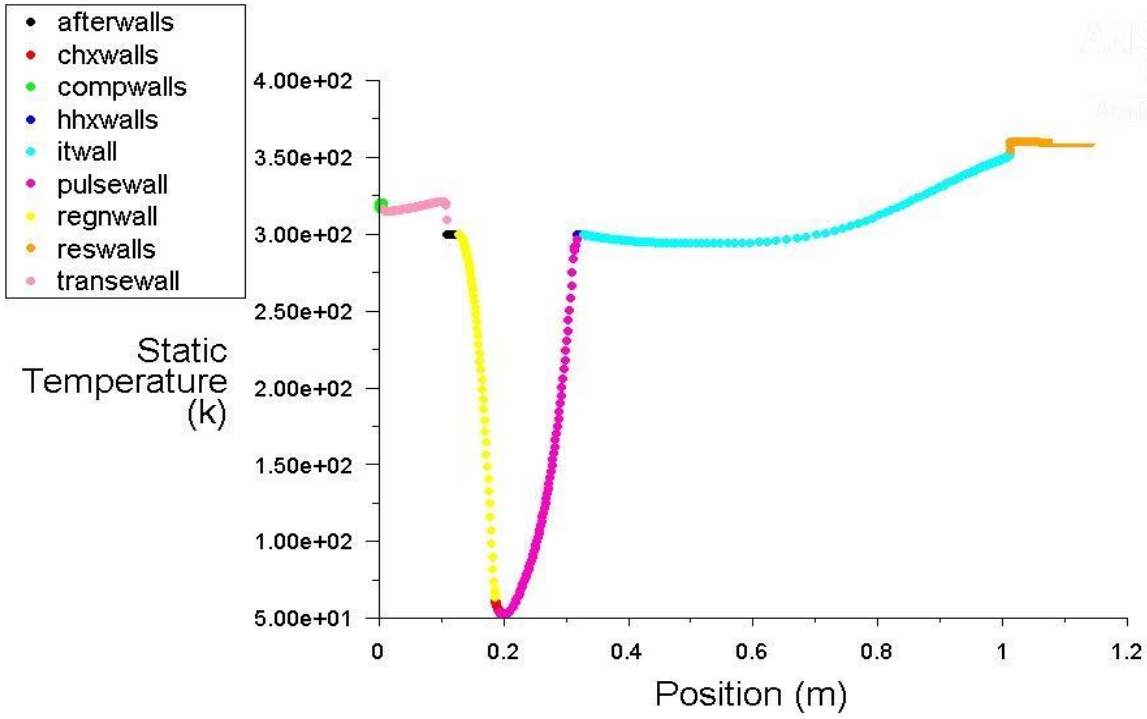

Figure 5.16: Static temperature variation along axial direction.

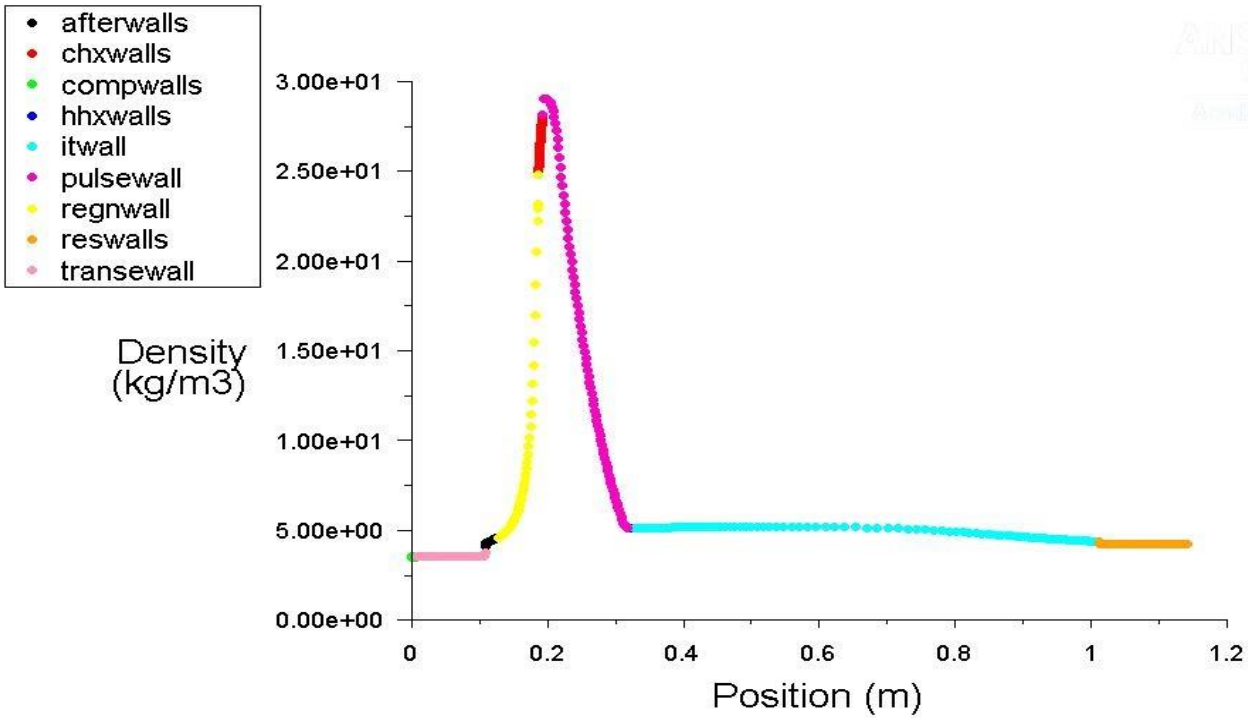

Figure 5.17: Density variation along axial direction.

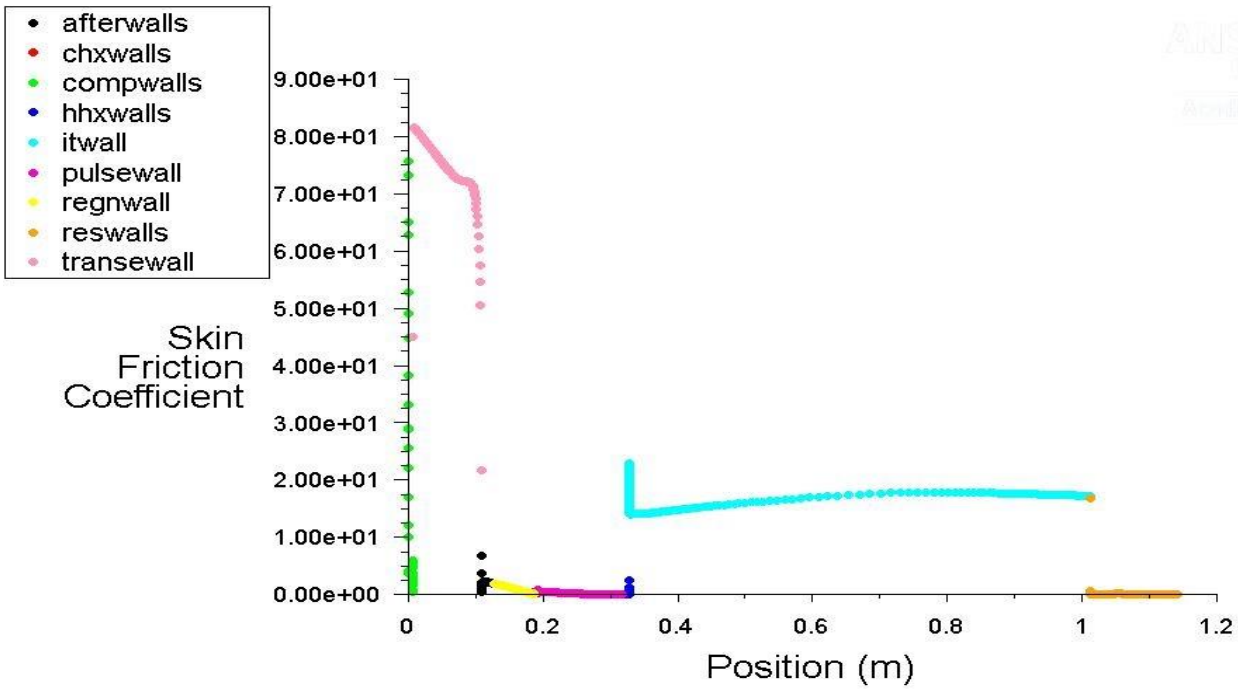

Figure 5.18: Skin friction coefficient variation along axial direction.

Chapter 6

Conclusions and Suggestion for Future Work

6.1 Conclusions

In the present work detailed mathematical study of regenerator and pulse tube refrigerator has been performed. Based on the mathematical models, two software packages have been developed, namely CRESP-REGEN and CRESP-PTR for regenerator and pulse tube refrigerator respectively. A detailed parametric study is performed to identify the effect of various geometrical and operating parameters on cold production. General conclusions that stemmed from this analysis are presented here, together with a brief recapitulation of some of the important remarks made earlier. From the parametric investigation, it is conccluded that:

- With increase in pressure ratio at cold end of the regenerator, it is possible to increase the refrigeration capcity but it is impossible to get a pressure ratio above a particular value in practical applications due to the limitations in the pressure wave generator.
- With increase in operating frequency, refrigeration power increases due to the production of inertance effect in the inertance tube.
- With increase in charging pressure, net refrigeration power increases and becomes maximum at an optimum point, thereafter it starts decreasing.

- Ineffectiveness of regenerator increases monotonously with increase in charging pressure.
- Both COP and exergy efficiency increase with increase in charging pressure till the optimum value, then start decreasing.
- With increase in pressure ratio at the cold end of the regenerator, second law efficiency, COP, isothermal refrigeration power, gross refrigeration power, net refrigeration power and inefficiency of regenerator increase.
- With increase in area to mass flow rate ratio at cold end of regenerator, COP and exergy efficiency increase up to a maximum point and then decrese.
- Refrigeration power and ineffctiveness decrease with increase in area to mass flow rate ratio at cold end of regenerator.
- With increase in length of regenerator, COP and exergy increase and become maximum at optimum point, then starts decreasing due to increase in viscous loss.
- With increase in operating frequency, exergy efficiency and COP start increasing and become maximum at the optimum point and thereafter start to decrease due to the increase in heat loss.
- Increase in operating frequency increases net refrigeration power due to increase in inertance effect in the ineratnce tube.
- Optimum phase angle at cold end of regenerator is found to be about −30°. Further increase in this value decreases COP and second law efficiency.
- With increase in hot end temperature of regenerator, COP, net refrigeration power, ineffectiveness and exergy efficiency decrease due to increase in regenerator loss.
- With increase in refrigeration temperature, ineffectiveness and regenerator loss starts decreasing, whereas, net refrigeration power, COP and second law efficiency starts increasing.

- Second law efficiency of regenerator, COP and net refrigeration power decrease with increase in thickness of regenerator due to increase in wall conduction.
- Both exergy efficiency and COP of regenerator is maximum for a particular range of values of porosity, it decreses further beyond this range.
- Variation of pressure with respect to time is mostly siusoidal in almost all componenets of pulse tube refrigerator except in the reservoir (here, it is nearly constant and equal to charging pressure).
- With increase in length of ineratnce tube, COP starts growing, and become maximum at the optimum point, then it starts decreasing.
- Amplitude of dynamic pressure decreses mostly in regenerator as compared to other components.
- Pressure ratio decreases consistently along the regenerator and incresaes along pulse tube.
- Amplitude of temperature oscillation is more at the end of pulse tube and hot heat exchanger, whereas its value is comparatively less in the aftercooler and nearly constant in buffer.
- Variations of solid temperature and fluid temperature at cold end of regenerator is nearly sinusoidal and amplitude of fluid temperature is greater than solid temperature.
- Most of the exergy destruction takes place in the regenerator due to irreversibility and generation of entropy, whereas, considerable amount of exergy drop occurs along cold heat exchanger, hot heat exchanger and cold end of pulse tube.
- From CFD analysis of inertance type pulse tube refrigerator, it is concluded that with increase in operating frequency, the cooldown time starts to decrease, also the cooling temperature is less.
- Flow is turbulent inside the transfer line and inertance tube whereas, in all other componenets the flow is laminar.

6.2 Suggestion for future work

The proposed formulation to develop the software packaages is capable of simulating a class of regenerative and recuperative cryocoolers. The suggested procedure may be beneficial to further develop the software package to include other types of cryocoolers as given below:

- CRESP-REGEN software can be extended by adding temperature dependent properties of both fluid and solid materials to improve its accuracy compatible with experimental results. Also, sinusoidal and trapezoidal variations of mass flow rate and pressure variations can be included for simulations of Stirling-type and GM-type cryocoolers.

- CRESP-PTR software has been validated with a few available computational results. So there is a need to perform experiments on various types of pulse tube cryocoolers which may be beneficial to validate the present simulation results.

- The present software can be extended to simulate other types of regenerative and recuperative cryocoolers (Stirling, GM-type and VM-type etc.) including temperature dependent thermo-physical properties. The software can also be extended to multistage pulse tube refrigerator.

- CFD analysis can be performed for other types of pulse tube refrigerators to investigate the multi-dimensional effects and results may be corroborated with CRESP-PTR.

References

[1] W. E. Gifford and R. Longsworth, "Pulse-tube refrigeration," *Journal of Engineering for Industry*, vol. 86, pp. 264-268, 1964.

[2] W. E. Gifford and R. Longsworth, "Surface heat pumping," in *Advances in Cryogenic Engineering*, ed: Springer, 1966, pp. 171-179.

[3] E. Mikulin, A. Tarasov, and M. Shkrebyonock, "Low-temperature expansion pulse tubes," in *Advances in cryogenic engineering*, ed: Springer, 1984, pp. 629-637.

[4] R. Radebaugh, J. Zimmerman, D. R. Smith, and B. Louie, "A comparison of three types of pulse tube refrigerators: new methods for reaching 60K," in *Advances in Cryogenic Engineering*, ed: Springer, 1986, pp. 779-789.

[5] Z. Shaowei, W. Peiyi, and C. Zhongqi, "Double inlet pulse tube refrigerators: an important improvement," *Cryogenics*, vol. 30, pp. 514-520, 1990.

[6] D. Gedeon, "DC gas flows in Stirling and pulse tube cryocoolers," in *Cryocoolers 9*, ed: Springer, 1997, pp. 385-392.

[7] D. Gardner and G. Swift, "Use of inertance in orifice pulse tube refrigerators," *Cryogenics*, vol. 37, pp. 117-121, 1997.

[8] K. D. Timmerhaus and T. M. Flynn, *Cryogenic process engineering*: Springer Science & Business Media, 2013.

[9] W. Gifford, "The Gifford-McMahon Cycle," in *Advances in Cryogenic Engineering*, ed: Springer, 1966, pp. 152-159.

[10] R. A. Ackermann, *Cryogenic regenerative heat exchangers*: Springer Science & Business Media, 2013.

[11] W. Dai, Y. Matsubara, and H. Kobayashi, "Experimental results on VM type pulse tube refrigerator," *Cryogenics*, vol. 42, pp. 433-437, 2002.

[12] R. Radebaugh, "Development of the pulse tube refrigerator as an efficient and reliable cryocooler," in *Proceedings of Institute of Refrigeration*, 2000, pp. 1999-2000.

[13] J. Yuan and J. Pfotenhauer, "Thermodynamic analysis of active valve pulse tube refrigerators," *Cryogenics*, vol. 39, pp. 283-292, 1999.

[14] S. Zhu, Y. Kakimi, and Y. Matsubara, "Investigation of active-buffer pulse tube refrigerator," *Cryogenics*, vol. 37, pp. 461-471, 1997.

[15] M. Shiraishi and M. Murakami, "Visualization of oscillating flow in a double-inlet pulse tube refrigerator with a diaphragm inserted in a bypass-tube," *Cryogenics*, vol. 52, pp. 410-415, 2012.

[16] R. Radebaugh, "Cryocoolers: the state of the art and recent developmentsContribution of NIST; not subject to copyright in the US," *Journal of Physics: Condensed Matter*, vol. 21, p. 164219, 2009.

[17] S. Kasthurirengan, G. Srinivasa, G. Karthik, D. Nadig, U. Behera, and K. Shafi, "Experimental and theoretical studies of a two-stage pulse tube cryocooler operating down to 3 K," *International Journal of Heat and Mass Transfer*, vol. 52, pp. 986-995, 2009.

[18] K. Shafi, N. M. Sajid, S. Kasthurirengan, and B. Upendra, "Investigations of a two-stage pulse tube cryocooler operating down to 2.5 K," *Proceedings of the Institution of Mechanical Engineers, Part C: Journal of Mechanical Engineering Science*, vol. 224, pp. 1255-1260, 2010.

[19] L. Qiu, Q. Cao, X. Zhi, L. Han, Z. Gan, Y. Yu, *et al.*, "Operating characteristics of a three-stage Stirling pulse tube cryocooler operating around 5K," *Cryogenics*, vol. 52, pp. 382-388, 2012.

[20] T. J. Hofler, "Thermoacoustic refrigerator design and performance," 1986.

[21] T. I. Mulcahey, "Convective instability of oscillatory flow in pulse tube cryocoolers due to asymmetric gravitational body force," 2014.

[22] G. Swift and S. Backhaus, "Why high-frequency pulse tubes can be tipped," 2008.

[23] G. Swift and S. Backhaus, "The pulse tube and the pendulum," *The Journal of the Acoustical Society of America,* vol. 126, pp. 2273-2284, 2009.

[24] L. Yang, Y. Zhou, and J. Liang, "DC flow analysis and second orifice version pulse tube refrigerator," *Cryogenics,* vol. 39, pp. 187-192, 1999.

[25] J. Gerster, M. Thürk, L. Reißig, and P. Seidel, "Hot end loss at pulse tube refrigerators," *Cryogenics,* vol. 38, pp. 679-682, 1998.

[26] S. Zhu, S. Kawano, M. Nogawa, and T. Inoue, "Work loss in double-inlet pulse tube refrigerators," *Cryogenics,* vol. 38, pp. 803-807, 1998.

[27] W. M. Kays and A. L. London, "Compact heat exchangers," 1984.

[28] A. Hill and A. J. Willmott, "Accurate and rapid thermal regenerator calculations," *International journal of heat and mass transfer,* vol. 32, pp. 465-476, 1989.

[29] A. Willmott and R. Thomas, "Analysis of the long contra-flow regenerative heat exchanger," *IMA Journal of Applied Mathematics,* vol. 14, pp. 267-280, 1974.

[30] A. J. Willmott, "The development of thermal regenerator theory: 1931-the present," *JOURNAL-INSTITUTE OF ENERGY,* pp. 54-54, 1993.

[31] A. Willmott, "Digital computer simulation of a thermal regenerator," *International Journal of Heat and Mass Transfer,* vol. 7, pp. 1291-1302, 1964.

[32] A. Willmott and C. Hinchcliffe, "The effect of gas heat storage upon the performance of the thermal regenerator," *International Journal of Heat and Mass Transfer,* vol. 19, pp. 821-826, 1976.

[33] A. Willmott and D. Knight, "Improved collocation methods for thermal regenerator simulations," *International journal of heat and mass transfer,* vol. 36, pp. 1663-1670, 1993.

[34] A. Willmott, D. Scott, and L. Zhang, "Matrix formulations of linear simulations of the operation of thermal regenerators," *Numerical Heat Transfer,* vol. 23, pp. 43-65, 1993.

[35] A. Willmott and B. Kulakowski, "Numerical acceleration of thermal regenerator simulations," *International Journal for Numerical Methods in Engineering,* vol. 11, pp. 533-551, 1977.

[36] A. Willmott, "The regenerative heat exchanger computer representation," *International Journal of Heat and Mass Transfer,* vol. 12, pp. 997-1014, 1969.

[37] A. Hill and A. J. Willmott, "A robust method for regenerative heat exchanger calculations," *International journal of heat and mass transfer,* vol. 30, pp. 241-249, 1987.

[38] A. Willmott, "Simulation of a thermal regenerator under conditions of variable mass flow," *International Journal of Heat and Mass Transfer,* vol. 11, pp. 1105-1116, 1968.

[39] S. Sarangi and J. Barclay, "Analysis of compact heat exchanger performance," Los Alamos National Lab., NM (USA)1984.

[40] R. Sahoo and S. Sarangi, "Effect of temperature-dependent specific heat of the working fluid on the performance of cryogenic regenerators," *Cryogenics,* vol. 25, pp. 583-590, 1985.

[41] S. Sarangi and H. Baral, "Effects of axial conduction in the fluid on cryogenic regenerator performance," *Cryogenics,* vol. 27, pp. 505-509, 1987.

[42] J. A. Barclay and S. Sarangi, "Selection of regenerator geometry for magnetic refrigerator applications," Los Alamos National Lab., NM (USA)1984.

[43] R. Radebaugh, Y. Huang, A. O'Gallagher, and J. Gary, "Calculated regenerator performance at 4 K with helium-4 and helium-3," in *ADVANCES IN CRYOGENIC ENGINEERING: Transactions of the Cryogenic Engineering Conference-CEC, Vol. 53,* 2008, pp. 225-234.

[44] J. Gary, D. E. Daney, and R. Radebaugh, "A computational model for a regenerator," in *Proc. of the Third Cryocooler Conference,* 1985, pp. 199-211.

[45] D. Daney and R. Radebaugh, "Non-ideal regenerator performance—the effect of void volume fluid heat capacity," *Cryogenics,* vol. 24, pp. 499-501, 1984.

[46] R. Radebaugh and B. Louie, "A simple, first step to the optimization of regenerator geometry," in *In its Proc. of the 3rd Cryocooler Conf. p 177-198 (SEE N86-11367 02-31)*, 1985, pp. 177-198.

[47] Z. Gan, W. Dong, L. Qiu, X. Zhang, H. Sun, Y. He, *et al.*, "A single-stage GM-type pulse tube cryocooler operating at 10.6 K," *Cryogenics,* vol. 49, pp. 198-201, 2009.

[48] Z.-h. Gan, G.-j. Liu, Y.-z. Wu, Q. Cao, L.-m. Qiu, G.-b. Chen, *et al.*, "Study on a 5.0 W/80 K single stage Stirling type pulse tube cryocooler," *Journal of Zhejiang University SCIENCE A,* vol. 9, pp. 1277-1282, 2008.

[49] J. Pfotenhauer, J. Shi, and G. Nellis, "A parametric optimization of a single stage regenerator using REGEN 3.2," in *Cryocoolers 13*, ed: Springer, 2005, pp. 463-470.

[50] Q. Cao, Z. Gan, G. Liu, Z. Li, Y. Wu, L. Qiu, *et al.*, "Theoretical and experimental study on a pulse tube cryocooler driven with a linear compressor," *Cryocoolers,* vol. 15, pp. 149-156, 2009.

[51] P. J. Storch and R. Radebaugh, "Development and experimental test of an analytical model of the orifice pulse tube refrigerator," in *Advances in cryogenic engineering*, ed: Springer, 1988, pp. 851-859.

[52] S. Zhu and Z. Chen, "Isothermal model of pulse tube refrigerator," *Cryogenics,* vol. 34, pp. 591-595, 1994.

[53] P. Wu and S. Zhu, "Mechanism and numerical analysis of orifice pulse tube refrigerator with a valveless compressor," in *Cryogenic and Refrigeration proceeding of International Conference, Hangzhou China*, 1989, pp. 22-26.

[54] J. Lee and H. Dill, "The influence of gas velocity on surface heat pumping for the orifice pulse tube refrigerator," in *Advances in Cryogenic Engineering*, ed: Springer, 1990, pp. 1223-1229.

[55] P. De Boer, "Pressure heat pumping in the orifice pulse-tube refrigerator," in *Advances in cryogenic engineering*, ed: Springer, 1996, pp. 1373-1382.

[56] R. Richardson, "Valved pulse tube refrigerator development," *Cryogenics,* vol. 29, pp. 850-853, 1989.

[57] A. Razani, C. Dodson, N. Abhyankar, and B. Flake, "A model for energy and exergy flow in an orifice pulse tube refrigerator," in *Cryocoolers 13*, ed: Springer, 2005, pp. 353-362.

[58] X. Zhang, L. Qiu, Z. Gan, and Y. He, "Effects of reservoir volume on performance of pulse tube cooler," *International journal of refrigeration,* vol. 30, pp. 11-18, 2007.

[59] W. Rawlins, R. Radebaugh, P. Bradley, and K. Timmerhaus, "Energy flows in an orifice pulse tube refrigerator," in *Advances in cryogenic engineering*, ed: Springer, 1994, pp. 1449-1456.

[60] C. Wang, P. Wu, and Z. Chen, "Numerical modelling of an orifice pulse tube refrigerator," *Cryogenics,* vol. 32, pp. 785-790, 1992.

[61] P. Kittel, "Ideal orifice pulse tube refrigerator performance," *Cryogenics,* vol. 32, pp. 843-844, 1992.

[62] M. David, J.-C. Maréchal, Y. Simon, and C. Guilpin, "Theory of ideal orifice pulse tube refrigerator," *Cryogenics,* vol. 33, pp. 154-161, 1993.

[63] C. Wang, P. Wu, and Z. Chen, "Modified orifice pulse tube refrigerator without a reservoir," *Cryogenics,* vol. 34, pp. 31-36, 1994.

[64] B. Huang and M. Chuang, "System design of orifice pulse-tube refrigerator using linear flow network analysis," *Cryogenics,* vol. 36, pp. 889-902, 1996.

[65] P. R. Roach and A. Kashani, "A Simple modeling program for orifice pulse tube coolers," in *Cryocoolers 9*, ed: Springer, 1997, pp. 327-334.

[66] P. Nika, "Étude paramétrique comparée des performances des réfrigérateurs à tube à gaz pulsé classique et hybride," *International journal of thermal sciences,* vol. 38, pp. 175-183, 1999.

[67] M. Xu, Y. He, and Z. Chen, "Analysis of an orifice pulse tube refrigerator using the method of characteristics," *Cryogenics,* vol. 39, pp. 751-757, 1999.

[68] F. Kuriyama and R. Radebaugh, "Analysis of mass and energy flow rates in an orifice pulse-tube refrigerator," *Cryogenics,* vol. 39, pp. 85-92, 1999.

[69] X. Zhang, L. Qiu, Z. Gan, and Y. He, "CFD study of a simple orifice pulse tube cooler," *Cryogenics,* vol. 47, pp. 315-321, 2007.

[70] Y. Ju, C. Wang, and Y. Zhou, "Numerical simulation and experimental verification of the oscillating flow in pulse tube refrigerator," *Cryogenics,* vol. 38, pp. 169-176, 1998.

[71] L. Ying-wen and H. Ya-ling, "A new tapered regenerator used for pulse tube refrigerator and its optimization," *Cryogenics,* vol. 48, pp. 483-491, 2008.

[72] C. Wang, P. Wu, and Z. Chen, "Numerical analysis of double-inlet pulse tube refrigerator," *Cryogenics,* vol. 33, pp. 526-530, 1993.

[73] H. Mirels, "Double inlet pulse tube cryocooler with stepped piston compressor," in *Advances in cryogenic engineering*, ed: Springer, 1994, pp. 1425-1431.

[74] P. Nika and Y. Bailly, "Comparison of two models of a double inlet miniature pulse tube refrigerator: Part A thermodynamics," *Cryogenics,* vol. 42, pp. 593-603, 2002.

[75] Y. Bailly and P. Nika, "Comparison of two models of a double inlet miniature pulse tube refrigerator: Part B electrical analogy," *Cryogenics,* vol. 42, pp. 605-615, 2002.

[76] J. Xiao, J. Yang, and Z. Tao, "Miniature double-inlet pulse tube cryocooler: design by thermoacoustic theory compared with preliminary experimental results," in *Advances in cryogenic engineering*, ed: Springer, 1996, pp. 1435-1441.

[77] A. Hofmann, "Numeric Code for the Design of Pulse Tube Coolers," in *Cryocoolers 13*, R. Ross, Jr., Ed., ed: Springer US, 2005, pp. 323-332.

[78] Y.L. He, J. Huang, C.F. Zhao, and Y.W. Liu, "First and second law analysis of pulse tube refrigerator," *Applied thermal engineering,* vol. 26, pp. 2301-2307, 2006.

[79] P. De Boer, "Characteristics of the double inlet pulse tube," *Cryogenics,* vol. 43, pp. 379-391, 2003.

[80] M. Chokhawala, K. Desai, H. Naik, and K. Narayankhedkar, "Phasor analysis for double inlet pulse tube cryocooler," *Advances in cryogenic engineering,* vol. 45, pp. 159-166, 2000.

[81] Y. Banjare, R. Sahoo, and S. Sarangi, "CFD simulation of a Gifford–McMahon type pulse tube refrigerator," *International Journal of Thermal Sciences,* vol. 48, pp. 2280-2287, 2009.

[82] Y. P. Banjare, "Theoretical and Experimental Studies on Pulse Tube Refrigerator," 2009.

[83] Y. Ju, L. Wang, and Y. Zhou, "Dynamic simulation of the oscillating flow with porous media in a pulse tube cryocooler," *Numerical Heat Transfer, Part A Applications,* vol. 33, pp. 763-777, 1998.

[84] G. Dash, T. Nandi, and P. Das, "Exergy destruction in the double inlet pulse tube cryocooler (DIPTC): A parametric study," *International Journal of Energy Research,* vol. 33, pp. 1290-1308, 2009.

[85] C. Wang, P. Wu, and Z. Chen, "Theoretical and experimental studies of a double-inlet reversible pulse tube refrigerator," *Cryogenics,* vol. 33, pp. 648-652, 1993.

[86] B. Zhou, P. Wu, S. Hu, and G. Chen, "Experimental results of the internal process of a double inlet pulse tube refrigerator," *Cryogenics,* vol. 32, pp. 24-27, 1992.

[87] M. Tanaka, S. Kawamatsu, T. Kodama, T. Nishitani, E. Kawaguchi, and M. Yanai, "Behavior of the gas temperature and pressure in the pulse tube refrigerator," *Cryogenics,* vol. 32, pp. 32-35, 1992.

[88] A. Ravex, P. Rolland, and J. Liang, "Experimental study and modelisation of a pulse tube refrigerator," *Cryogenics,* vol. 32, pp. 9-12, 1992.

[89] J. Cai, Y. Zhou, J. Wang, and W. Zhu, "Experimental analysis of double-inlet principle in pulse tube refrigerators," *Cryogenics,* vol. 33, pp. 522-525, 1993.

[90] I. Charles, L. Duband, and A. Ravex, "Permanent flow in low and high frequency pulse tube coolers–experimental results," *Cryogenics,* vol. 39, pp. 777-782, 1999.

[91] Z. Gan, G. Chen, G. Thummes, and C. Heiden, "Experimental study on pulse tube refrigeration with helium and nitrogen mixtures," *Cryogenics,* vol. 40, pp. 333-339, 2000.

[92] P. De Boer, "Performance of the inertance pulse tube," *Cryogenics,* vol. 42, pp. 209-221, 2002.

[93] E. Luo, R. Radebaugh, and M. Lewis, "Inertance tube models and their experimental verification," in *ADVANCES IN CRYOGENIC ENGEINEERING: Transactions of the Cryogenic Engineering Conference-CEC*, 2004, pp. 1485-1492.

[94] P. R. Roach and A. Kashani, "Pulse tube coolers with an inertance tube: theory, modeling, and practice," in *Advances in cryogenic engineering*, ed: Springer, 1998, pp. 1895-1902.

[95] L. O. Schunk, G. Nellis, and J. Pfotenhauer, "Experimental investigation and modeling of inertance tubes," *Journal of fluids engineering,* vol. 127, pp. 1029-1037, 2005.

[96] S. Zhu and Y. Matsubara, "Numerical method of inertance tube pulse tube refrigerator," *Cryogenics,* vol. 44, pp. 649-660, 2004.

[97] J. J. Cha, "CFD Simulation of multi-dimensional effects in inertance tube pulse tube cryocoolers," 2004.

[98] E. Luo, R. Radebaugh, W. Dai, M. Lewis, Z. Wu, and Y. Zhang, "Thermoacoustic turbulent-flow model for inertance tubes used for pulse tube refrigerators," *Proceedings of ICEC,* vol. 20, pp. 383-386, 2005.

[99] W. Dai, J. Hu, and E. Luo, "Comparison of two different ways of using inertance tube in a pulse tube cooler," *Cryogenics,* vol. 46, pp. 273-277, 2006.

[100] J. Ko, S. Jeong, and T. Ki, "Effect of pulse tube volume on dynamics of linear compressor and cooling performance in Stirling-type pulse tube refrigerator," *Cryogenics,* vol. 50, pp. 1-7, 2010.

[101] Y. Ju, G. He, Y. Hou, J. Liang, and Y. Zhou, "Experimental measurements of the flow resistance and inductance of inertance tubes at high acoustic amplitudes," *Cryogenics,* vol. 43, pp. 1-7, 2003.

[102] S.-J. Park, Y.-J. Hong, H.-B. Kim, S.-Y. Kim, and W.-S. Jung, "A study on the in-line type inertance tube pulse tube cryocooler for cooling Superconductor filter," *Progress in Superconductivity and Cryogenics,* vol. 6, pp. 46-50, 2004.

[103] M. Xu, Y. He, P. Wu, and Z. Chen, "Experimental research of a miniature coaxial pulse tube refrigerator using nylon tube," *Cryogenics,* vol. 36, pp. 131-133, 1996.

[104] T. Ashwin, "CFD Studies of Pulse Tube Refrigerators," 2012.

[105] E. Marquardt, R. Radebaugh, and P. Kittel, "Design equations and scaling laws for linear compressors with flexure springs," *Cryocoolers,* vol. 7, pp. 783-804, 1992.

[106] E. Marquardt and R. Radebaugh, "Design optimization of linear-arm flexure bearings," in *Cryocoolers 8*, ed: Springer, 1995, pp. 293-304.

[107] D.Y. Koh, Y.J. Hong, S.J. Park, H.B. Kim, and K.S. Lee, "A study on the linear compressor characteristics of the Stirling cryocooler," *Cryogenics,* vol. 42, pp. 427-432, 2002.

[108] G. Choe and K.J. Kim, "Analysis of Nonlinear Dynamics in a Linear Compressor," *JSME International Journal Series C,* vol. 43, pp. 545-552, 2000.

[109] A. Biswas and S. K. Ghosh, "Experimental and numerical investigation on performance of a double inlet type cryogenic pulse tube refrigerator," *Heat and Mass Transfer,* pp. 1-10, 2015.

[110] R. Richardson, "Development of a practical pulse tube refrigerator: co-axial designs and the influence of viscosity," *Cryogenics,* vol. 28, pp. 516-520, 1988.

[111] J. Wang, Y. Zhou, W. Zhu, and J. Cai, "Development of a liquid nitrogen precooled co-axial pulse tube refrigerator," *Cryogenics,* vol. 33, pp. 463-465, 1993.

[112] W. Ding, P. Huang, Y. He, Y. Liu, and W. Tao, "Factors influencing the lowest refrigerating temperature of the miniature co-axial pulse tube refrigerator," *Heat Transfer—Asian Research,* vol. 34, pp. 219-225, 2005.

[113] H. Dang, "High-capacity 60K single-stage coaxial pulse tube cryocoolers," *Cryogenics,* vol. 52, pp. 205-211, 2012.

[114] T. Haruyama, K. Kasami, H. Inoue, S. Mihara, and Y. Matsubara, "Development of a High-Power Coaxial Pulse Tube Refrigerator for a Liquid Xenon Calorimeter," in *ADVANCES IN CRYOGENIC ENGEINEERING: Transactions of the Cryogenic Engineering Conference-CEC*, 2004, pp. 1459-1466.

[115] M. Tanaka, T. Kodama, T. Nishitani, T. Araki, E. Kawaguchi, and M. Yanai, "Two stage pulse tube refrigerator with double rotary valves," *Cryogenics,* vol. 34, pp. 159-162, 1994.

[116] Y. Matsubara and J. Gao, "Multi-staged pulse tube refrigerator for superconducting magnet applications," *Cryogenics,* vol. 34, pp. 155-158, 1994.

[117] Y. Matsubara and J. Gao, "Novel configuration of three-stage pulse tube refrigerator for temperatures below 4 K," *Cryogenics,* vol. 34, pp. 259-262, 1994.

[118] K. Narayankhedkar and B. Gawali, "Design and development of an orifice/inertance pulse tube cryocooler using a linear compressor," in *ADVANCES IN CRYOGENIC ENGEINEERING: Transactions of the Cryogenic Engineering Conference-CEC*, 2004, pp. 1380-1387.

[119] C. Wang, Y. Ju, and Y. Zhou, "The experimental investigation of a two-stage pulse tube refrigerator," *Cryogenics,* vol. 36, pp. 605-609, 1996.

[120] C. Wang, G. Thummes, and C. Heiden, "Experimental study of staging method for two-stage pulse tube refrigerators for liquid 4 He temperatures," *Cryogenics,* vol. 37, pp. 857-863, 1997.

[121] C. Wang, G. Thummes, and C. Heiden, "A two-stage pulse tube cooler operating below 4 K," *Cryogenics,* vol. 37, pp. 159-164, 1997.

[122] C. Wang, "Numerical analysis of 4 K pulse tube coolers: Part I. Numerical simulation," *Cryogenics,* vol. 37, pp. 207-213, 1997.

[123] C. Wang, "Numerical analysis of 4 K pulse tube coolers: Part II. Performances and internal processes," *Cryogenics,* vol. 37, pp. 215-220, 1997.

[124] Y. Ju, "Computational study of a 4 K two-stage pulse tube cooler with mixed Eulerian–Lagrangian method," *Cryogenics,* vol. 41, pp. 49-57, 2001.

[125] A. Markan, A. Dash, and M. Atrey, "StirlinGUIDE-graphical user interface design and education of stirling type machines," *Indian Journal of Cryogenics,* vol. 40, pp. 182-187, 2015.

[126] R. Jahanbakhshi, M. H. Saidi, and A. R. Ghahremani, "Numerical modeling of pulse tube refrigerator and sensitivity analysis of simulation," *HVAC&R Research,* vol. 19, pp. 242-256, 2013/04/03 2013.

[127] D. Gedeon, "Sage User's Guide," *Gedeon Associates, Athens, OH,* 2011.

[128] B. Ward, J. Clark, and G. Swift, "Design Environment for Low (amplitude Thermoacoustic Energy Conversion DeltaEC Version 6.3 b11 Users Guide," *Los Alamos national laboratory,* 2012.

[129] M. P. Mitchell and L. Bauwens, "Modeling Pulse Tube Coolers with the MS* 2 Stirling Cycle Code," in *Cryocoolers 10*, ed: Springer, 2002, pp. 379-385.

[130] M. Atrey, S. Bapat, and K. Narayankhedkar, "Cyclic simulation of Stirling cryocoolers," *Cryogenics,* vol. 30, pp. 341-347, 1990.

[131] M. Atrey and K. Narayankhedkar, "Development of second order isothermal model of orifice type pulse tube refrigerator (OPTR) with linear compressor," in *18th International Cryogenic Engineering Conference (ICEC-18)*, 2000, pp. 519-522.

[132] S. Jacob, K. Sriram Prabhu, R. Karunanithi, and V. Ramanarayanan, "Design and Analysis of Power Controller for Moving Magnet Linear Motor Compressor," 2008.

[133] R. Radebaugh, Y. Huang, A. O'Gallagher, J. Gary, and J. Weisend, "Optimization calculations for a 30 Hz, 4 K regenerator with helium-3 working fluid," in *AIP Conference Proceedings*, 2010, p. 1581.

[134] J. Pfotenhauer, Z. Gan, and R. Radebaugh, "Approximate design method for single stage pulse tube refrigerators," in *ADVANCES IN CRYOGENIC ENGINEERING: Transactions of the Cryogenic Engineering Conference-CEC, Vol. 53*, 2008, pp. 1437-1444.

[135] P. Neveu and C. Babo, "A simplified model for pulse tube refrigeration," *Cryogenics*, vol. 40, pp. 191-201, 2000.

[136] J. Liang, A. Ravex, and P. Rolland, "Study on pulse tube refrigeration Part 1: Thermodynamic nonsymmetry effect," *Cryogenics*, vol. 36, pp. 87-93, 1996.

[137] J. Liang, A. Ravex, and P. Rolland, "Study on pulse tube refrigeration Part 2: Theoretical modelling," *Cryogenics*, vol. 36, pp. 95-99, 1996.

[138] P. Kush and M. Thirumaleshwar, "Design of regenerators for a Gifford-McMahon cycle cryorefrigerator," *Cryogenics*, vol. 29, pp. 1084-1091, 1989.

[139] Y. Ju, Y. Jiang, and Y. Zhou, "Experimental study of the oscillating flow characteristics for a regenerator in a pulse tube cryocooler," *Cryogenics*, vol. 38, pp. 649-656, 1998.

[140] R. F. Barron, "Cryogenic systems," 1966.

[141] A. Boroujerdi, A. Ashrafizadeh, and S. M. Naeenian, "Numerical analysis of stirling type pulse tube cryocoolers," *Cryogenics*, vol. 51, pp. 521-529, 2011.

[142] M. Arablu and A. Jafarian, "Investigation of synchronous effects of multi-mesh regenerator and double-inlet on performance of a Stirling pulse tube cryocooler," *Cryogenics*, vol. 54, pp. 1-9, 2013.

[143] M. Arablu and A. Jafarian, "A modified two-stage pulse tube cryocooler utilizing double-inlet and multi-mesh regenerator," *Cryogenics*, vol. 58, pp. 26-32, 2013.

[144] M. Arablu, A. Jafarian, and P. Deylami, "Numerical simulation of a two-stage pulse tube cryocooler considering influence of abrupt expansion/contraction joints," *Cryogenics*, vol. 57, pp. 150-157, 2013.

[145] U. Bin-Nun and D. Manitakos, "Low cost and high performance screen laminate regenerator matrix," *Cryogenics*, vol. 44, pp. 439-444, 2004.

[146] J. H. Baik, "Design methods in active valve pulse tube refrigerator," UNIVERSITY OF WISCONSIN–MADISON, 2003.

[147] A. F. U. s. Guide, "Release 15.0," *ANSYS, Inc.: Canonsburg, PA*, 2013.

[148] F. ANSYS, "Fluent user's manual," *Software release*, vol. 13, 2006.

[149] P. Linstrom and W. Mallard, "NIST Chemistry WebBook, NIST Standard Reference Database Number 69, National Institute of Standards and Technology, Gaithersburg MD, 20899," ed, 2010.

[150] H. Versteeg and W. Malalasekera, "An Introduction to computational fluid dynamics. 1995," *Harlow: Pearson Education Limited*, 1995.

[151] S. Patankar, *Numerical heat transfer and fluid flow*: CRC press, 1980.

APPENDIX-I: Solution Method for Adiabatic Model of Pulse Tube Refrigerator

All the governing equations are coupled equations of differential equations, linear equations, and conditional equations. The integral equations have been solved by Numerical integration methods. Here fourth order RK method has been implemented to solve these equations. The mass flow rate through the orifice valve, double inlet valve and regenerator are conditional equations because these equations will be solved based on the values of pressure. Suitable initial conditions must be assumed to get converged solutions within a small period. In the present work, the initial pressure is assumed to be mean pressure everywhere. Changes of the pressure of the compressor, reservoir, pulse tube, change of temperature of pulse tube are functions of temporal and spatial coordinates. Hence, fourth order Runge-Kutta method has been implemented to calculate $\frac{dP_{cp}}{dt}, \frac{dP_{pt}}{dt}, \frac{dP_{res}}{dt}, \frac{dT_{pt}}{dt}$. This procedure will repeat until one cycle will finish. After completion of one cycle convergence criteria has been checked, if the convergence criteria satisfied then, iteration terminated else it will again repeat. The detailed has been explained in the flow chart.

Derivatives

$$\begin{aligned}
\frac{dP_{cp}}{dt} &= f\left(P_{cp}, P_{pt}, P_{res}, T_{pt}\right) \\
\frac{dP_{pt}}{dt} &= f\left(P_{cp}, P_{pt}, P_{res}, T_{pt}\right) \\
\frac{dP_{res}}{dt} &= f\left(P_{cp}, P_{pt}, P_{res}, T_{pt}\right) \\
\frac{dT_{pt}}{dt} &= f\left(P_{cp}, P_{pt}, P_{res}, T_{pt}\right)
\end{aligned} \tag{A.1}$$

Runge-Kutta first orders coefficients

$$\begin{aligned}
K_1^{P_{cp}} &= h.f\left(P_{cp}, P_{pt}, P_{res}, T_{pt}\right) \\
K_1^{P_{pt}} &= h.f\left(P_{cp}, P_{pt}, P_{res}, T_{pt}\right) \\
K_1^{P_{res}} &= h.f\left(P_{cp}, P_{pt}, P_{res}, T_{pt}\right) \\
K_1^{T_{pt}} &= h.f\left(P_{cp}, P_{pt}, P_{res}, T_{pt}\right)
\end{aligned} \tag{A.2}$$

Runge-Kutta second order coefficients

$$K_2^{P_{cp}} = h.f\left(P_{cp} + \frac{K_1^{P_{cp}}}{2}, P_{pt} + \frac{K_1^{P_{pt}}}{2}, P_{res} + \frac{K_1^{P_{res}}}{2}, T_{pt} + \frac{K_1^{T_{pt}}}{2}\right)$$

$$K_2^{P_{pt}} = h.f\left(P_{cp} + \frac{K_1^{P_{cp}}}{2}, P_{pt} + \frac{K_1^{P_{pt}}}{2}, P_{res} + \frac{K_1^{P_{res}}}{2}, T_{pt} + \frac{K_1^{T_{pt}}}{2}\right) \tag{A.3}$$

$$K_2^{P_{res}} = h.f\left(P_{cp} + \frac{K_1^{P_{cp}}}{2}, P_{pt} + \frac{K_1^{P_{pt}}}{2}, P_{res} + \frac{K_1^{P_{res}}}{2}, T_{pt} + \frac{K_1^{T_{pt}}}{2}\right)$$

$$K_2^{T_{pt}} = h.f\left(P_{cp} + \frac{K_1^{P_{cp}}}{2}, P_{pt} + \frac{K_1^{P_{pt}}}{2}, P_{res} + \frac{K_1^{P_{res}}}{2}, T_{pt} + \frac{K_1^{T_{pt}}}{2}\right)$$

Runge-Kutta third order coefficients

$$K_3^{P_{cp}} = h.f\left(P_{cp} + \frac{K_2^{P_{cp}}}{2}, P_{pt} + \frac{K_2^{P_{pt}}}{2}, P_{res} + \frac{K_2^{P_{res}}}{2}, T_{pt} + \frac{K_2^{T_{pt}}}{2}\right)$$

$$K_3^{P_{pt}} = h.f\left(P_{cp} + \frac{K_2^{P_{cp}}}{2}, P_{pt} + \frac{K_2^{P_{pt}}}{2}, P_{res} + \frac{K_2^{P_{res}}}{2}, T_{pt} + \frac{K_2^{T_{pt}}}{2}\right) \quad \text{(A.4)}$$

$$K_3^{P_{res}} = h.f\left(P_{cp} + \frac{K_2^{P_{cp}}}{2}, P_{pt} + \frac{K_2^{P_{pt}}}{2}, P_{res} + \frac{K_2^{P_{res}}}{2}, T_{pt} + \frac{K_2^{T_{pt}}}{2}\right)$$

$$K_3^{T_{pt}} = h.f\left(P_{cp} + \frac{K_2^{P_{cp}}}{2}, P_{pt} + \frac{K_2^{P_{pt}}}{2}, P_{res} + \frac{K_2^{P_{res}}}{2}, T_{pt} + \frac{K_2^{T_{pt}}}{2}\right)$$

Runge-Kutta fourth order coefficients

$$K_4^{P_{cp}} = h.f\left(P_{cp} + K_3^{P_{cp}}, P_{pt} + K_3^{P_{pt}}, P_{res} + K_3^{P_{res}}, T_{pt} + K_3^{T_{pt}}\right)$$

$$K_4^{P_{pt}} = h.f\left(P_{cp} + K_3^{P_{cp}}, P_{pt} + K_3^{P_{pt}}, P_{res} + K_3^{P_{res}}, T_{pt} + K_3^{T_{pt}}\right)$$

$$K_4^{P_{res}} = h.f\left(P_{cp} + K_3^{P_{cp}}, P_{pt} + K_3^{P_{pt}}, P_{res} + K_3^{P_{res}}, T_{pt} + K_3^{T_{pt}}\right) \quad \text{(A.5)}$$

$$K_4^{T_{pt}} = h.f\left(P_{cp} + K_3^{P_{cp}}, P_{pt} + K_3^{P_{pt}}, P_{res} + K_3^{P_{res}}, T_{pt} + K_3^{T_{pt}}\right)$$

Numerical integration

$$K^{P_{cp}} = \frac{K_1^{P_{cp}} + 2K_2^{P_{cp}} + 2K_3^{P_{cp}} + K_4^{P_{cp}}}{6}$$

$$K^{P_{pt}} = \frac{K_1^{P_{pt}} + 2K_2^{P_{pt}} + 2K_3^{P_{pt}} + K_4^{P_{pt}}}{6} \quad \text{(A.6)}$$

$$K^{P_{res}} = \frac{K_1^{P_{res}} + 2K_2^{P_{res}} + 2K_3^{P_{res}} + K_4^{P_{res}}}{6}$$

$$K^{T_{pt}} = \frac{K_1^{T_{pt}} + 2K_2^{T_{pt}} + 2K_3^{T_{pt}} + K_4^{T_{pt}}}{6}$$

Integrated new values

$$\begin{aligned} t^{l+1} &= t^l + h \\ P_{cp}^{l+1} &= P_{cp}^l + K^{P_{cp}} \\ P_{pt}^{l+1} &= P_{pt}^l + K^{P_{pt}} \\ P_{res}^{l+1} &= P_{res}^l + K^{P_{res}} \\ T_{pt}^{l+1} &= T_{pt}^l + K^{T_{pt}} \end{aligned} \quad \text{(A.7)}$$

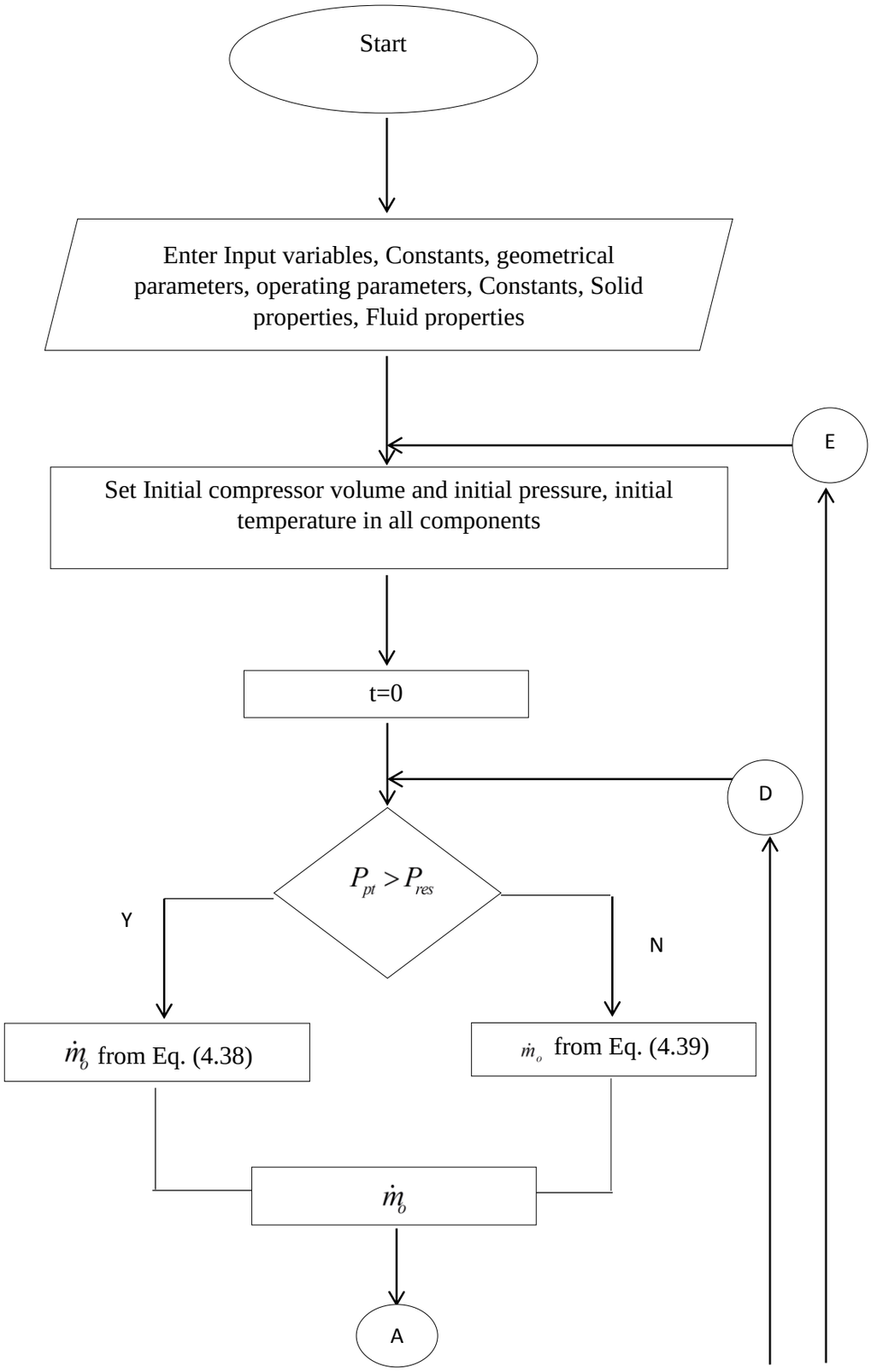
Start
Enter Input variables, Constants, geometrical parameters, operating parameters, Constants, Solid properties, Fluid properties
E
Set Initial compressor volume and initial pressure, initial temperature in all components
t=0
D
$P_{pt} > P_{res}$
Y
N
$\dot{m}_o$ from Eq. (4.38)
$\dot{m}_o$ from Eq. (4.39)
$\dot{m}_o$
A

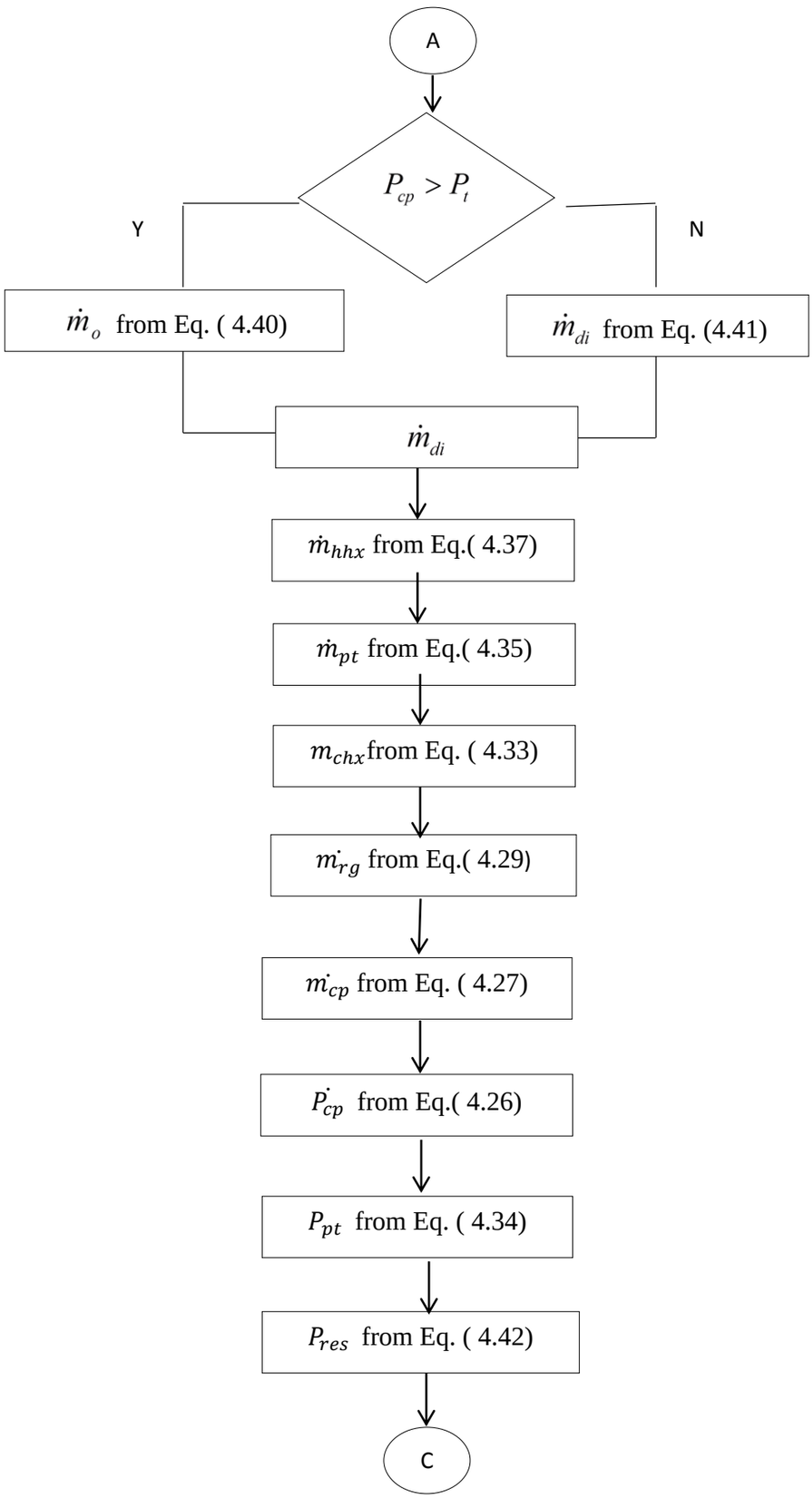
A
$P_{cp} > P_t$
Y
N
$\dot{m}_o$ from Eq. (4.40)
$\dot{m}_{di}$ from Eq. (4.41)
$\dot{m}_{di}$
$\dot{m}_{hhx}$ from Eq.(4.37)
$\dot{m}_{pt}$ from Eq.(4.35)
$m_{chx}$from Eq. (4.33)
$\dot{m_{rg}}$ from Eq.(4.29)
$\dot{m_{cp}}$ from Eq. (4.27)
$\dot{P_{cp}}$ from Eq.(4.26)
P_{pt} from Eq. (4.34)
P_{res} from Eq. (4.42)
C

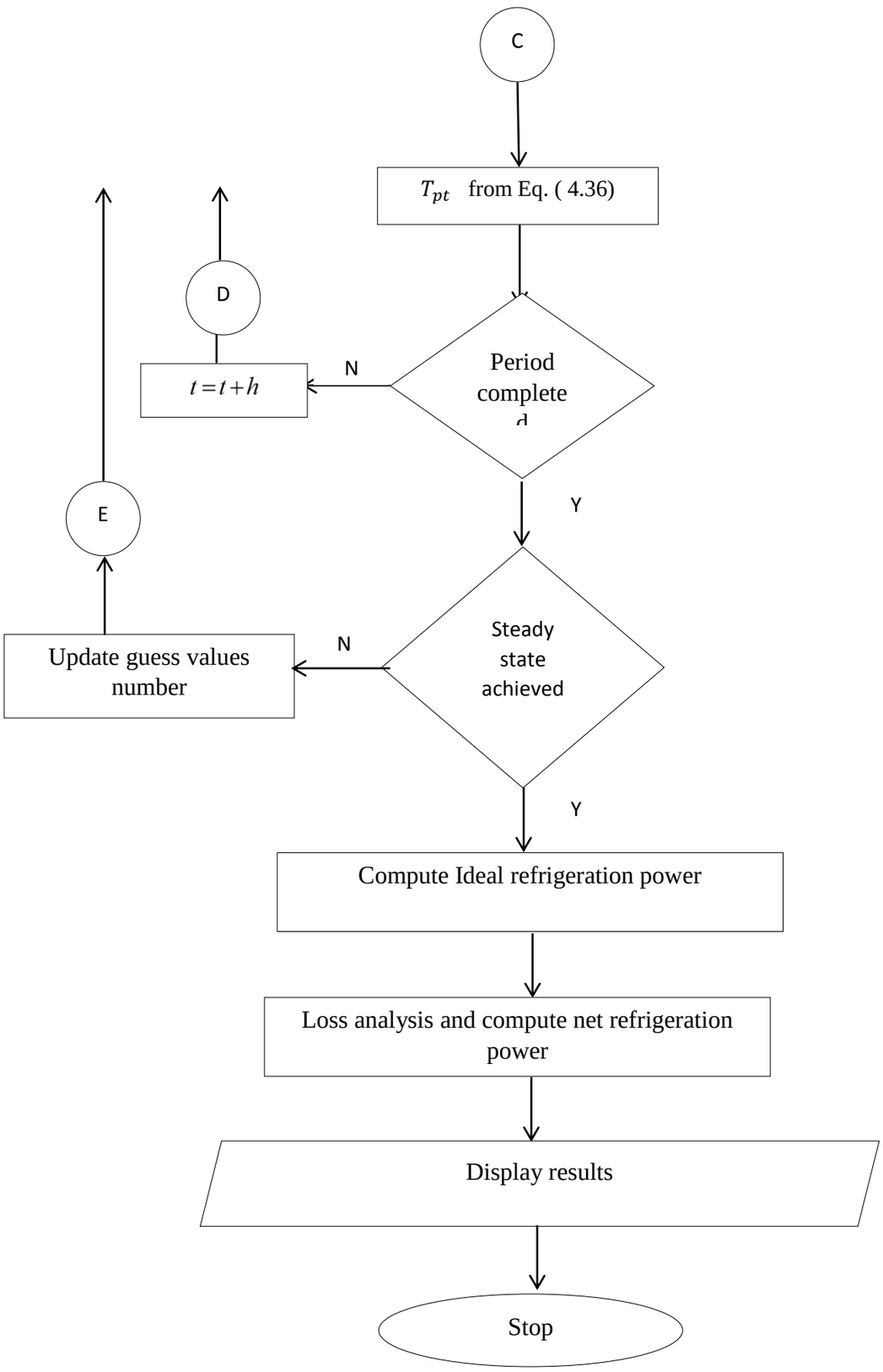

Figure A-I.1: Flow diagram for adiabatic model.

APPENDIX-II: Flow Chart of Numerical Model of Pulse Tube Refrigerator

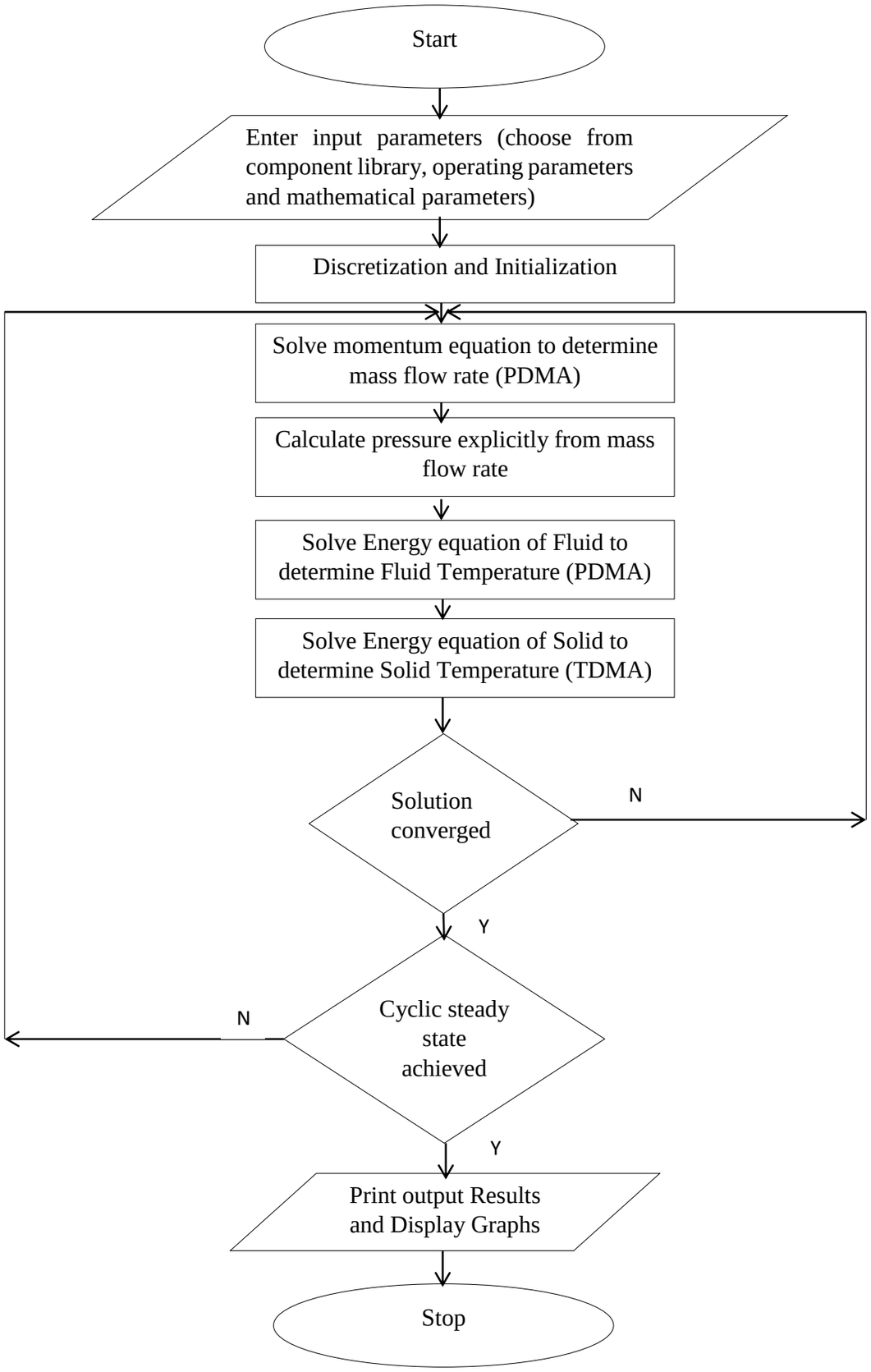

Figure A-II.1: Flow chart of numerical model.

Dissemination

1. D. Panda, K.N.S.Manoj, S. K. Sarangi, R. K. Sahoo. "A Mathematical Model and Design Software for Pulse Tube Refrigerator". *Proc. of International Cryogenic Engineering Conference-International Cryogenic Materials Conference* (ICEC26-ICMC 2016), March 2016, New Delhi, India.

2. K.N.S.Manoj**,** S. Panda, D. Panda, R.K. Sahoo, S.K. Sarangi. "Design and Fabrication of a High Cooling Capacity G-M Type Pulse Tube Refrigerator", *Proc. of International Cryogenic Engineering Conference-International Cryogenic Materials Conference* (ICEC26-ICMC 2016), March 2016, New Delhi, India.